AN ABSTRACT OF THE DISSERTATION OF

Yolanda H. Tennico for the degree of Doctor of Philosophy in Chemistry
presented on February 10, 2010
Title: Magnetic Particles for Selective Extraction of Trace Analytes in Microfluidic Devices

Abstract approved:

Vincent T. Remcho

The development of micro total analysis systems (μTAS), also called "lab-on-a-chip", or microfluidic analysis systems, is presented in this dissertation. Various research areas, covering subjects from magnetic particles synthesis to novel microchip fabrication techniques, are explored to develop a lab-on-a-chip system capable of performing magnetic bead-based bioassays. These devices are proven not only to be cost-effective (due to their reduced reagent consumption), but also time-efficient (shorter analysis time), and may be disposable (they are inherently compact and inexpensive to produce), making them very attractive to be used in biomedical applications.

The research starts with the utilization of functionalized magnetic particles as sorbents for an in-line extraction in confines of capillary columns. The synthesized silica-coated iron oxide particles functionalized with C18 groups were used as reversed-phase sorbents. Magnets were used to locally immobilize these particles inside the capillary. The results showed that extraction, elution, and detection of the analytes were performed sequentially without interruption or need for sample handling.

The work continued with the development of bonding techniques for creating polymer-based microfluidic devices through surface modification process. This technique readily produced complete microfluidic chips via plasma oxidation followed by silane reagent treatment (tetraethyl orthosilicate) to facilitate siloxane bonds between the two polymers. It provides a versatile approach to bond dissimilar polymer substrates and between a hard polymer substrate to polydimethylsiloxane or glass.

The two previous studies were combined allowing for the integration of magnetic particles in a microfluidic chip format. The benefits of each component were utilized to develop an on-chip aptamer-based fluorescence assay for thrombin detection and quantification based on sandwich ELISA principles. Aptamer-functionalized magnetic beads were utilized to capture the target analyte, while a second aptamer, functionalized with quantum dots, was employed for on-chip detection. Disposable microfluidic devices were employed as the platform to enable rapid and sensitive thrombin detection with the benefits of reduced costs, minimized material consumption, and simplified washing process. This work has opened up a new chapter in the development of magnetic beads-based materials and devices in a wide variety of applications for detection of target proteins of biomedical importance.

Magnetic Particles for Selective Extraction of Trace Analytes in Microfluidic Devices

by
Yolanda H. Tennico

A DISSERTATION

submitted to

Oregon State University

in partial fulfillment of
the requirements for the
degree of

Doctor of Philosophy

Presented February 10, 2010
Commencement June 2010

Doctor of Philosophy dissertation of Yolanda H. Tennico
presented on February 10, 2010.

APPROVED:

Major Professor, representing Chemistry

Chair of the Department of Chemistry

Dean of the Graduate School

I understand that my dissertation will become part of the permanent collection of Oregon State University libraries. My signature below authorizes release of my dissertation to any reader upon request.

Yolanda H. Tennico, Author

ACKNOWLEDGEMENTS

I would like to express my deepest gratitude to my research advisor, Dr. Vincent Remcho, for his guidance, understanding, and encouragement throughout my graduate career at OSU. His continuous support and enthusiasm have provided me with an excellent atmosphere in pursuing research. His mentorship has helped me to grow as a scientist and independent thinker. My appreciation also for my committee members, Dr. Chih-hung (Alex) Chang, Dr. Michael Lerner, Dr. Alexey Shvarev, and Dr. Alena Paulenova, for their commitment, input, and valuable discussions. Special thanks to Dr. Manish Gupta for his willingness to participate in my defense committee at the last moment.

I would like to thank all of the members of the Remcho research groups, Myra Koesdjojo, Jintana (Dao) Nammoonnoy, Tae-Hyeong Kim, Esha Chatterjee, David Mandrell, Saki Kondo, Natalia Pylypiuk, and Adeniyi Adenuga, for their countless help and valuable suggestions, for the friendship and much needed humor that have provided me with an enjoyable working environment. My sincere thanks also to the past group members with whom I have been fortunate to work with: Corey Koch, Jack Rundel, and Carlos Gonzalez.

I would like to acknowledge and thank my collaborators, especially Dr. Daniela Hutanu and Dr. Cheryl Moody Bartel for their guidance during my internship at Life Technologies and assistance in editing chapter 4 of this

dissertation. I am grateful for the rewarding internship experience and the opportunity to work, learn, and prepare for my future career. Thanks to ONAMI for the permission to use their facilities. I also thank the OSU Department of Chemistry, the faculties, and staffs for their assistance and for the access to all the facilities during my stay at OSU.

Many thanks to my friends, especially Defne Cakin Koch, Xenia Tombokan, Rina Permanasari, Hasini Perera, Zoe Lin, and Marian Lin for their moral supports and encouragements throughout these years.

Lastly and most importantly, I would like to thank my family for their continuous supports and encouragements. Special thanks to my parents, Justinus and Merry, and my sister, Methilda, for their understanding, patience and love that allow me to complete my study at OSU.

CONTRIBUTION OF AUTHORS

Dr. Vincent T. Remcho edited and assisted in writing of all chapters in this dissertation. His name appears on all published and submitted work contained herein. Dr. Myra Koesdjojo was involved with the design and writing of chapter 3 and 4. Saki Kondo and David Mandrell assisted with data collection in chapter 3.

TABLE OF CONTENTS

Page

TABLE OF CONTENTS (Continued)

Page

TABLE OF CONTENTS (Continued)

Page

TABLE OF CONTENTS (Continued)

Page

LIST OF FIGURES

Figure Page

LIST OF FIGURES (Continued)

Figure Page

LIST OF FIGURES (Continued)

Figure Page

LIST OF TABLES

MAGNETIC PARTICLES FOR SELECTIVE EXTRACTION OF TRACE ANALYTES IN MICROFLUIDIC DEVICES

CHAPTER 1

INTRODUCTION TO MAGNETIC NANOPARTICLES, FABRICATION TECHNOLOGY, AND CAPILLARY ELECTROPHORESIS

This chapter is divided into three sections. The first section focuses on the synthesis and properties of magnetic iron oxide nanoparticles. The next section highlights the advances of microfluidics and the fabrication technologies used to create the device. The last section describes the basic theoretical concepts and operational principles of capillary electrophoresis (CE). These discussions are intended to provide background and recent developments in the area of magnetic particles and microfabrication techniques. Their applications in capillary and microfluidic devices will be discussed in chapter 2, 3, and 4.

1.1 Magnetic particles

1.1.1 Properties of magnetic particles

Nanoparticles are defined as submicron moieties made of inorganic or organic materials, which have many novel properties compared to their bulk materials [1]. Magnetic nanoparticles (MNPs) have been growing in popularity in the past decade due to their superparamagnetic properties [2]. In the presence of a magnetic field, the particles exhibit very strong paramagnetic properties with a large susceptibility enabling the control and manipulation to externally applied

magnetic fields [3]. However, they do not retain any magnetism after the removal of magnetic field. In addition, their physical and chemical properties can be altered or modified based on their uses and applications. Magnetic iron oxide nanoparticles have been widely used as solid support due to their biocompatibility, stability and easily modifiable surface, which allows for their conjugation with biomolecules of interest [4-5]. They have been utilized in various fields of studies, including biomedical applications such as in drug delivery, magnetic resonance imaging contrast enhancement, magnetic cell separation, and biosensors [6-8].

Iron oxide NPs have been successfully synthesized with several methods, such as coprecipitation, thermal decomposition, hydrothermal synthesis, microemulsion, and sonochemical synthesis [9]. These approaches aim to produce MNPs that are monodisperse (with control over size and shape of the resulting particles), stable, and biocompatible. The effectiveness of the synthesized MNPs is highly dependent on the following parameters [10]:

1. High magnetic susceptibility for an effective magnetic enrichment
2. Size and shape of the resulting particles
3. Superparamagnetic property that determines their dispersion. No residual magnetic force remains between the particles after removal of the magnetic fields.
4. Tailored surface chemistry for specific biomedical applications

The surface of iron oxide NPs is hydrophobic with a large surface area-to-volume ratio. Therefore, these particles possess high surface energies. Consequently, they tend to aggregate (to minimize their surface energy) and form large clusters, resulting in an increase in particle size. Moreover, iron oxide NPs are easily oxidized in air (especially magnetite) which can result in loss of magnetism. Therefore, strategies are developed to maintain their stability by providing the proper surface coating during the particles synthesis. These strategies comprise of coating the particles with organic molecules (such as small organic molecules or surfactants, polymers, and biomolecules), or an inorganic layer (such as silica, metal or nonmetal elements, metal oxide or metal sulfide). Surface coating provides not only stability to the synthesized NPs, but can also be used for further functionalization. This chapter highlights the synthetic method and functionalization strategy used to produce the iron oxide NPs discussed in chapter 2.

1.1.2 Synthesis of iron oxide nanoparticles by co-precipitation technique

Iron oxide (Fe_3O_4 or γ-Fe_2O_3) NPs can be synthesized through the coprecipitation of Fe^{2+} and Fe^{3+} aqueous salt solutions by the addition of a base at room temperature or at elevated temperature, according to Fig. 1.1 below [11-14].

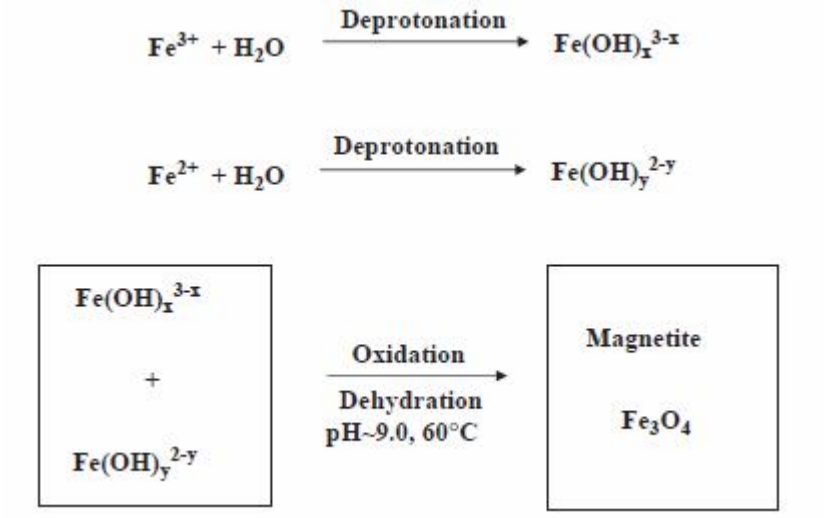

Fig. 1.1 Schematic drawing of the reaction of iron oxide particles precipitation from an aqueous mixture of ferrous and ferric salt solutions by addition of a base [10]

The overall chemical reaction of Fe_3O_4 precipitation is given below [15-16]:

$$Fe^{2+} + 2Fe^{3+} + 8OH^- \rightarrow Fe_3O_4 + 4H_2O \quad (1.1)$$

This reaction results in a black precipitation of magnetite that is expected to occur at pH between 9 and 14, while maintaining Fe^{2+}:Fe^{3+} molar ratio of 1:2; under a non-oxidizing oxygen free environment.

Fe_3O_4 NPs are not very stable under ambient conditions and are easily oxidized according to the following reaction.

$$Fe_3O_4 + 0.25O_2 + 4.5H_2O \rightarrow 3Fe(OH)_3 \quad (1.2)$$

Therefore, to minimize oxidation and have better control over the reaction kinetics, the synthesis is usually performed in an oxygen-free environment by streaming nitrogen gas through the solution during reaction.

This route is the most conventional method of producing iron oxide NPs. The control over size, shape, and composition of synthesized NPs depends on the type of salts used (such as chlorides, sulfates, nitrates, or perchlorates), Fe^{2+} and Fe^{3+} ratio, reaction temperature, pH and ionic strength of the media, and other reaction parameters (such as stirring rate, rate of addition of basic solution) [17]. The synthesis of Fe_3O_4 NPs by coprecipitation method and their corresponding morphology, structure, and magnetic properties at different reaction temperature has been reported [18].

1.1.3 Surface functionalization of magnetic nanoparticles

The surface of magnetic particles can be modified by the conjugation of inorganic metallic (such as gold) or oxide surfaces (such as silica or alumina) or organic molecules (such as polymers or silane agents). The surface can be further functionalized for the attachment of various bioactive molecules.

1.1.3.1 Surface functionalization by inorganic coating

Iron oxide NPs have been coated with inorganic molecules, such as silica or gold [19-20]. These coating materials provide not only the stability to the particles in solutions, changes in pH or electrolyte concentration, but also help in binding to the various biological ligands at the NPs surface for various applications. The coating materials also minimize oxidation and agglomeration during the precipitation synthesis process.

Silica is the most common molecule for preparing the functionalized iron oxide NPs. An advantage of having a surface enriched in silica is the presence of surface silanol groups that can easily react with silane coupling agents for binding to biomolecules. In addition, the silica surface has chemical and biochemical inertness, good mechanical stability, hydrophilic to avoid non-specific interactions, and retains the biospecific activity of antibodies after immobilization procedure.

Iron oxide NPs have been coated with silica by several methods, such as Stöber methods, sol–gel process, and aerosol pyrolysis [21]. Silica coating typically increases the size of the resulting NPs. The technology of preparing size tunable NPs with silica coating has already matured. The silica thickness can be tuned by varying the concentration of basic solution (such as ammonia) and the tetraethyl orthosilicate (TEOS) to water ratio. Silica can be coated via the hydroxyl groups on the surface of iron oxide NPs, according to the Stöber method and sol–gel process [9].The hydrolysis of TEOS under basic condition produces silanol group on the surface of the Fe_3O_4 NPs.

1.1.3.2 Surface functionalization by organic coating

The silane agent is one of the commonly used organic materials for modifying the surface of iron oxide NPs. They have the advantages of biocompatibility as well as high density of surface functional end groups which allow for conjugation to other metal, polymer or biomolecules [22-23]. Some commonly used agents include 3-aminopropyltriethyloxysilane (APTES),

p-aminophenyl trimethoxysilane (APTS), and mercaptopropyltriethoxysilane (MPTES), which contains amino and sulfhydryl functional groups. APTES offers the advantage of maintaining the morphology of the synthesized NPs, rendering the particles stability and water dispersibility, and protection against mild acid and alkaline environments.

The resulting silane-coated iron oxide NPs maintains the physical properties of bare NPs. The particles still possess high saturation magnetization (a decrease value of saturation magnetization is usually less than 10 emu/g). Some silane agents mostly employed for modifying the surface of iron oxide NPs along with their physiochemical characteristics are depicted in Fig. 1.2 [24]. The hydroxyl groups on the iron oxide NPs surface can be reacted with the methoxy or ethoxy groups of the silane molecules leading to the formation of Si–O bonds and high density functional end groups for conjugation to other molecules.

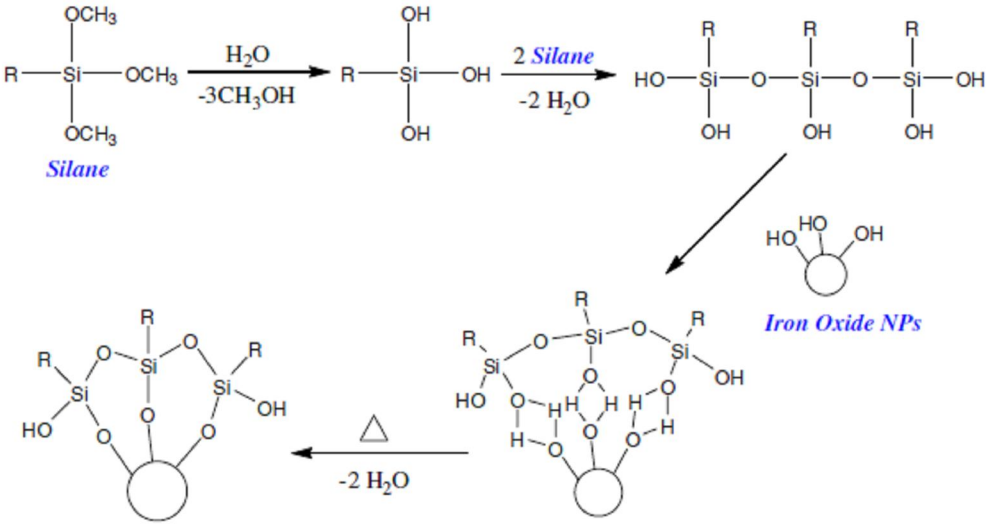

Fig. 1.2 Physiochemical mechanism for modifying the silane agents on the surface of iron oxide NPs [24].

Various biological molecules, such as protein, antibody, or biotin and avidin [25-27] can be conjugated to the surface of iron oxide NPs through the proper functional end groups (such as amide or ester bonds) to make the NPs target specific. Linker molecules, such as 1-ethyl-3- (3-dimethylaminopropyl) carbodiimide hydrochloride (EDC), N-succinimidyl 3-(2-pyridyldithio) propionate (SPDP), N-hydroxysuccinimide or N, N' methylene *bis* acrylamide (MBA) are commonly used to attach the surface of the hydrophilic coated particles to the functional group of the bioactive molecules [28]. Some crosslinker molecules used for biomolecules conjugations to the magnetic particles are provided in Fig. 1.3.

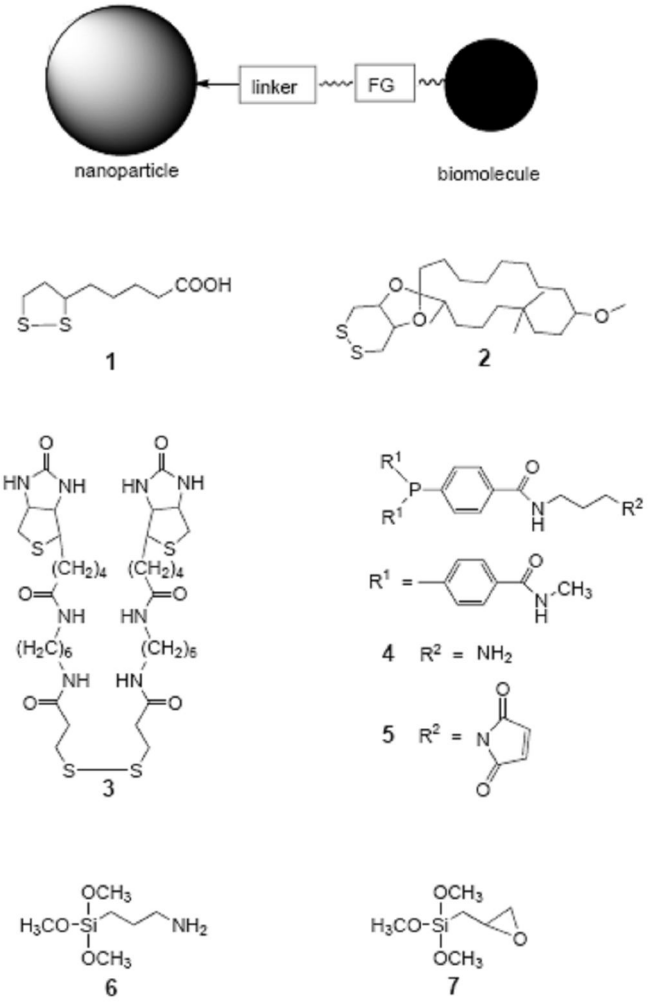

Fig. 1.3 Cross-linker molecules used for biomolecules conjugations to the magnetic particles [29]

The functionalized magnetic NPs have been used in effective separation of proteins, DNA, cells, aptamers, or other biomolecules. An application of magnetic particles functionalized with aptamers will be discussed in chapter 4. Fig. 1.4 shows the synthetic scheme of producing antibody-conjugated magnetic particles.

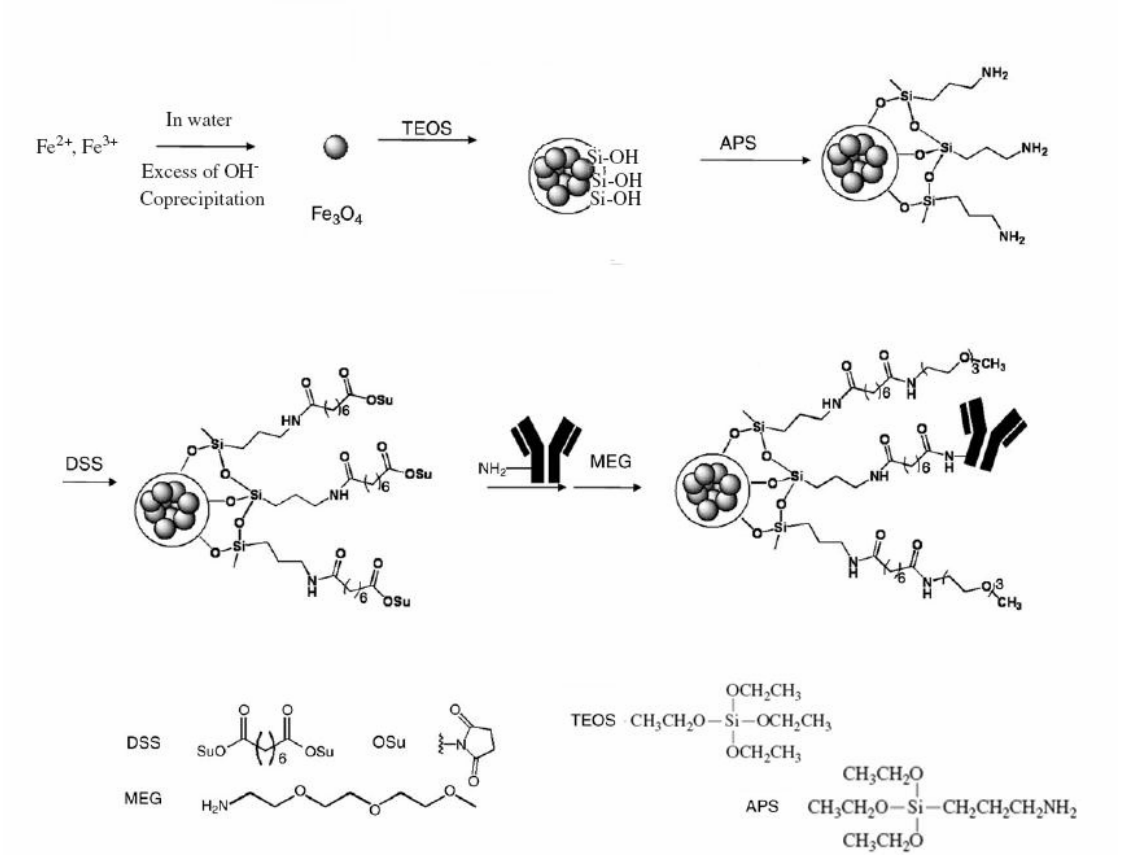

Fig. 1.4 Synthetic scheme of antibody-conjugated iron oxide nanoparticles [13-14]

1.1.4 Applications of magnetic particles in microfluidic devices

The use of magnetic particles are ideal for microfluidic applications as they possess a large surface area-to-volume ratio, which in turn may enhance the signal sensitivity due to higher efficiency of interactions between samples and reagents, and provide a relatively large numbers of binding sites for biochemical reactions. In addition, their superparamagnetic properties enable them to be externally controlled and manipulated by simple permanent magnets. This property makes them attractive to be integrated into microfluidic systems. They can be employed

as solid supports for SPE sorbents using magnets to retain the beads in a microfluidic device. This way, the challenges of microfabrication to create frits are eliminated. Moreover, they can be positioned anywhere in the microchip, and the beads are easily unloaded for downstream analysis and testing by simply removing the magnet. The beads can then be immobilized after each analysis, eliminating the need to regenerate the solid supports.

1.2 Introduction to microfluidics

Since the introduction of miniaturization concept in the early 1990s, significant progress has been made in the development of microfluidics for biological and chemical analysis [30]. Microfluidics, also known as lab-on-a-chip systems or micrototal analysis system (μTAS) is the study of fluids manipulation and analysis in micron-sized channels. Microfluidic devices offer many promising analytical tools that can enhance the effectiveness and performance of routine chemical analysis. They allow for the integration of fluid delivery (such as pumps, valves, filters, mixers), sample handling, chemical or biochemical analysis (such as extraction, separation by chromatography or electrophoresis), and detection systems (fluorescence, electrochemical detection) into a single device for a complete on-chip analysis.

In addition, microfluidics offer unique benefits, such as reduced component size, decreased consumption of reagents and sample, reduced waste generation, reduced analysis time, and increased synthesis rate due to short mixing time. The

miniaturization of microfluidic devices has also made possible the development of portable analytical instrumentation where lower voltages and smaller power supplies are needed. These devices can be interfaced to allow highly integrated parallel operations for the development of micro total analysis systems (μTAS). This integration makes complex analyses simpler to perform. All the steps in the analysis, including sample processing, separation, and detection, are all performed on one chip. Moreover, μTAS devices can reduce the chance of human error, such as mislabeling and contamination, by decreasing the number of times a sample is handled.

Glass has been the dominant substrate material for production of microfluidic systems [31-32]. They possess many characteristics, such as high thermal stability, biocompatibility, solvent compatibility, optical transparency, and surface properties that are well suited for use in μTAS. They are fabricated by preexisting microfabrication techniques (photolithography and chemical etching) that have been well established in the microelectronics industry. While the use of glass substrates in microfluidic systems is very attractive, they also have some limitations. The fabrication of glass microchips is often expensive, time-consuming, and the process involves the use of harmful hydrofluoric acid (HF) and clean room facilities. These disadvantages have made manufacturers to seek alternative materials for microchips fabrication.

Polymers have great potential to be used as alternative materials for making microfluidic devices. They offer low cost, ease of fabrication, and greater

flexibility over silicon and glass. The expensive microfabrication step is only required to make the master structure, which then can be replicated many times into the polymer substrate. This offers benefits where high volume production is required. Moreover, existing mass replication technologies (such as hot embossing and injection molding) as well as methods for rapid prototyping (including casting or laser machining) can be directly applied to polymer fabrication. Polymer substrates offer optical characteristics, temperature stability, chemical resistance and biocompatibility. These are very important parameters to be considered in the fabrication process and application of the resulting device. The cost effective and relatively rapid fabrication procedures of these polymeric materials have made the development of single use, disposable microchips feasible.

Polymers are large molecules (macromolecules) composed of connected repeating structural units. An important parameter in fabrication of polymeric devices is their glass transition temperatures (Tg). The glass transition temperature is the temperature range at which the polymer substrate changes from a rigid glassy material to a soft (yet not molten) material [33]. It differs from the melting temperature in that the melting temperature is the temperature at which the polymer flows, and usually occurs at a much higher temperature than Tg. At temperatures above Tg, the materials become viscous. Cooling to below the glass transition temperature will result in hard, brittle, glass-like materials. Therefore, demolding of the materials is performed below their Tg to protect their geometric stability from relaxation occurred during demolding process.

Thermoplastic polymers consist of weakly linked or unlinked chain molecules [33]. At a temperature above Tg, these materials behave as plastics and can be molded into specific shapes. They will retain their shape when demolded below Tg. Examples are poly(methyl methacrylate) (PMMA), polycarbonate (PC), or polyethylene terephthalate [34-36]. Elastomeric polymers also consist of weakly cross-linked polymer chains. Their molecular chains can be stretched in response to an external force. In the absence of external force, they relax and return to their original state. Polydimethylsiloxane (PDMS) [37] is the widely used elastomeric material used in microfluidic device fabrication. A list of standard polymer materials and their properties is summarized in Table 1.1 below.

Table 1.1 Standard polymer materials and their properties [33].

Thermoplastic materials	Density ($x10^3$ kg/m^3)	Glass temp. T_g (^oC)	Thermal conductivity λ (W/mK)	Linear expansion coefficient α (10^{-6} /K)
Polyamine 6 (PA 6)	1.13	60	0.29	80
Polyamide 6.6 (PA 6.6)	1.14	70	0.23	80
Polycarbonate (PC)	1.2	150	0.21	65
Polyoxymethylene (POM)	1.41-1.42	-60	0.23-0.31	90-110
Cycloolefin copolymer (COC)	1.01	138	N/A	60
Polymethylmetharcylate (PMMA)	1.18-1.19	105	0.186	70-90
Polyethylene low density (PE-LD)	≤ 0.92	-10	0.349	140
Polyethylene high density (PE-HD)	≤ 0.954	-	0.465	200
Polypropylene (PP)	0.896-0.915	0-10	0.22	100-200
Polystyrene (PS)	1.05	80-100	0.18	70

The wide range of polymers available allows manufacturers to choose the material properties that are suitable for their specific applications. These parameters include their chemical resistance, mechanical and UV stability, and aging. As an example, for applications requiring laser induced fluorescence (LIF) detection, PMMA and special grades PC are often the chosen materials as they have low autofluorescence (their fluorescence is comparable to standard borofloat glass substrates). The physical and chemical properties of the most commonly used thermoplastics materials are listed in Table 1.2.

Table 1.2. Basic chemical properties of polymer materials [33].

Thermoplastic materials	Solvent resistance	Acid and alkaline resistance	Trade name
Polyamine 6 (PA 6)	Resistant against: ethanol, benzene, aromatic and aliphatic hydrocarbons, mineral oils, fats, ether, ester, ketones	Not resistant against: diluted and concentrated mineral acids, formic acid	Perlon Durethan (Bayer) Ultramid (BASF)
Polyamide 6.6 (PA 6.6)	Same as above	Same as above	Nylon Nylind (DuPont) Celanese (Ticona) Ultramid (BASF)
Polycarbonate (PC)	Resistant against: water, benzene, mineral oils Conditionally resistant against: alcohols, ether, ester	Resistance against: diluted mineral acids	Makrolon (Bayer)
Polyoxymethylene (POM)	Resistant against: fuels, mineral oils, usual solents	Not resistant against: anorganic acids, acetic acid, oxidating solvents	Hostaform (Hoechst)
Cycloolefin copolymer (COC)	Resistant against: acetone, methylethylketone, methanol, isopropanol	Resistant against: diluted and concentrated mineral acids and alkalines, 30% H_2O, 40% formaldehyde, detergents in water	Topas (Ticona) Zeonex (Nippon Zeon)
Polymethylmetharcylate (PMMA)	Resistant against: water, mineral oils, fuel, fatty oils	Resistant against: up to 20% diluted acids, diluted alkalines, NH_3	Plexiglas (Rohm) Lucryl (BASF) Perspex (ICI)
Polyethylene (PE)	Resistant against: alcohols, benzene, toluene, xylene	Resistant against: NH_3, diluted HNO_3, H_2SO_4, HCl, KOH, NaOH	Lupolen (BASF)
Polypropylene (PP)	Resistance against: diluted solutions of salts, lubricating oils, chlorinated hydrocarbons, alcohols	Resistant against: most diluted acids and alkalines	Hostalen (Hoechst)
Polystyrene (PS)	Resistant against: alcohols, polar solvents Nor resistant against: ether, benzene, toluene, chlorinated hydrocarbons, acetone, ethereal oils	Resistant against: diluted and concentrated acids (except HNO_3) and alkalines	Polystrol (BASF)

1.2.1 Fabrication of polymer-based microfluidic devices

Fabrication of polymeric devices has been performed using several mass replication technologies, such as hot embossing, injection molding, laser ablation, soft lithography or casting [38-42]. As a general rule, the selection of a fabrication method is determined by several factors, including the available technologies and equipment, cost, speed, fabrication capabilities, and the preferred material substrates.

1.2.1.1 Photolithography

Photolithography has been a widely used method for fabrication of master templates. The process starts by patterning features on the master (usually silicon) using a photoresist (a photo-active polymer, such as SU-8). The photoresist is masked with a transparency that contains the pattern features of interest and irradiated using an emissive source (electron, ion, X-ray, UV or visible light source) that leads to a photochemical reaction of the resist material. In negative photoresists (such as SU-8), the solubility of the irradiated areas decreases relative to the unexposed regions. When SU-8 is exposed to a UV source, the polymer chains cross-link to form a chemical and temperature-resistant material with high mechanical strength. The non-irradiated areas are then removed by a developer. Fig. 1.5 shows the schematic diagram of a photolithography process.

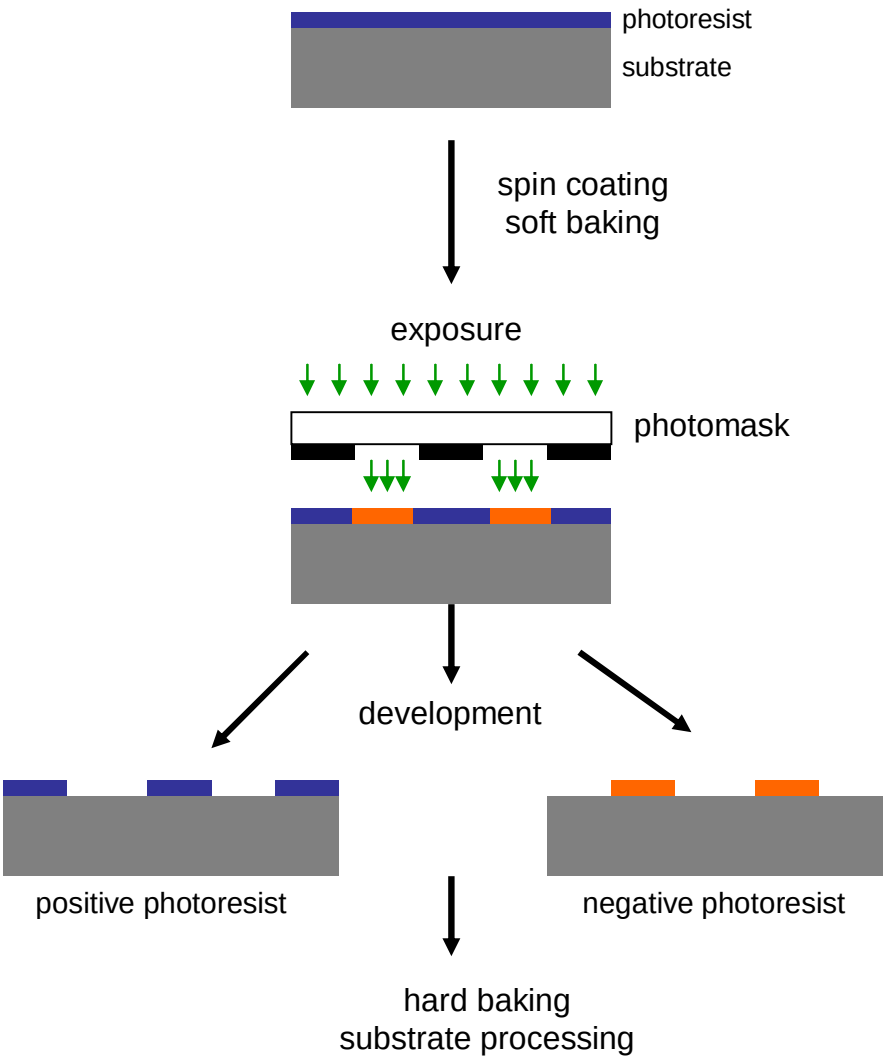

Fig. 1.5 Photolitographic process for fabricating microchip devices

1.2.1.2 Hot embossing

Hot embossing has been described as the most widely used and low cost process to replicate microstructures for microfluidic applications [33]. The process is rapid, inexpensive, simple and straightforward. After the fabrication of the master template by process such as photolithography, both the master and the substrate are mounted into the hot embossing tool (Fig. 1.6a), and are heated to a

temperature above the glass transition temperature, T_g, of the polymer material. The embosser is brought into contact with the substrate, and uniform pressure is applied in the substrate. Still applying the pressure, the substrate is then cooled down to just below their Tg to stabilize the structure.

A)

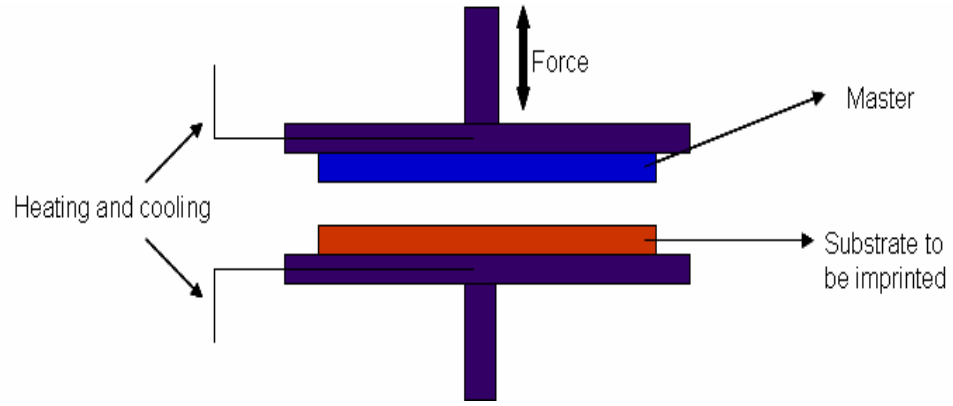

B)

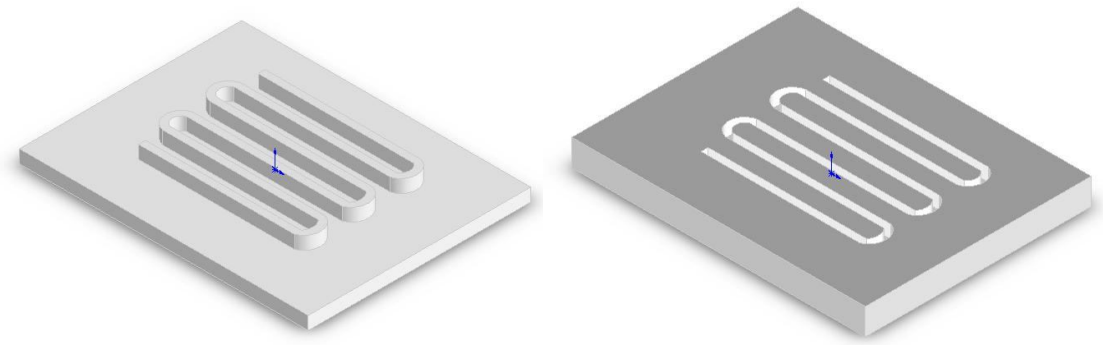

Fig. 1.6 A) The diagram of a hot embossing tool, B) Raised features (left) used as the master mold to replicate structure with recessed features (left) by single step hot embossing technique [43].

Hot embossing typically employs a single processing step in which a master mold with *negative* features is used to emboss *positive* features into a thermoplastic substrate (the term "positive" refers to the geometry of the desired features whereas the term "negative" refers to the inverse of the desired features) (see Fig. 1.6b). Our group has developed a two stage embossing technique for fabrication of polymer microfluidic chips [43]. The method involves two processing steps to produce the final product. In the first step, a primary mold with *positive* features was embossed into a thermoplastic substrate to create a secondary mold with *negative* features. In the second step, the secondary mold is used to emboss *positive* features into another polymeric substrate to form the final product. It is essential for the secondary mold to have a much higher Tg compared to the final product to avoid feature deformation of the secondary mold during the second embossing step. Fig. 1.7 shows the schematic diagram of two-stage embossing technique.

The motivation of using the two stage embossing method instead of the conventional one-step embossing technique is the need for co-planarity of bonding surfaces at the interface between substrates in a microfluidic chip [43]. With this technique, tedious procedures of fabricating the primary mold can be avoided, and thus decreasing the time needed for mold fabrication.

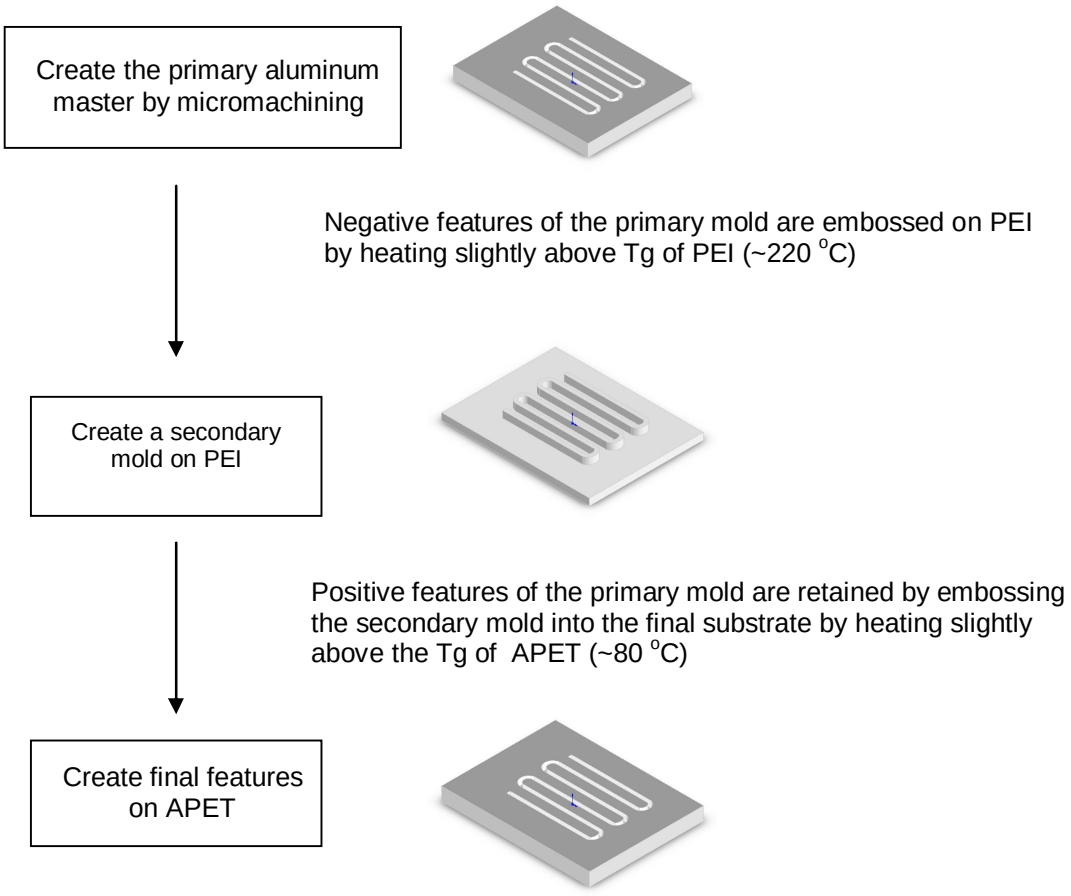

Fig. 1.7 Schematic diagram of the two-stage embossing procedure [43].

1.2.1.3 Casting

The process of casting microfluidic chips using silicone-based elastomers (such as PDMS) has found its use in the academic environment due to its simplicity. The process is shown in Fig. 1.8. A mixture of elastomer and curing agent is poured on the master mold and cured for several hours. After curing, the PDMS can be peeled off the mold and placed on a planar surface, such as glass

slide. The microchannel is formed by conformal sealing (a reversible process) or exposing PDMS to oxygen plasma or other strong oxidizing sources (for irreversible or permanent bonding).

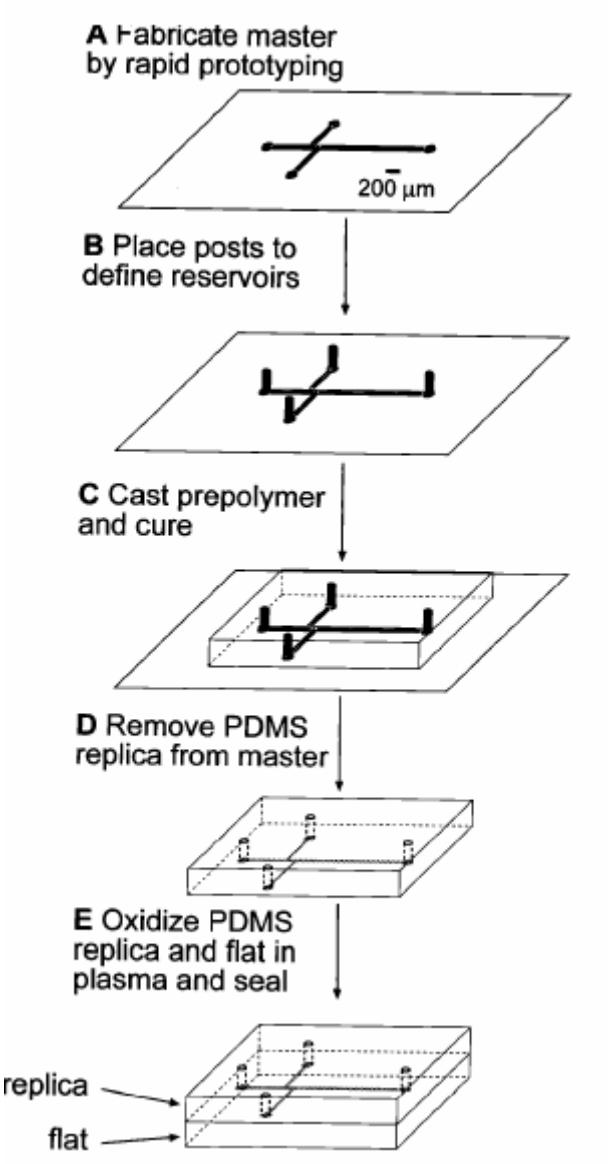

Fig. 1.8 Schematic of microfluidic devices replica molding using PDMS. (A) Master is fabricated by rapid prototyping, (B) Posts are positioned on the master to define reservoirs, (C) Prepolymer is casted on the master and cured, (D) PDMS replica is removed from the master, and (E) The replica and a planar substrate are exposed to air plasma to form an irreversible seal [37].

1.2.2 Bonding of microfluidic devices

A major challenge for creating polymer-based microfluidic devices is in the process of bonding parts together or layering-up. After fabrication, the microchannels are normally open on the mold-contacting side. Sealing of microchannels to a blank piece is necessary to create a fully functional system. The challenge is to achieve this seal without clogging or altering the channel dimensions during the bonding process. This step often limits high volume chips fabrication. A successful bonding process must preserve channel integrity, geometry and structure, and offer high bonding strength for specific applications. Several bonding techniques, such as thermal bonding, solvent welding, lamination, laser welding, and the use of adhesives [44-47], have been reported for bonding polymer-based microchips.

1.2.2.1 Thermal and pressure bonding

Thermal bonding is the most popular method for sealing plastic chips. The microchannel is sealed by placing two pieces of identical materials (one having the embossed features) in contact with one another in a thermal press, heating the plates and applying pressure. This process creates microchannels with uniform surfaces since they composed of entirely the same materials. However, the bond strength (1000 kN/m^2) created by this method is usually much lower than that of solvent-bonded chips [48]. In addition, the heating process during thermal bonding in plastic chips may cause channel deformation. Therefore, careful approach must

be taken to avoid any variance in the temperature and pressure applied to preserve the channel geometry.

1.2.2.2 Solvent welding

Solvent bonding has been proven to create microchips with high bond strength. Unlike thermal bonding, the bonding process is performed at room temperature, and thus thermal distortion of the microstructure can be avoided. The use of solvents, however, has some disadvantages as they can cause clogging or channel deformation during sealing. One way to resolve this issue is by using a sacrificial layer to protect the channels from the bonding solvent. Prior to device sealing, the channel in the embossed chip is filled with paraffin waxes or low melting temperature alloy [49] that forms a solid sacrificial layer at room temperature. This layer prevents channel deformation from the solvent during bonding which otherwise will fill and softens the channel. After the bonding process, the sacrificial layer needs to be removed from the microchannel. Removal of sacrificial layers, such as paraffin wax, is performed by heating the assembly to melt the wax out of the channel. However, an incomplete removal may occur and causes some residual materials to be trapped inside the channel, affecting CE analysis and compromising results.

We have developed a solvent welding technique using ice as the sacrificial layer [44]. Water was chosen as the sacrificial layer as it is readily available, non toxic, has a low evaporation rate, a high freezing point relative to dicholorethane,

and a low melting point that makes it easier to be removed after sealing. Removal of the sacrificial layer can be done by simply letting the ice melt out of the channel at room temperature. Fig. 1.9 summarizes the solvent bonding procedure using ice as sacrificial layer to create the final PMMA microchips.

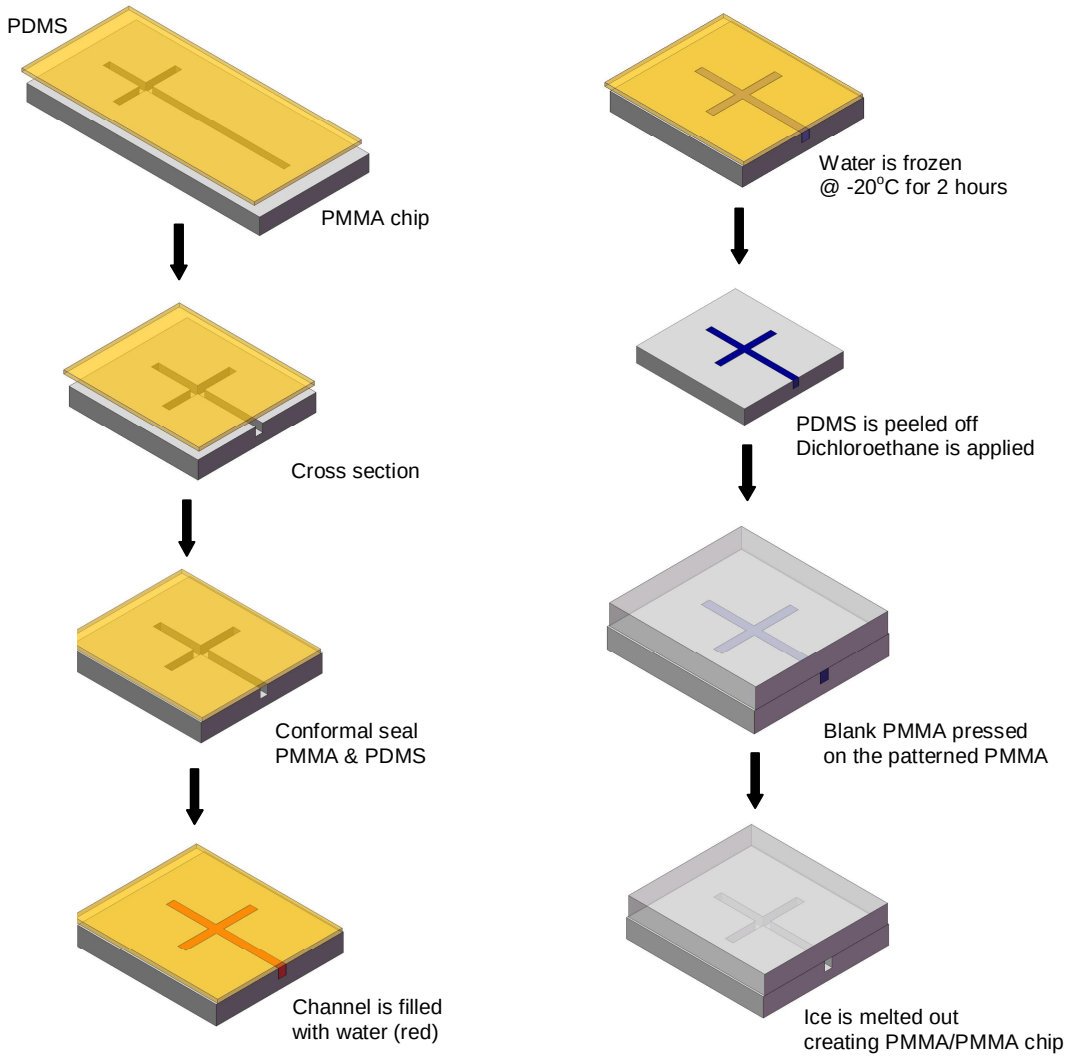

Fig. 1.9 A schematic of the bonding procedure to create PMMA/PMMA microchip. The PMMA chip was conformally sealed with a piece of PDMS. The channel is then filled with water. The PMMA/PDMS assembly was placed in a freezer at -20 ^{o}C for 2 hours until all of the water inside the channel solidified, forming a solid sacrificial layer for solvent welding. After the water solidified, the PMMA/PDMS assembly is removed from the freezer onto a cooling block (-20 ^{o}C). The PDMS piece was peeled off from the PMMA, and a uniform layer of dichlororethane (~300 µL) was applied onto the PMMA chip. A blank piece of PMMA chip was pressed on top of the patterned PMMA chip with an applied pressure of ~5 psi for 2 minutes for bonding. After 2 minutes, the applied pressure is released, and the PMMA chip is removed from the cooling block to allow the ice to melt off at room temperature [44].

1.2.2.3 Gluing and the use of adhesives

The process typically uses a thin adhesive layer that is rolled onto the structure to seal the channels. With very small channels that are typical of microfluidic devices, the adhesives can partially or fully clog the channel. An inhomogeneous interface between the capping layer and the channel can also be resulted due to the differences in the materials used. This leads to parameter variability, such as changes in refractive index at the interface.

1.2.2.4. Laser welding

Laser welding results in sealing of microchannels by local melting of the polymers due to the heat generated by a laser. The margins of the features to be sealed must be traced by the laser, and thus long welding times might be resulted for microchannels with large distances.

1.3 Introduction to Capillary Electrophoresis (CE)

Capillary electrophoresis (CE), also known as capillary zone electrophoresis (CZE), is defined as the migration of ions or solutes under the influence of an electrical field in confines of capillary columns. A CE system consists of having a positive electrode (anode) and negative electrode (cathode) that are placed in a solution containing ions. A voltage is applied across the capillary causing the ions of different charges (anions and cations) to migrate towards the electrode of opposite charge. Separation of analytes is based on the

differences in their electrophoretic mobilities, determined by their charge to mass ratio.

The schematic diagram of a basic CE instrument is shown in Fig. 1.10. A CE system consists of a capillary, two electrodes (cathode and anode), an autosampler, detection, and data acquisition system. Both ends of the capillary are placed in separate buffer reservoirs (inlet and outlet). The electrodes are connected to a high-voltage power supply capable of generating up to 30 kV. Samples can be introduced into the capillary by applying either electric potential (electrokinetic injection) or pressure (hydrodynamic injection) at one end of the capillary (usually the anode). Once the sample is in the capillary, an electric potential is applied across the capillary causing the ionic species in the sample plug to migrate. Analytes will be separated and will eventually pass through a detector near the opposite end of capillary where information is collected and stored by a data acquisition system.

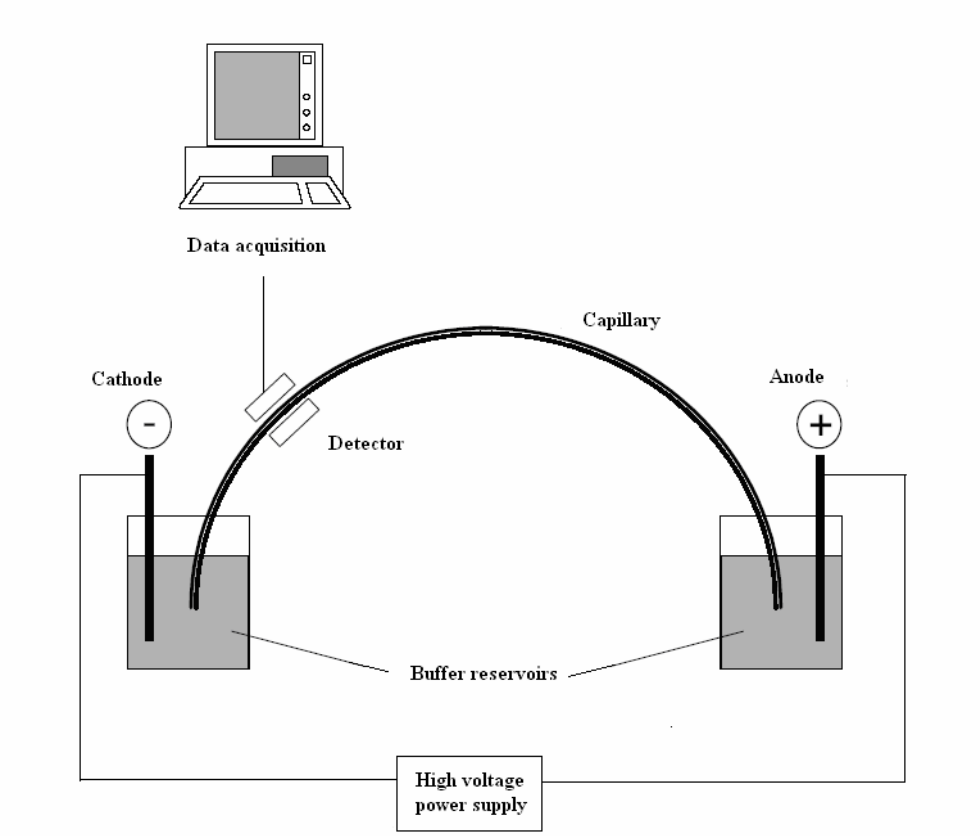

Fig. 1.10 Schematic diagram of a CE system.

CE offers the advantage of small amounts of reagents and samples required (due to the small size of capillaries). Narrow-bore capillaries having an internal diameter (ID) from 25 to 100 μm (360 μm OD) are usually employed in CE. The application of high fields (30 kV) during CE run can allow for rapid analysis time. Furthermore, high separation efficiencies are usually obtained in CE due to their flat flow profile (see section 1.3.1.2). CE has been used as a powerful separation technique for a wide range of sample types, such as proteins, oligonucleotides, chiral compounds, surfactants, pharmaceuticals, and environmental samples [50-57].

1.3.1 Electrophoresis Theory

1.3.1.1 Electrophoretic mobility

Electrophoretic mobility is a parameter that drives the movement of analytes in the capillary. Each ion or solute migrates with a finite electrophoretic mobility. Separation of mixtures of different ions and solutes in electrophoresis must then be determined by the differences in their electrophoretic mobility.

The Debye-Huckle-Henry theory gives an equation in relation to the electrophoretic mobility (μ_{ep}) of a charged species [55]:

$$\mu_{ep} = q / (6\pi\eta r) \qquad (1.3)$$

In equation 1.3, q refers to the charge on the ion, η is the viscosity of the buffer and r is the ion radius. Therefore, both charge and radius have an effect in electrophoretic mobility. The charge on the ion (q) is determined by the pH of buffer solution, whereas the ion radius (r) can be affected by many factors, such as counter-ion effects, non-spherical shape or other non-ideal behaviors of molecules. Equation 1.3 shows that the differences in the charge-to-size ratio of analytes will result in the differences in their electrophoretic mobility. The size of an analyte is often approximated as the mass of the molecule, and thus the analytes are separated based on their “Charge to Mass Ratio”. An ion with higher charge and smaller size will have greater mobility, whereas lower charge and larger size means lower mobility.

In the presence of applied electric field, different ions and solutes have different migration velocities (u_{ep}) according to equation 1.2 below [58]:

$$u_{ep} = \mu_{ep} E \qquad (1.4)$$

where u_{ep} is ion migration velocity (ms^{-1}), μ_{ep} is electrophoretic mobility ($m^2V^{-1}s^{-1}$) and E is electric field strength (Vm^{-1}). The electric field strength is a function of the applied voltage divided by the total capillary length. Equation 1.4 states that the actual migration velocity of an ion takes into account the ions individual electrophoretic mobility and the applied voltage.

Based on the electrophoretic mobility alone, the migration of ions under normal polarity (inlet – detector - outlet) is as follows. Only cations will pass through the detector. The neutral analytes will stay at the inlet whereas anions will be driven away from the detector. Therefore, there must be other force than electrophoretic mobility that drives the movement of analytes in the capillary. This force is called “electroosmotic flow (EOF)”, which plays a critical role in analytes mobility and will be discussed in the next section.

1.3.1.2 Electroosmotic Flow (EOF)

EOF is the bulk flow of liquid through the capillary that will drive all the movements in the capillary toward the detector. An important characteristic of EOF is its flat flow profile, as opposed to the parabolic or laminar flow profile generated by an external pump used in HPLC, shown in Fig. 1.11. The generation of a flat profile comes from the evenly distributed charge on the capillary wall, resulting in uniform flow velocity across the capillary. The pressure-driven flow, on the other hand, induces a parabolic or laminar flow profile due to the frictional

forces at the column walls. Broad peaks will be resulted due to the dispersive nature of the broad range in flow velocity. With a flat profile, zone broadening is minimized, leading to high separation efficiencies.

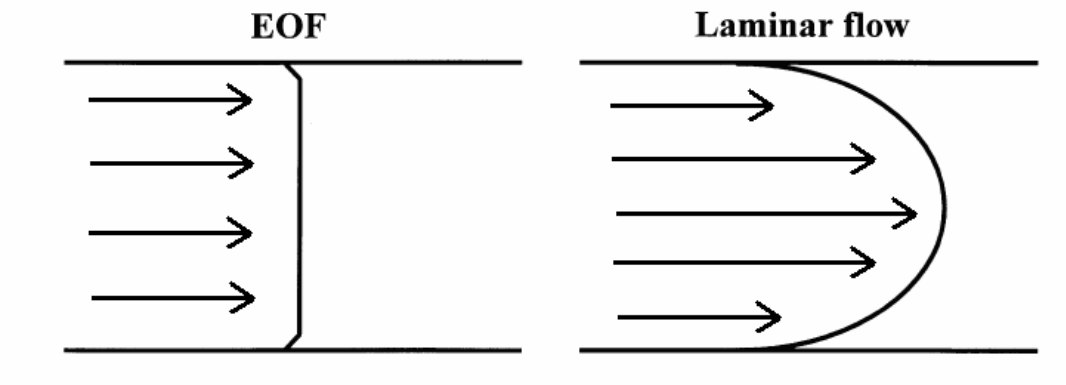

Fig 1.11 Flowprofiles of EOF and laminar flow.

The generation of EOF inside the capillary can be explained using Stern model, as presented in Fig. 1.12 [59]. The inner wall of a fused silica capillary possesses ionizable silanol groups on the surface. During electrophoresis, these silanol groups dissociate to give the capillary wall a negative charge (SiO^-). In contact with buffer solution, this attracts the positively charged ions from the buffer solution, giving rise to electrical double layer. The layer of ions closest to the surface is called the “Stern layer” and is essentially rigid or immobile. A more diffuse layer is formed distal to the Stern layer and is known as the “Gouy layer”. This mobile layer is rich in cations and decays into the bulk liquid.

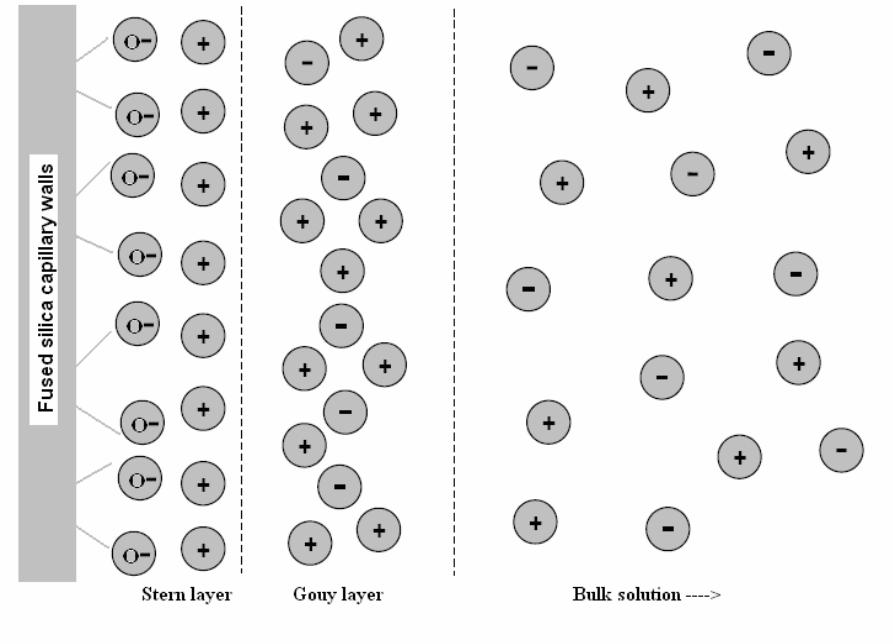

Fig. 1.12 Schematic representation of the electrical double-layer at a negatively charged capillary wall.

The formation of electrical double layer gives rise to a potential that falls off exponentially as a function of distance from the capillary surface. The potential drop between the silica wall and the interface of the diffuse layer and bulk solution is called the zeta potential, ζ, with values ranging from 0-100mV. The distance between Stern layer and a point in the bulk liquid at which the potential is 0.37 times the potential at the interface between Stern and diffuse layer, is defined as the thickness of the double layer (δ).

Knox [60] gives an equation describing δ (the thickness of double layer):

$$\delta = [\varepsilon_r \varepsilon_o RT/2cF^2]^{1/2} \qquad (1.5)$$

where δ= thickness of double layer, ε_r = dielectric constant or relative permitivity of medium, ε_o = permitivity of a vacuum, R = universal gas constant, T = absolute temperature, c = molar concentration, and F = Faraday constant.

From equation 1.5, for a monovalent electrolyte at a concentration of 0.001M in water (ε_r = 80), the thickness of the electrical double layer is calculated to be 10nm, and is 1nm at a concentration of 0.1M.

The zeta potential (ζ) is dependent on δ and the charge density σ according to the following equation [61]:

$$\zeta = (\delta\sigma)/(\varepsilon_o \varepsilon_r) \qquad (1.6)$$

The relationship between EOF linear velocity u_{eo} and ζ is given by Smoluchowski equation as follows:

$$u_{eo} = \varepsilon_o \varepsilon_r \zeta E/\eta \qquad (1.7)$$

where ε_o = the permitivity of a vacuum, ε_r = dielectric constant of the eluent, ζ = zeta potential, E = electric field strength, and η viscosity of the solvent. Equation 1.7 summarizes that electroosmotic flow depends on the surface charge density, the field strength, the thickness of the electrical double layer, and the viscosity of the separation medium which in turn is dependent on the temperature.

In the presence of applied electric field, cations in the diffuse (Gouy) layer are free to migrate toward the cathode, carrying the bulk solution with them. The

result is a net flow in the direction of the cathode, known as the electroosmotic flow (EOF).

The main factor affecting EOF mobility is buffer pH and ionic strength. EOF mobility will be significantly greater at high pH compared to low pH. At high pH (pH>9), silanols on the capillary surface are completely ionized and thus, EOF mobility is at its greatest. At low pH (pH<4), ionization of silanols is low and the EOF mobility is insignificant.

In summary, a solute apparent electrophoretic mobility (μ_a) is dependent on two parameters, its individual electrophoretic mobility (μ_e) and EOF mobility (μ_{eo}).

$$\mu_a = \mu_{ep} + \mu_{eo} \qquad (1.8)$$

Under normal polarity, samples are introduced at the anode and EOF migrates toward the cathode. Cations have positive μ_{ep}, neutrals have zero μ_{ep}, and anions have negative μ_{ep}. In other words, cations migrate faster than the EOF and anions migrate more slowly than the EOF, whereas neutrals migrate with the same velocity as the EOF. To determine EOF velocity experimentally, a neutral marker can be injected into the capillary under a given set of conditions. EOF is determined by calculating the time that it takes for the neutral marker to reach the detector.

1.4 References

[1] LaConte, L., Nitin, N., Bao, G. *Mater. Today* **2005**, *8*, 32

[2] Goya, G.F., Berquo, T.S., Fonseca, F.C. *J. Appl. Phys.* **2003**, *94*, 3520–3528

[3] Tartaj, P., Morales, M.P., Veintemillas-Verdaguer, S., Gonzalez-Carreno, T., Serna, C.J. *J. Phys. D: Appl. Phys.* **2003**, *36*, R182–97

[4] Lim, C.T., Zhang, Y. *Biosensors and bioelectronics* **2007**, *22*, 1197-1204

[5] Yang, H-H., Zhang, S-Q., Len, X-L., Zhuang, Z-X., Xu, J-G., Wang, X-R. *Anal. Chem.* **2004**, *76*, 1316-1321

[6] Lazaro F.J., Abadia A.R., Romero M.S., Gutierrez L., Lazaro J., Morales M.P. *Biochim. Biophys. Acta*, **2005**, 434–445

[7] Gleich, B., Weizenecker, J. *Nature*, **2005**, 1214–1217

[8] Kuhara, M., Takeyama, H., Tanaka, T., Matsunaga, T. *Anal. Chem.* **2004**, 6207–6213

[9] Wu, W., He, Q., Jiang, C. *Nanoscale Res. Lett.* **2008**, *3*, 397–415

[10] Gupta, A.K., Gupta, M. *Biomaterials* **2005**, *26*, 3995-4021

[11] Shen, X.C., Fang, X.Z., Zhou, Y.H., Liang H. *Chem Letters* **2004**, *33*, 1468-1469

[12] Kang, Y.S., Risbud S., Rabolt, J.F., Stroeve, P. *Chem. Mater.*, **1996**, 2209-2211

[13] He, Y.P., Wang, S.Q., Li, C.R., Miao, Y.M., Wu, Z.Y., Zou, B.S. *J. Phys D: Appl. Phys.* **2005**, *38*, 1342-1350

[14] Lin, P., Chou, P., Chen, S., Liao, H., Wang, K., Chen, Y., Lin, C. *Small* **2006**, *2*, 485-489

[15] Cornell, R.M., Schertmann, U. *Iron oxides in the laboratory; preparation and characterization*, Wiley-VCH, Weinheim, **1991**

[16] Cotton, F.A., Wilkinson, G. *Advanced inorganic chemistry*, Wiley Interscience, New York, **1988**

[17] Hadjipanayis, G.C., Siegel, R.W. *NATO ASI Series: Applied Sciences*, Kluwer, Dordrecht, **1993**

[18] Wu, W., He, Q., Hu, R., Huang, J., Chen, H. *Rare Metal Mater. Eng.* **2007**, *34*, 238

[19] Ashtari, P., He, X., Wang, K., Gong, P. *Talanta* **2005**, *67*, 548

[20] Chen, M., Yamamuro, S., Farrell, D., Majetich, S.A. *J Appl Phys* **2003**, *93*, 7551–7553

[21] Tartaj, P., Gonzalez-Carreno, T., Serna, C.J. *Langmuir* **2002**, *18*, 4556–4558

[22] Shen, X., Fang, X., Zhou, Y., Liang, H., *Chem. Lett.* **2004**, *33*, 1468

[23] Ma, M., Zhang, Y., Yu, W., Shen, H., Zhang, H., Gu, N. *Colloid Surf. A* **2003**, *212*, 219

[24] Arales, B. *Chem. Technology* **1997**, *7*, 766

[25] He, H., Liu, H., Zhou, K., Wang, W., Rong, P. *J. Cent. South Univ. Technol.* **2006**, *13*, 6

[26] Tiefenauer, L.X., Kuhne, G. , Andres, R.Y. *Bioconjug. Chem.* **1993**, *4*, 347

[27] Weizmann, Y., Patolsky, F., Lioubashevski, O., Willner, I. *J. Am. Chem. Soc.* **2004**, *126*, 1073

[28] Roberts, M.J., Bentley, M.D., Harris, J.M. *Adv Drug Del Rev* **2002**, *54*, 459-476

[29] Niemeyer, C.M. *Angew. Chem. Int. Ed.* **2001**, *40*, 4128 – 4158

[30] Manz, A., Graber, N., Widmer, H.M. *Sens. Actuators, B* **1990**, *1*, 244-248

[31] Manz, A., Fettinger, J. C., Verpoorte, E., Ludi, H., Widmer, H. M., Harrison, D. J. *Trends Anal. Chem.* **1991**, *10*, 144

[32] Jacobson, S. C., Hergenroder, R., Koutny, L. B., Warmack, R. J., Ramsey, J.M. *Anal. Chem.* **1994**, *66*, 1107

[33] Becker, H.; Gartner, C. *Electrophoresis.* **2000**, *21*, 12-26

[34] Soper, S.A., Henry, A.C., Vaidya, B., Galloway, M., Wabuyele, M., McCarley, R.L. *Anal. Chim. Acta* **2002**, *470*, 87–99

[35] Nugen, S.R., Asiello, P.J., Connelly, J.T., Baeumner, A.J. *Biosens. Bioelectron.* **2009**, *24*, 2428–2433

[36] Sun, Y. Kwok, Y.C. *Anal. Chim. Acta* **2006**, *556*, 80–96

[37] McDonald, J.C., Duffy, D.C., Anderson, J.R., Chiu, D.T., Wu, H. , Schueller, O.J.A., Whitesides, G.M. *Electrophoresis* **2000**, *21*, 27-40

[38] Fiorini, G.S., Chiu, D.T. *BioTechniques*, **2005**, *38*, 429–446

[39] Sun, Y., Kwok, Y.C., Nguyen, N.T. *J. Micromech. Microeng.* **2006**, *16*, 1681-1688

[40] Blanco, F.J., Agirregabiria, M., Garcia, J., Berganzo, J., Tijero, M., Arroyo, M.T., Ruano, J.M., Aramburu, I., Mayora, K. *J. Micromech. Microeng.* **2004**, *14*, 1047–1056

[41] Duffy, D.C., McDonald, J.C., Schueller, O.J.A., Whitesides, G.M. *Anal. Chem.* **1998**, *70*, 4974–4984

[42] Waddell, E.A. *Methods Mol Biol.* **2006**, *321*, 27-38

[43] Koesdjojo, M.T., Tennico, Y.H., Rundel, J.T., Remcho, V.T. *Sens. Actuators, B* **2008**, *131*, 692

[44] Koesdjojo, M.T., Tennico, Y.H., Remcho, V.T. *Anal. Chem.* **2008**, *80*, 2311-2318

[45] Zhu, X., Liu, G., Guo, Y., Tian, Y. *Microsyst Technol.* **2007**, *13*, 403–407

[46] Koesdjojo, M.T., Koch, C.R., Remcho, V. T. *Anal. Chem.* **2009**, *81*, 1652

[47] Ussing, T., Petersen, L. V., Nielsen, C. B., Helbo, B., Højslet, L. *Int. J. Adv. Manuf. Technol.* **2007**, *33*, 198–205

[48] Brown, L., Koerner, T., Horton, J.H., Oleschuk, R.D. *Lab Chip* **2006**, *6*, 66–73

[49] Kelly, R.T., Pan, T., Woolley, A.T. *Anal. Chem.* **2005**, *77*, 3536-3541

[50] Altria, K.D., Bryan, S.M, Hadgett, T.A. *J.Pharm. Biomed. Anal.* **1997**, *15*, 1091-1101

[51] Chee, G.L, Wan T.S.M. *J. Chromatogr*, **1993**, *612*, 172-177

[52] Altria, K.D., Chanter, Y.L. *J Chromatogr A*, **1993**, *652*, 459-463

[53] Gilpin, R.K, Pachla, L.A. *Anal. Chem*, **2003**, 75R

[54] Shafaati, A, Clark, B.J. *Analytical Proceedings*, **1993**, *30*, 481-483

[55] Landers, J.P. *Handbook of Capillary Electrophoresis*, CRC Press, Boca Raton, **1997**

[56] Monnig, C.A., Kennedy, R.T. *Anal Chem* **1994**, *66*, 280R-314R

[57] Thorman, W., Molteni, S., Caslavska, J., Schmutz, A. *Electrophoresis*, **1994,** *15*, 3-12

[58] Jorgenson, J.W., Lukacs, K.D. *Anal. Chem.* **1981**, *53*, 1298

[59] Remcho, V.T. *Chem. Educator*, **1997**, *2*

[60] Knox, J.H., Grant, I.H. *Chromatographia*, **1987**, *24*, 135-143

[61] Shaw, D.J. *Electrophoresis*, Academic Press, London, **1969**

CHAPTER 2

A NOVEL APPROACH TO IN-LINE EXTRACTION EMPLOYING FUNCTIONALIZED MAGNETIC PARTICLES AND CAPILLARY ELECTROPHORESIS

2.1. Abstract

We have reported a new approach of performing inline extraction employing magnetic particles by capillary electrophoresis. Iron oxide nanoparticles were synthesized and were used as the solid support to produce silica-coated iron oxide particles functionalized with C18 groups. These particles were used as reversed-phase sorbents for in-line solid phase extraction followed by capillary electrophoresis. As the particles are superparamagnetic, magnets were used to locally immobilize these particles inside the capillary. Extraction and separation were performed in-line; the extraction approach was fully integrated into the CE setup, which enabled a significantly faster analysis time compared an off-line approach. Extraction, elution, and detection of the analytes were performed sequentially without interruption or need for sample handling. Mixtures of parabens were successfully extracted from solution using the synthesized magnetic sorbents. CE was able to completely separate the analytes in the present study within 10 minutes. The results confirmed the applicability of using functionalized magnetic particles for performing inline extraction in the capillary setup.

2.2 Introduction

Magnetic particles have become a popular platform for analyte extraction and sequestration in the past decade.[1-4] Owing to their magnetic properties, they can be externally manipulated using simple permanent magnets or electromagnets.[5-8] Their ability to be manipulated it possible for them to be integrated into existing systems. They can be used as solid supports for SPE sorbents, and magnets can be used to retain the particles.[9-12] This will greatly simplify the fabrication process in situations where it is desirable to have a sorbent plug upstream of an open capillary or microchannel. In this way, the challenges of creating frits or monoliths are eliminated. Moreover, the particle bed can be positioned anywhere in the device, and can easily be unloaded for disposal, waste, downstream analysis, or replacement by simply removing the magnet.

Iron oxide nanoparticles have seen much use as a support due to their biocompatibility, stability and easily modifiable surface, which allows for conjugation with molecules of interest.[13-15] They have been used in various fields of study including biomedical applications such as in drug delivery, magnetic resonance imaging contrast enhancement, magnetic cell separation, and biosensing.[16-18] Iron oxide nanoparticles are excellent solid supports as they possess a large surface area-to-volume ratio, which in turn can enhance signal sensitivity due to increased efficiency of interactions between samples and reagents, and increased numbers of binding sites for chemical reactions. Moreover,

surface modification can also be easily carried out on these particles to add multiple functionalities to the device.

Sample preparation procedures play a very important role in chemical analyses as they enable the isolation and concentration of target analytes from complex matrices prior to their introduction to analytical instrumentation for subsequent analysis. Solid phase extraction (SPE) in particular is a widely applied sample preparation technique because it is simple, rapid, inexpensive, easy to automate, and requires lower consumption of organic solvent compared to more classical sample preparation techniques, such as liquid-liquid extraction. These benefits have made SPE popular for pharmaceutical and environmental applications.[19-21], mostly in conjunction with analytical separation and detection.

Functionalized magnetic particles have also been used to perform extractions[1-4, 12, 22], though most techniques are performed "off-line". Here, the functionalized particles are added to the sample, the sample is agitated, then a magnet is placed external to the sample vessel such that the particles collect at the floor or wall of the vessel. The matrix components are removed through several washing steps, followed by desorption of analytes from the magnetic sorbents. The supernatant is then collected for analysis. An "in-line" technique, in which extraction, elution, and detection can be performed in an integrated manner would clearly be beneficial: it would reduce the time consuming sample preparation step, reduce the volume of solvent required for elution from the sorbent, facilitate automation, and reduce sample handling.[23]

As a proof of concept, in this paper we introduce an approach for automated extraction of several parabens and nonsteroidal anti inflammatory drugs (NSAIDs) using C18 functionalized magnetic particles in-line with capillary electrophoresis. The parabens are esters of p-hydroxybenzoic acid that are widely used as bactericides and preservative agents in cosmetics, pharmaceuticals, and personal care products[24]. Conventional methods for separation and detection of parabens in a variety of matrices are usually based on GC or LC.[25, 26] Capillary electrophoresis (CE) is making some inroads for in the analysis of pharmaceutical compounds, and has recently been applied for the simple and rapid analysis of a variety of parabens.[24, 27-29] The advantages of CE include simple analytical conditions, simultaneous determination of multiple drugs, rapid analysis, low running cost, small amount of samples, and environmental benefits due to low consumption of organic solvents.[30] Although each paraben can be identified by these methods, extensive sample cleanup procedures are required to remove matrix components that might interfere with the analysis.

In this study, magnetic reversed-phase packing materials were synthesized and used as sorbents for extraction of several parabens. The magnetic particles consisted of silica-coated Fe_3O_4 were functionalized with C18 groups. Iron oxide nanoparticles (NPs) were synthesized by coprecipitation of Fe^{2+} and Fe^{3+} aqueous salt solutions by addition of a base.[31-33] The wet chemical routes are simple and inexpensive with control over size, composition, and shape of the resulting NPs. Iron oxide NPs can be coated with inorganic molecules such as silica or gold.[33]

These coating materials provide the stability to the NPs in solution and provide an ideal surface for immobilization of various ligands at the NP surface. An advantage of having a surface enriched in silica is its chemical and biochemical inertness, good mechanical stability, and also the presence of surface silanol groups that can easily react with silane coupling agents, and hence is well suited to our applications.

In this paper we report the synthesis of reversed-phased magnetic particles and their use as extraction sorbents in-line with capillary electrophoresis. The novelty of this method lies in its ability to extract compounds of interest "inline" on magnetic sorbents, which means that extraction, elution, and detection can be performed in a single capillary equipped with external magnets. This technique allows multiple analytes to be detected in the same sample solution. Strong permanent magnets are easily integrated into the capillary cassette in order to immobilize the particles for the in-line extraction. Moreover, the sorbents can easily be regenerated for later use by simply flushing them from the capillary and collecting them for treatment.

The in-line extraction steps are similar to those of conventional SPE methods (Fig. 2.1). After capillary conditioning (step 1), a suspension of samples and functionalized particles are directly injected into the CE capillary and are retained by the magnets inside the capillary (step 2). The analytes of interest will interact with the sorbent, whereas the impurities elute (step 3). Later, an elution solvent is introduced to desorb the analytes of interest (step 4).

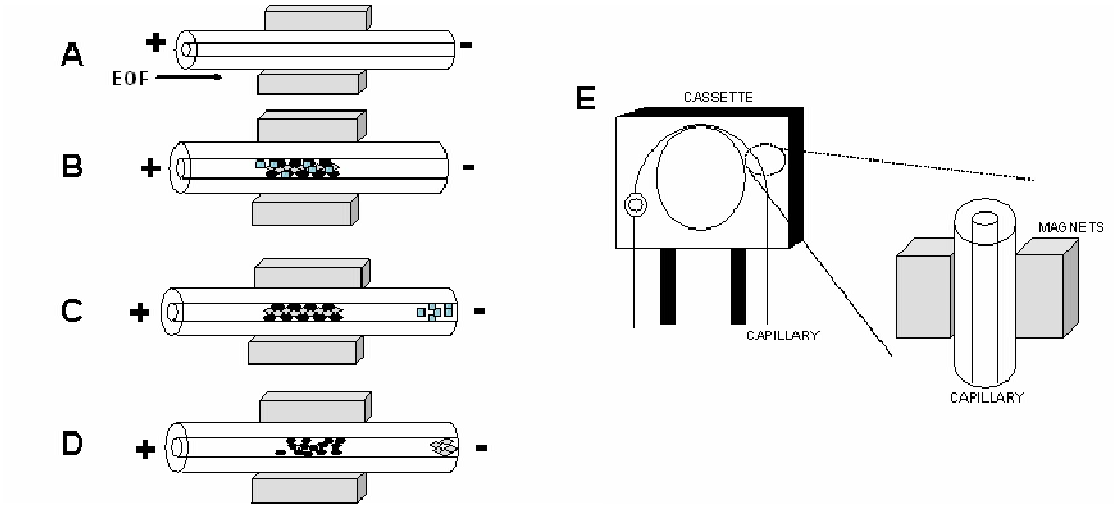

Fig. 2.1 Schematic illustration of the mechanism for performing inline magnetic extraction with capillary electrophoresis. A) Conditioning step: capillary is conditioned, NdFeB permanent magnets are placed around the capillary, B) Sample loading: sample mixtures containing magnetic particles are introduced into the capillary and are retained by the magnets C) Washing step: analytes of interests will interact with the sorbents, while interfering components are eluted, D) Elution step: retained analytes are eluted by applying a stronger eluent, E) a diagram showing how the magnets sandwiched the capillary in the cassette.

2.3 Experimental

2.3.1 Chemicals

All chemicals were reagent grade and were used without further purification. Ferrous chloride tetrahydrate ($FeCl_2 \cdot 4H_2O$ ≥99.0%), ferric chloride hexahydrate ($FeCl_3 \cdot 6H_2O$ ≥99.0%), tetraethylorthosilicate (TEOS ≥99.0%), trimethoxy(octadecyl)silane (ODS >90%), butyl paraben, propyl paraben, methyl paraben, benzoic acid, ibuprofen, sodium tetraborate were purchased from Aldrich (Milwaukee, WI, USA) and were used as received. The solvents (acetonitrile, methanol, ethanol, ammonium hydroxide, toluene, N-N-dimethylformamide) were either HPLC or ACS analytical grade and were purchased from Fisher Scientific

(Pittsburgh, PA, USA) or Mallinckrodt (Phillipsburg, NJ, USA). Fused silica tubing of 50 μm ID x 360 μm OD was purchased from Polymicro Technologies, Inc. (Phoenix, AZ, USA).

2.3.2 Synthesis of iron oxide functionalized C18 particles (Fe_3O_4-Si-C18)

Briefly, iron oxide nanoparticles (NPs) were synthesized using a modification of a method first presented by Stroeve et al.[34-35] The NPs were prepared by chemical coprecipitation of $FeCl_2$ and $FeCl_3$ in basic solution. Next, the resulting particles were silanized by a sol-gel process with the addition of tetraethyl orthosilicate (TEOS). The hydrolysis of TEOS produced a silica-cladding on the surface of the Fe_3O_4 NPs under basic conditions. The silica-coated Fe_3O_4 posses –OH (hydroxyl) functional groups on the surface, which were covalently modified with octadecyl (-C18) functional groups by the addition of n-octadecyltriethoxysilane (ODS).

The detailed synthesis consisted of three steps (Fig. 2.2). First, to synthesize iron oxide nanoparticles, stock solutions of $FeCl_2 \cdot 4H_2O$ (0.6 M) and $FeCl_3 \cdot 6H_2O$ (1.2 M) were prepared by dissolving each reagents in deionized water. Five mL of each iron solution was then transferred into a three-necked flask such that the molar ratio of Fe^{2+} to Fe^{+3} was 1:2, followed by the addition of 24 mL of deionized water. Next, 16 mL of 1.5 M NH_4OH was rapidly added into the flask (pH ~9) with vigorous stirring under N_2 at 40^{o}C. A black precipitate formed instantly and the reaction was allowed to proceed for another 30 minutes. The

precipitate was then collected using a magnet and the supernatant was removed by decanting. The particles were washed several times with deionized water, followed by ethanol, and vacuum dried overnight.

To produce the desired silica cladding, the nanoparticles obtained in the first step were dispersed in 4:1 (v/v) ethanol:H_2O solution and loaded into a three necked flask under N_2 with stirring. The pH of the solution was adjusted to ~9 with 1.5 M ammonium hydroxide. Next, 0.24 M TEOS was added dropwise to the flask. Stirring continued at room temperature for 16 hours, followed by heating at 50^{o}C to further hydrolyze the particles for an additional 8 hours. Particles were then collected using a magnet, washed with deionized water and ethanol, and vacuum dried overnight.

The C18 functionalized silica-clad Fe_3O_4 nanoparticles were synthesized by dispersing the particles obtained from the previous step with 3:2 (v/v) dimethylformamide:toluene solution and then loaded into a three-necked flask under stirring and N_2. Next, 0.24 M ODS was added dropwise under stirring and was allowed to stir for 24 hours at room temperature. The resulting particles were collected with a magnet, washed multiple times with toluene, and vacuum dried overnight. After drying, the samples were dissolved in ethanol. Before usage, the vial was shaken and aliquots of the samples were pipetted into a vial and then washed several times to remove the solvent.

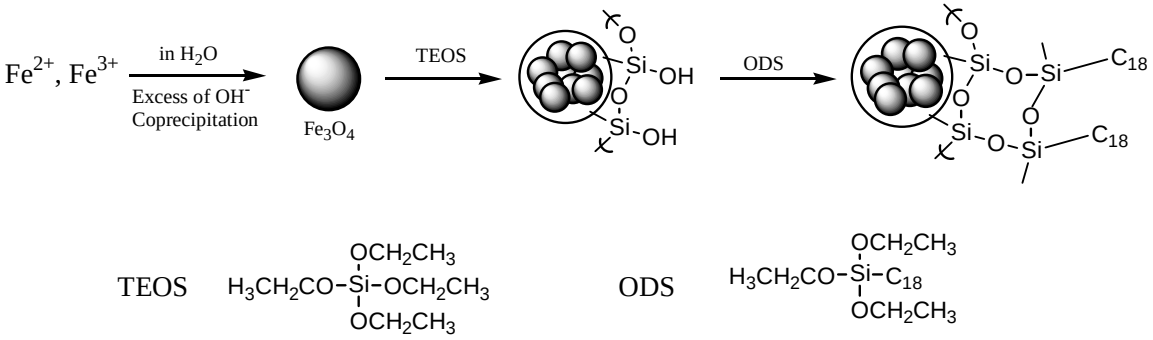

TEOS $H_3CH_2CO-Si(OCH_2CH_3)_3$ ODS $H_3CH_2CO-Si(OCH_2CH_3)_2-C_{18}$

Fig. 2.2 Synthetic scheme for preparations of C18-conjugated iron oxide particles.

2.3.3 Characterization

Particles characterization was performed in the solid phase. X-ray diffraction (XRD) was performed using a Rigaku Miniflex II using the X-ray beam from the Cu Kα radiation to study the structural properties of the Fe_3O_4 powders.

Fourier-transform infrared (FTIR) spectroscopy was used to verify surface modification of the silica clad NPs. Characterization was performed using a Nicolet 5DXB FTIR spectrometer in the range of 4000-400 cm^{-1} with KBr pellets of the NPs, produced by grinding about 2 mg of NPs with ~200 mg KBr and compacting them in a pellet press.

Particle size and morphology were examined via transmission electron microscope (TEM) analysis performed on a Philips CM-12 operating at 80 kV. TEM grids consisted of carbon-coated Cu. A drop of particle suspension in ethanol was carefully placed on the copper grid surface and air dried to let ethanol to evaporate.

Magnetic properties were studied using a Quantum Design Physical Property Measurement System (PPMS) at room temperature to generate a hysteresis loop, a curve of magnetic moment versus external magnetic field applied, to confirm the superparamagnetic behavior of the iron oxide NPs.

Imaging of particles inside the capillary with and without the presence of magnets was observed under an optical microscope (Zeiss Axiotron, Carl Zeiss SMT, Germany) at 10, 20, and 50x magnification.

2.3.4 Extraction and in-line capillary zone electrophoresis (CZE)

2.3.4.1 Instrumentation

Capillary electrophoresis (CE) was employed as a method for separation and detection of analytes, preceded by in-line SPE in the CE capillary facilitated by magnetic immobilization of SPE sorbent. The CE consisted of an Agilent/HP 3D CE system (Waldbronn, Germany), and a fused silica capillary with an ID of 50 μm, total length of 35.5 cm, and effective length (length to the detection window) of 27 cm and UV detection at 200 nm. Data acquisition and processing were performed with the Agilent Chem Station software. The CE running buffer was 35mM sodium tetraborate, pH 9. Samples were injected hydrodynamically at a constant pressure at 30 mbar for 10 sec, and separations were performed at 10 kV at 25^{o}C.

2.3.4.2 Extraction procedure

Before initial use, the bare fused-silica capillaries were flushed with 0.1 M NaOH for 15 min, washed with deionized water for 15 min, and then conditioned with the running buffer for 15 min. Before extraction, the capillary was flushed with 0.1M NaOH (5min), followed by deionized water (5 min), and then with the running buffer (5 min). A new capillary was used at the beginning of each day. Two Neodymium (NdFeB) bar magnets of 1”x1/8”x1/16”, grade N42, (K&J Magnetics) sandwiched the capillary 12 cm from the capillary inlet inside the CE cassette in order to trap the particles as they moved through the capillary (Fig. 2.1).

In-line SPE was performed with two different sample types. First, a mixture of non-polar aromatic hydrocarbons including butyl paraben (BP), propyl paraben (PP), and methyl paraben (MP) was analyzed. The second sample consisted of aromatic carboxylic acids (NSAIDs) including benzoic acid (BA) and ibuprofen (IBU). Stock solutions of each analyte were prepared in a 50:50 (v/v/) methanol/H_2O mixture; sample solutions were prepared by diluting the stock solutions in the CE running buffer to a final concentration of 10 μg/mL. Standards for calibration curves for each analyte were prepared in the CE running buffer solution. Analyte concentrations were measured from the calibration curves. Extraction efficiencies (E, %) were evaluated by adding increments of C18 particles into a vial containing mixtures of BP and BA until a minimum level of BP was detected.

The in-line extraction procedure consisted of three steps (Fig. 2.1). First, aliquots of the functionalized particles were pipetted into a CE vial, and then washed several times with acetonitrile, methanol, and the running buffer solution. Sample mixtures containing 10 μg/mL BP and BA were then added into the vial, mixed, and then injected into the CE system. The second step consisted of washing with 35mM sodium tetraborate, which separated BA from the analyte of interest (BP), retained by the magnetic sorbent. The third step consisted of elution of the trapped parabens by injecting a plug of methanol/acetonitrile into the capillary. Three elutions were performed to ensure complete extraction of the parabens. CE conditions were the same as those applied to the extraction, except that a running buffer of 25:25:50 (v/v) ACN:MeOH:35mM sodium tetraborate buffer (pH 9) was used as the elution buffer.

2.4. Results and discussion

The synthesized iron oxide nanoparticles were first characterized by X-ray diffraction (XRD) to confirm the synthesis. Fig. 2.3a shows the XRD pattern of the synthesized Fe_3O_4 powder. The core material exhibited an XRD pattern corresponding to pure magnetite (Fe_3O_4). The broad peak near 2θ of ~24^o was observed when the iron oxide nanoparticles were coated with silica. The coated and uncoated samples have very similar XRD patterns that indicated that the crystallinity of the magnetic core was retained following the coating procedure.

FTIR spectroscopy was used to study the surface modification of the functionalized particles. As can be seen from Fig. 2.3b, the appearances of peaks at 575 cm^{-1}, 3441 cm^{-1}, 1650 cm^{-1}, which correspond to the Fe-O stretching vibration, O-H stretching vibration, and O-H deformed vibration, confirm the synthesis of iron oxide nanoparticles. The existence of silica can be seen from the appearance of a strong absorption band for the Si-O stretching vibration at around 1090 cm^{-1}, suggesting that Si-O-Si bonds were formed after the silanization reaction with TEOS, confirming successful silica cladding of the Fe_3O_4.

TEM was used to examine the particle size distribution and morphology. It has been reported that agglomeration occurs with uncoated particles due to electrostatic interaction between the particles.[33] In order to prevent agglomeration, particles are usually modified with organic or inorganic coatings such as silica or gold after precipitation.[33] As shown in Fig. 2.3c, the functionalized particles consist of particles that are spherical in shape (~500nm in diameter) with no aggregation observed. These monodisperse nanoparticles were obtained consistently following multiple replications of the synthetic procedure. After cladding with silica, the particles remain well dispersed for extended time periods. These particles were stable colloidally in the absence of magnetic fields. This was in contrast to the uncoated NPs, which agglomerated and settled to the bottom of the vial after only 1-2 minutes. When an external magnetic field was applied, silica-clad particles move toward the field leading to a complete separation from suspension (Fig. 2.3d). They were rapidly redispersed in solution when the

magnetic field was removed. The NPs do not retain magnetism even after several exposures to the magnetic field.

A

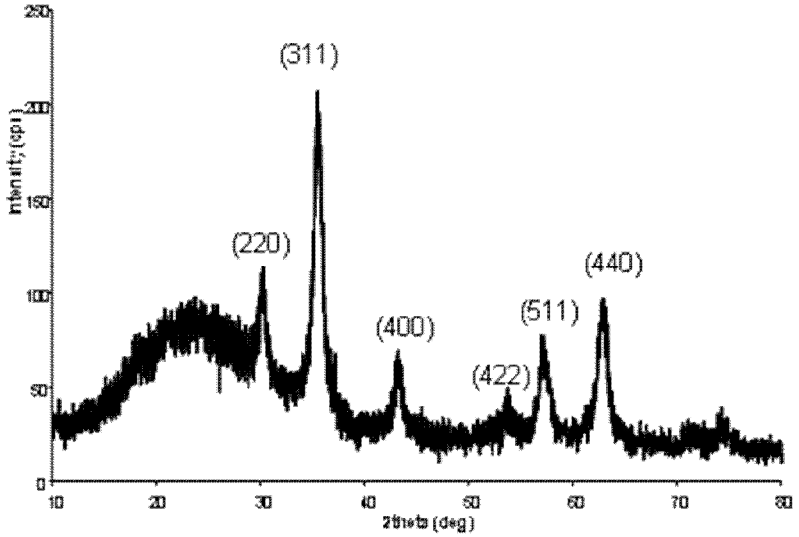

B

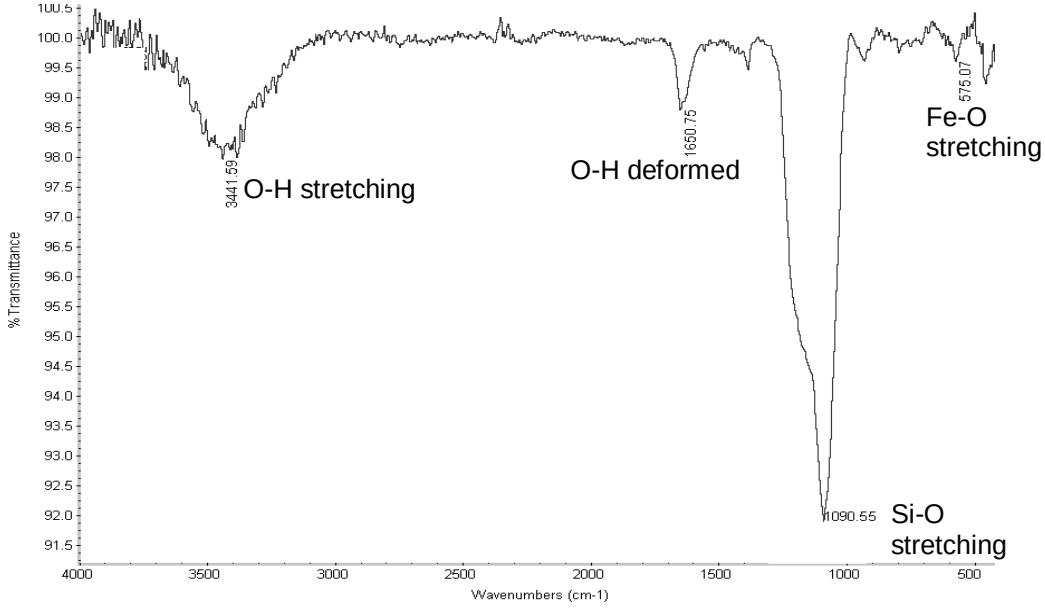

C

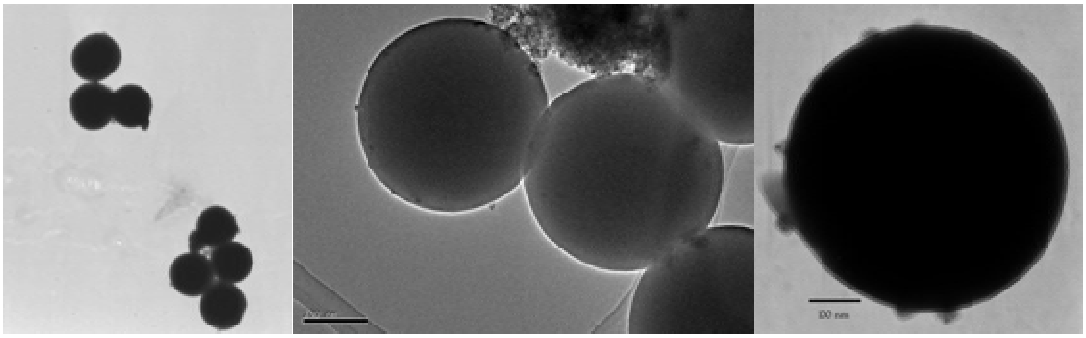

D

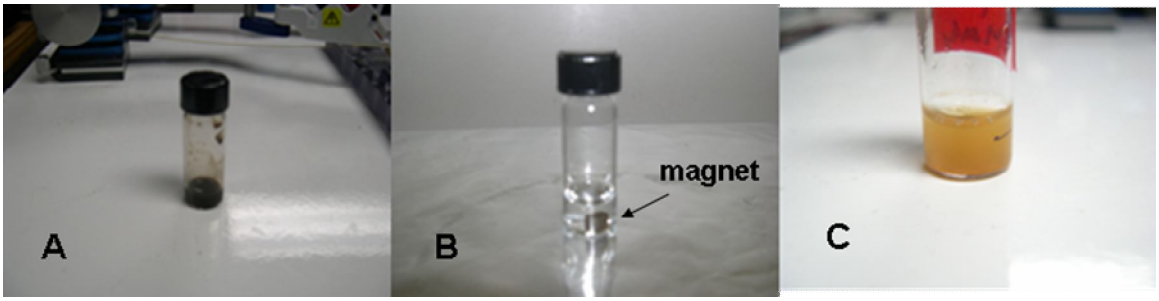

Fig. 2.3 A) XRD pattern of the synthesized Fe_3O_4-Si-C18 particles, B) FTIR spectrum of silica coated Fe_3O_4 particles, C) TEM images of Fe_3O_4-Si-C18 NPs at different magnification, and D) Fe_3O_4-Si-C18 particles before (a) and after (b) attraction to a magnet, (c) uncoated Fe_3O_4 particles after 3 months in solution.

The magnetic properties of iron oxide NPs were studied by measuring the hysteresis loop at room temperature for both the uncoated and coated particles. As can be seen in Fig. 2.4a, both samples exhibit a typical superparamagnetic behavior showing negligible coercivity and remanence. From the curve, saturation magnetization values were reached at a field of ~5 kOe and the values were 57.15 and 30.15 emu/g for the unfunctionalized and C18-functionalized NPs, respectively. This decrease in saturation magnetization value for the C18-functionalized particles is most likely attributable to the existence of the coating on

the surface of the magnetic nanoparticles. The magnetization values of these particles were higher than these of commercially available particles, such as Dynabeads (Invitrogen, Carlsbad, CA) or SeraMag (Seradyn Inc., Indianapolis, IN).[36-37] This shows that even after the coating procedure, the particles still exhibit superparamagnetic behavior with a high magnetization value, which is of high importance for this application.

Fig. 2.4b shows optical microscopy images of the particles immobilized inside a small section of the capillary. They were immobilized by attraction to a magnetic field supplied by NdFeB magnets. The particles formed a continuous bed that was uniform, stable, and robust, enabling analysis by electrophoresis without displacement of the NPs. The particles were “trapped” inside the capillary. However, after the magnetic field was removed, they were immediately released. In this way, the process of loading and unloading of sorbents can be simplified, and the sorbents can easily be recovered.

A

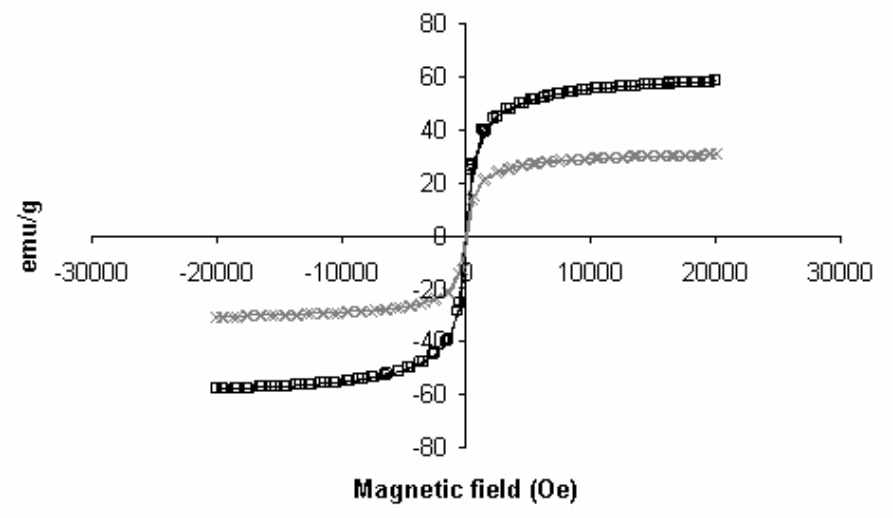

B

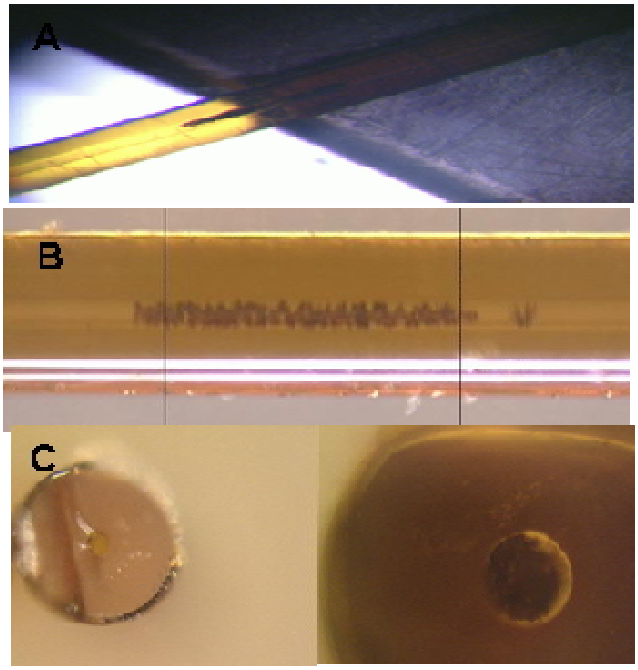

Fig. 2.4 A) Magnetization curve of uncoated Fe_3O_4 (represented by black squares in the figure) and Fe_3O_4-Si-C18 (grey), B) Optical images of 50 μm inner diameter fused silica capillaries packed with C18-functionalized iron oxide particles at different magnification. a) Particles are immobilized by magnet, b) 10x magnification of the trapped particles inside capillary, c) cross section of capillary before and after particles trapping at 20 and 50x magnification.

The use of functionalized magnetic particles for extraction of analytes from solutions or suspensions was demonstrated with the aim for developing a simple procedure for the extraction and subsequent analysis of target analytes. Several parabens were chosen as model compounds. A small amount of C18 functionalized sorbent was immobilized directly inside the bare fused-silica capillary using magnets within the CE cassette. The in-line SPE-CE coupling is particularly attractive since it allows direct injection of sample, with preconcentration and purification taking place automatically during the analytical run.

Fig. 2.5a shows a typical electropherogram for extracted benzoic acid (BA) and butyl paraben (BP) using C18 functionalized particles. For peak identification, the analytes were characterized by their retention times with quantification by measuring UV absorbance at 200 nm using the on-column UV detector. BP and BA can be separated by CE using sodium tetraborate as the running buffer solution and elute at ~5 and 7 minutes, respectively. When no magnets were placed in the cassette, a peak appeared at ~9 mins, which is attributed to the NPs that are transported past the detector. This peak was not observed when magnets were used, indicating that the particles were trapped between the magnets when introduced to the capillary.

The extraction efficiency of the C18-Fe_3O_4 particles was evaluated by measuring their binding affinity for butyl paraben and benzoic acid (Fig. 2.5b). The results were compared to a control study, in which no particles were added.

Since there was no sorbent, there was no measurable loss of analyte, which explains initial high absorbance values for BP and BA. When the sorbent was added to the BP/BA mixtures, BP was sorbed onto the NPs. Therefore the concentration of BP detected after each addition was progressively lower than the control. The BP peak was seen to decrease in height corresponding to the quantity of analyte that sorbed. As more sorbent was added, the BP concentration detected decreased steadily. The BA peak, on the other hand, remained very high, indicating little interaction with the C18 sorbent as would be expected: benzoic acid has little hydrophobic interaction with C18.

The experiments were conducted off-line in vials and in-line in a capillary in order to compare the results obtained with both techniques. In the off-line method, particles were added to a vial containing a mixture of BP and BA. The particles were sequestered at the side wall of the vial using a magnet and the supernatant was sampled for CE analysis. Extraction efficiency (E) was calculated from the ratio of concentrations of analytes before (control) and after extraction. The results from both off-line and in-line studies are summarized in Fig. 2.5c and were shown to be reproducible (RSD ~2-5%, n=5). There are no significant differences in the amount of BP extracted between the two methods, off-line and in-line.

A

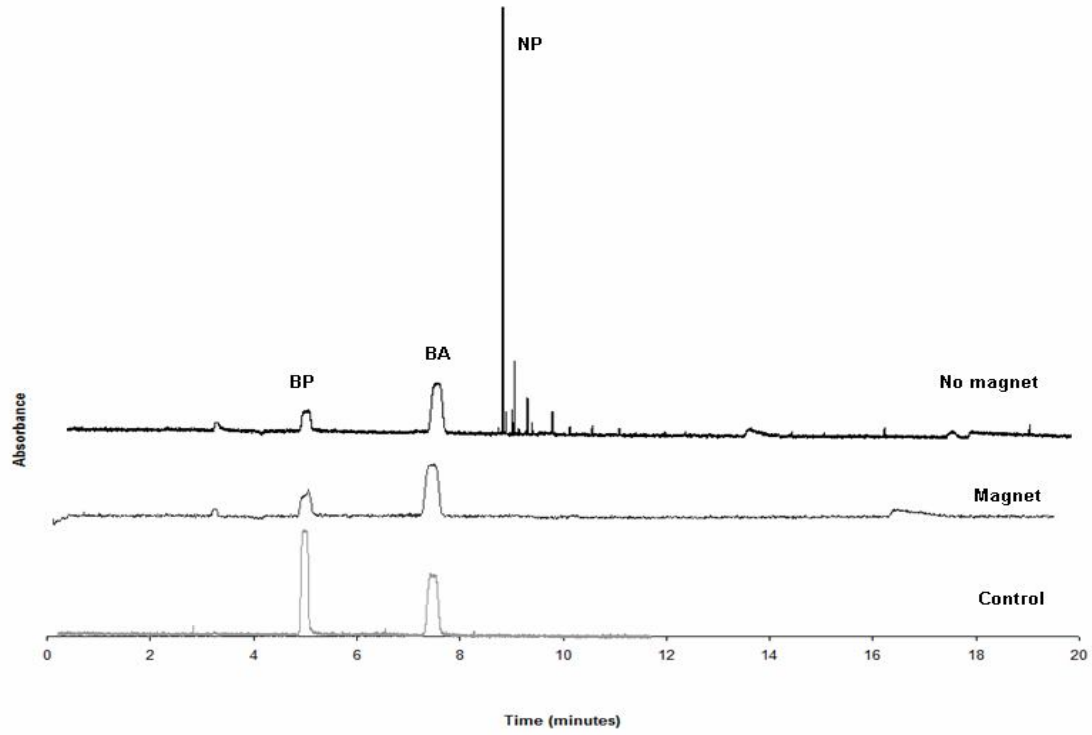
NP
BA
BP
No magnet
Magnet
Control
Absorbance
0
2
4
6
8
10
12
14
16
18
20
Time (minutes)

B

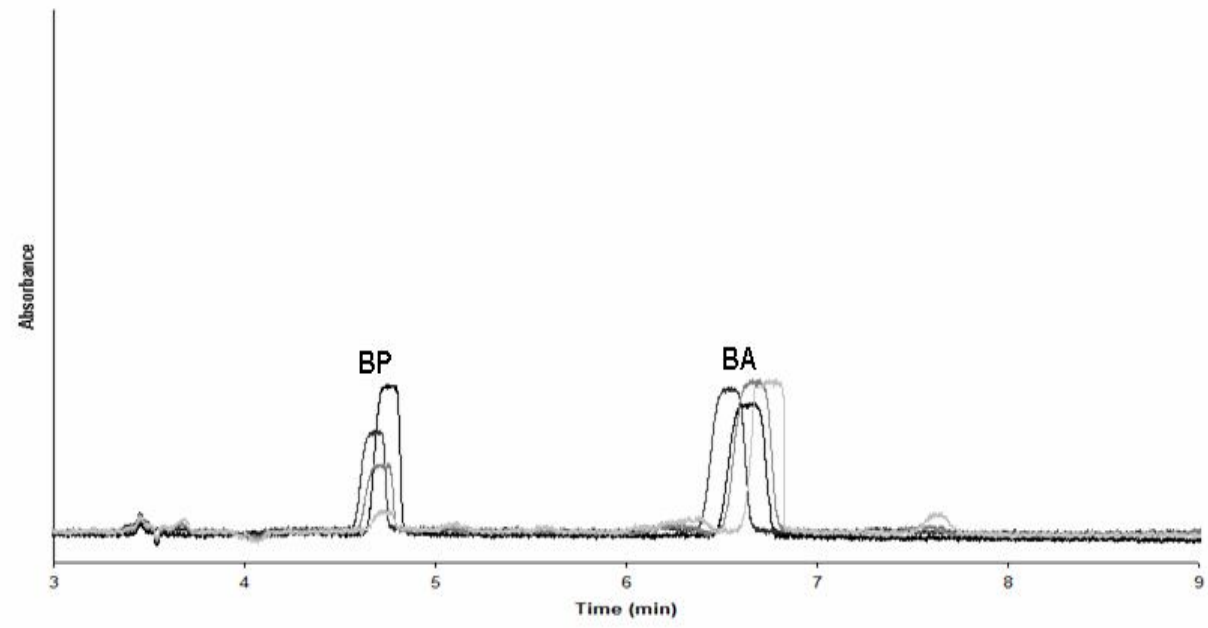
Absorbance
BP
BA
3
4
5
6
7
8
9
Time (min)

C

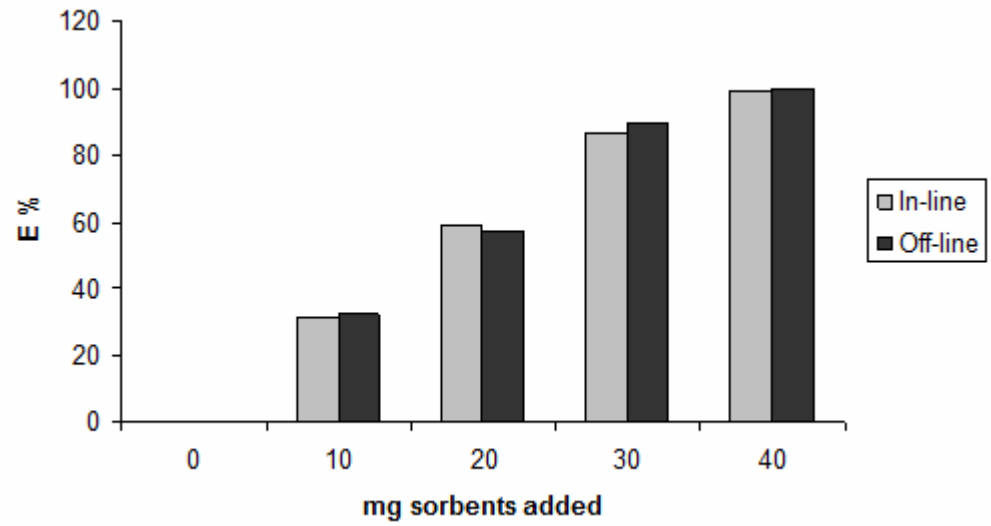

Fig. 2.5 A) Electropherogram of separation of magnetic particles, BP, and BA with and without magnets. The peaks between 9-10 minutes are due to particles, B) Electropherogram of in-line extraction of BP/BA using C18 magnetic particles, and C) Extraction efficiency (E, %) of butyl paraben to Fe_3O_4–Si-C18 sorbents (comparison offline vs. online method). Each curve corresponds to 10 mg increments of sorbents addition from 0, 10, 20 to 30 mg C18 particles.

A series of simple test compounds (non polar, weak acids) were also evaluated to demonstrate the efficacy of the automated in-line extraction process. Fig. 2.6a shows that the parabens can be extracted from the mixtures and also separated in-line, making this technique very attractive for simultaneous extraction, separation, and detection of molecules. Initial results show that the analytes can be separated with good peak shapes and efficiencies with reasonable analysis time using a simple eluent. The retention of each analyte shows a correlation with pKa and charge-to-mass ratio; the most acidic compound being

the most strongly retained. The pKa's of the parabens are in the range of 8-9, whereas the pKa of benzoic acid is ~4.[24] Therefore, at pH~9, the elution order was BP>PP>MP>BA. Under this condition, BA being the most anionic analyte traveled against the EOF and eluted last. Separation was therefore based mainly on the electrophoretic mobilities of the analytes.

Selectivity of the C18 sorbents was tested by extracting various parabens and NSAID mixtures. As can be seen in Fig. 2.6b, extraction of butyl paraben was the highest (~97%), followed by ibuprofen (71%), methyl paraben (~56%), and lastly benzoic acid which did not show any interaction with the sorbents (n=4). This result demonstrated the useful reversed-phase selectivity of the magnetic C18 sorbents. Increasing recovery of the non polar analytes indicated that adsorption was based on non specific, hydrophobic interactions with the sorbents.

A

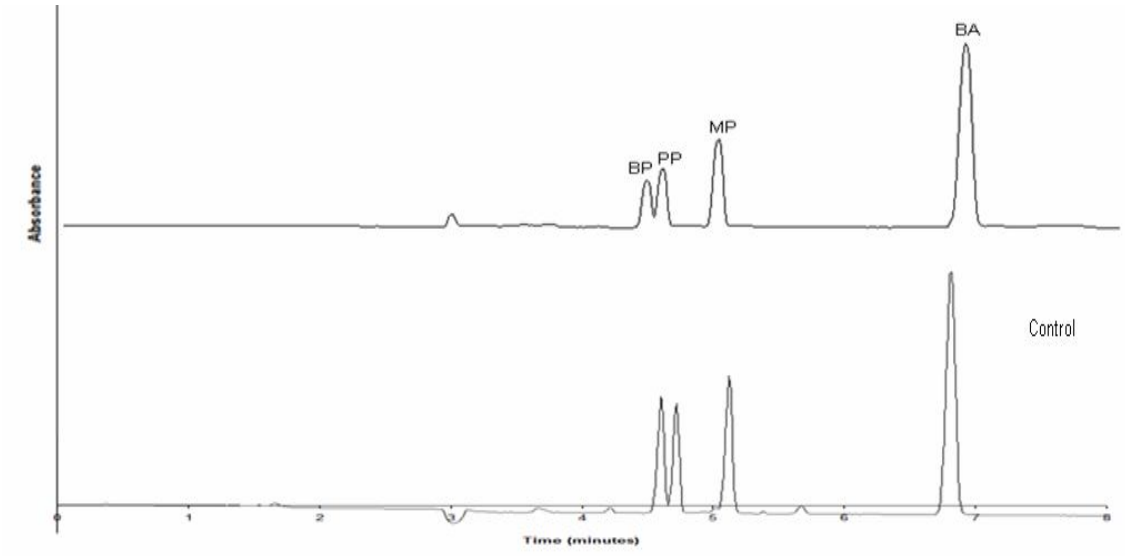

B

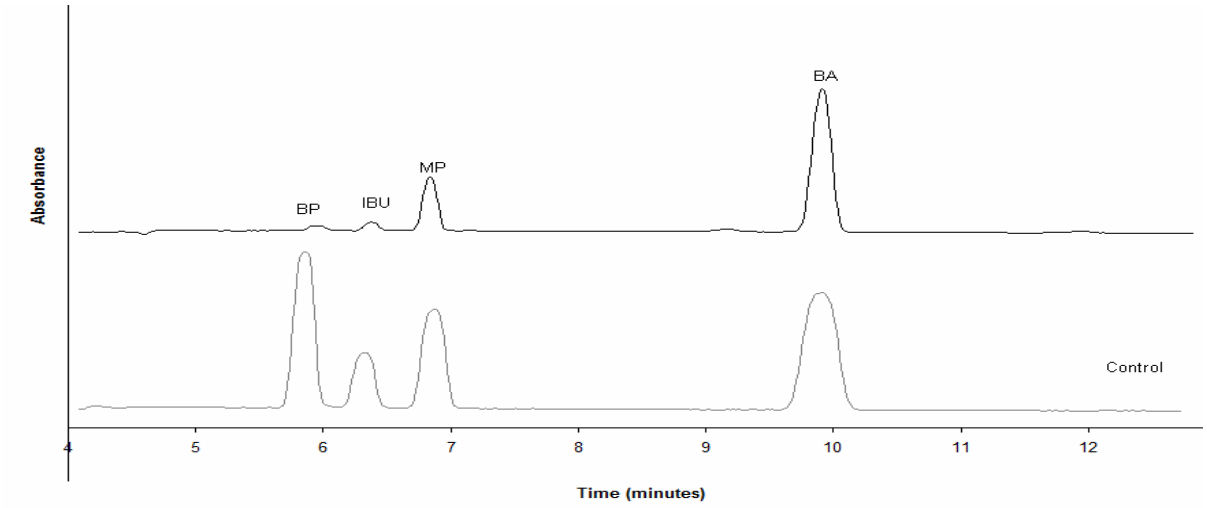

Fig. 2.6 A) Electropherogram of separation of BP/PP/MP/BA (extraction with 8mg sorbents vs. control), and B) Electropherogram of in-line extraction of BP/IBU/MP/BA with 30mg sorbents as compared to control.

Elution of the trapped parabens was performed using an acetonitrile (ACN)/methanol mixture. Different percentages of organic solvent were used to study elution behavior. Due to the suppression of electroosmotic flow (EOF) at a high percentage of organic solvents, elution solvents containing 25:25:50 (v/v) ACN:MeOH:sodium tetraborate buffer were selected in this study. The addition of organic solvents allowed the parabens to be eluted. The average recovery of butyl paraben was 64%, based on the mean of 5 extractions ranging from 57 to 71% (RSD ~6%). The recovery was based on the total BP recovered from the elutions performed by comparing the peak areas of BP extracted and eluted. Stronger eluents containing higher percentages of organic solvent could potentially be

applied in a pressure driven system (or combination pressure/EOF system) in order to obtain higher recoveries.

The reuse of analytical sorbents is very attractive as it leads to cost and time savings. After elution, sorbents can readily be collected by removing the magnetic field and inducing flow. These sorbents were reused for another experiment with no loss in performance. Good repeatability of extraction efficiencies was also observed with the reused sorbents, as calculated based on results obtained from six independent extractions performed on different days with RSD of ~4%.

2.5 Conclusions

We have demonstrated the feasibility of performing inline extraction with magnetic particles in a capillary setup. The in-line extraction approach is also transferable in a microchip format and work is ongoing in our lab that will demonstrate this application for microfluidics. The magnetic particles consisted of silica-clad iron oxide nanoparticles that were functionalized with C18 groups. The particles demonstrated high saturation magnetization and superparamagnetic properties that are of significant importance for magnetic applications. We showed the utility of these particles as extraction sorbents and used simple permanent magnets in order to carry out the inline extraction method. Extraction, elution, and detection of target analytes were performed in a single configuration with good repeatibility. The method is simple and inexpensive; eliminates the need to use any

frits to immobilize the sorbent, and reuse of the sorbent is possible. This approach is especially advantageous when the analysis must be performed in samples containing particulate matter, such that sample preparation is greatly simplified. Usage is not limited to this application: other extraction sorbents and/or separation/detection systems can be used depending on their specific applications.

2.6. Acknowledgement

The authors would like to thank Teresa Sawyer and Andrew Smith for assistance with TEM and PPMS experiments.

2.7. References

(1) Nakagawa, T.; Hashimoto, R.; Maruyama, K.; Tanaka, T.; Takeyama, H; Matsunaga, T. *Biotechnology and bioengineering* **2006**, *94*, 862-868.

(2) Huang, C.; Hu, B. *Spectrochimica Acta, Part B: Atomic Spectroscopy* **2008**, *63B*, 437-444.

(3) Zou, Z.; Ibisate, M.; Zhou, Y.; Aebersold, R.; Xia, Y.; Zhang, H. *Anal Chem.* **2008**, *80*, 1228-1234.

(4) Zhao, X.; Shi, Y.; Cai, Y.; Mou, S. *Environmental Science & Technology* **2008**, *42*, 1201-1206.

(5) Bronzeau,S.; Pamme, N. *Analytica chimica acta* **2008**, *609*, 105–112.

(6) Pamme, M. *Lab Chip*, **2006**, *6*, 24 – 38.

(7) Smistrup, K.; Hansen, O.; Bruus, H.; Hansen, M. F. *Journal of Magnetism and Magnetic Materials* **2005**, 293, 597-604

(8) Rida, A.; Gijs, M. A. M. *Anal Chem*. **2004**, *76*, 6239 – 6246.

(9) Peterson, D.S. *Lab on a chip* **2005**, *5*, 132-139.

(10) Zhao, X.; Shi, Y.; Wang, T.; Cai, Y.; Jiang, G. *Journal of Chromatography A* **2008**, *1188*, 140-147.

(11) Saiyed, Z. M.; Ramchand, C. N. *American Journal of Infectious Diseases* **2007**, *3*, 225-229.

(12) Liu, Y.; Jia, L. *Microchemical Journal* **2008**, *89*, 72-76.

(13) Lim, C.T.; Zhang, Y. *Biosensors and bioelectronics* **2007**, *22*, 1197-1204.

(14) Osaka, T.; Matsunaga, T.; Nakanishi, T.; Arakaki, A.; Niwa, D.; Iida, H. *Anal Bioanal Chem.* **2006**, *384*, 593-600.

(15) Yang, H-H.; Zhang, S-Q.; Chen, X-L.; Zhuang, Z-X.; Xu, J-G.; Wang, X-R. *Anal Chem.* **2004**, *76*, 1316-1321.

(16) Lazaro F.J.; Abadia A.R.; Romero M.S.; Gutierrez L.; Lazaro J.; Morales M.P. *Biochim Biophys Acta* **2005**, 434–45.

(17) Gleich, B.; Weizenecker, J. *Nature* **2005**, *435*, 1214–1217.

(18) Kuhara, M.; Takeyama, H.; Tanaka, T.; Matsunaga, T. *Anal Chem.* **2004**, *76*, 6207–6213.

(19) Delaunay-Bertoncini, D.; Hennion, M.-C. *Journal of Pharmaceutical and Biomedical Analysis* **2004**, *37*, 717-736.

(20) Zou, Z.; Ibisate, M.; Zhou. Y.; Aebersold, R.; Xia, Y.; Zhang, H. *Anal Chem.* **2008**, *80*, 1228-1234.

(21) Haginaka, J. *Trends in Anal Chem.* **2005**, *24*, 407-415.

(22) Yoza, B.; Matsumoto, M.; Matsunaga, T. *Journal of Biotechnology* **2002**, *94*, 217-224.

(23) Tempels, F.W.A.; Underberg, W.J.M.; Somsen, G.W.; de Jong, G.J. *Electrophoresis* **2008**, *29*, 108-128.

(24) Blanco, E.; Casais, M.; Mejuto, M.; Cela, R. *Electrophoresis* **2008**, *29*, 3229-3238.

(25) Ye, X.; Kuklenyik, Z.; Bishop, A.M.; Needham, L.L.; Calafat, A.M. *Journal of Chromatography B* **2006**, *844*, 53-59.

(26) Canosa, P.; Rodriguez, I.; Rubi, E.; Bollain, M.H.; Cela, R. *Journal of Chromatography A* **2006**, *1124*, 3-10.

(27) Labat, L.; Kummer, E.; Dallet, P; Dubost, J.P. *Journal of Pharmeceutical and Biomedical analysis* **2000**, *23*, 763-769.

(28) Blanco, C.C.; Carretero, A.S.; Mata, L.G.; Gutierrez, A.F. *Chromatographia* **2001**, *53*, 414-418.

(29) Mahuzier, P.-E.; Altria, K.D.; Clark, B.J. *Journal of Chromatography A* **2001**, *924*, 465-470.

(30) Makino, K.; Itoh, Y.; Teshima, D.; Oishi, R. *Electrophoresis* **2004**, *25*, 1488-1495.

(31) Lin, P.-C; Chou, P.-H.; Chen, S.-H.; Liao, H.-K.; Wang, K.-Y.; Chen, Y.-J.; Lin, C.-C.; *Small* **2006**, *2*, 485-489.

(32) He, Y.P.; Wang, S.Q.; Li, C.R.; Miao, Y.M.; Wu, Z.Y.; Zou, B.S. *J. Phys D: Appl. Phys.* **2005**, *38*, 1342-1350.

(33) Gupta, A.K.; Gupta, M. *Biomaterials* **2005**, *26*, 3995-4021.

(34) Shen, X.C.; Fang, X.Z.; Zhou, Y.H.; Liang H. *Chem Letters* **2004**, *33*, 1468-1469.

(35) Kang, Y.S.; Risbud S.; Rabolt, J.F.; Stroeve, P. *Chem. Mater.* **1996**, 2209-2211.

(36) Shang, H.; Chang, W-S.; Kan, S.; Majetich, S.A.; Lee, G.U. *Langmuir* **2006**, *22*, 2516-2522.

(37) Baselt, D.R.; Lee. G. U.; Natesan, M.; Metzger, S.W.; Sheehan, P.E.; Colton, R.J. *Biosens. Bioelectron*. **1998**, *13*, 731.

SURFACE MODIFICATION-ASSISTED BONDING OF POLYMER-BASED MICROFLUIDIC DEVICES

Yolanda H Tennico; Myra T Koesdjojo; Saki Kondo; David T Mandrell; Vincent Remcho

Sensors and Actuators B: Chemical

1183 Westline Industrial Drive, St. Louis, MO 63146

Volume 143 (2010), Issue 2, 799-804

CHAPTER 3

SURFACE MODIFICATION-ASSISTED BONDING OF POLYMER-BASED MICROFLUIDIC DEVICES

3.1. Abstract

This paper reports on the development and application of a surface modification technique as an improved method for bonding polymer microfluidic substrates. This technique readily produced complete microfluidic chips via plasma oxidation followed by silane reagent treatment on the polymer surface. Characterization of the bonded chips was performed using scanning electron microscopy (SEM), water contact angle measurement, and tensile strength measurement. SEM images showed that the integrity of the channel features was successfully preserved. A bond strength approaching that of solvent welding was demonstrated. This technique has been successfully applied to bond dissimilar polymer substrates (polymethylmethacrylate (PMMA), amorphous polyethylene terephthalate (APET), polycarbonate (PC)), and is also applicable to bonding a hard polymer substrate to polydimethylsiloxane (PDMS) or glass.

3.2. Keywords

surface modification, tetraethyl orthosilicate, poly(methyl methacrylate), hot embossing, microfluidics, fabrication

3.3. Introduction

The field of microfluidics has rapidly expanded since its introduction in the early 1990s [1]. Microfluidic devices are becoming increasingly attractive as alternatives to their larger-scale conventional counterparts. Microfluidic solutions can offer smaller sample and reagent volumes, high separation efficiences due to their high surface area-to-volume ratio, rapid analysis time, improved sensitivity, and the possibility of integrating multiple chemical processes all in one chip, which allows for the development of micro total analysis systems (micro-TAS).

Glass was the first substrate used for fabrication of microfluidic devices due to its well established fabrication process and many benefits, such as its chemical resistance, high voltage tolerance, optical transparency, high thermal stability and biocompatibility. It has been employed successfully as the material of choice for many applications [2-3]. Despite their advantages, glass chips also have some limitations, namely their high unit cost and specialized fabrication procedure.

Recently, polymers [4-7] have become viable materials for microchips because they are easy and cost effective to fabricate, yet retain many of the desirable characteristics of glass. They are disposable, biocompatible, and possess excellent optical properties, such as low intrinsic autofluorescence and high transparency. Fabrication of polymeric devices has been performed using several mass replication technologies such as hot embossing, injection molding, laser ablation, soft lithography, and casting [8-12]. A wide variety of polymer materials

are available; each has unique physical and chemical characteristics, which make them suitable for different microfluidic applications. Of the available polymer materials, thermoplastic polymers (such as polymethylmethacrylate (PMMA) [13-16], polyethylene terephthalate (PETE) [17-18], polycarbonate [19]), and polydimethylsiloxane (PDMS) [11, 20], have been intensively studied. PDMS has been extensively used for making microchips due to its ease of fabrication. PMMA and PC are the most widely used materials for chip production due to their low cost, good mechanical strength, optical transparency, and biocompability. PETE is also an attractive material that is gaining popularity due to its physiochemical properties, mainly its resistance to aggressive solvents (acetonitrile, chloroform, tetrahydrofuran, etc.) [18].

Various bonding techniques have been reported for fabrication of polymer substrates, such as thermal bonding [21], solvent bonding [22], plasma oxidation [17, 18], the use of adhesives [2], UV/ozone surface treatment [16], and laser welding [23]. A successful bonding process must preserve channel integrity, geometry, and structure, and offer high bonding strength. Thermal bonding is the most popular method for sealing plastic chips. However, the bond strength ($1000kN/m^2$) created by this method is usually much lower than that of solvent-bonded chips [15]. Special care must be taken in thermal bonding and solvent welding since the substrates are subjected to high temperatures and strong solvents that lead to channel deformation. Sacrificial layers, such as paraffin wax, low melting temperature alloys, and ice [13, 24], have been utilized to protect the

channels from deforming; however, it can be difficult to completely remove the sacrificial materials from the channels. Due to these challenges with the bonding process, a need remains for effective bonding methods for microchip fabrication.

Low bond strengths between two polymer substrates are largely due to the low specific energy of the polymer surface [16], typical of hydrophobic or weakly hydrophilic polymers. Several methods have been developed to increase the surface energy, including surface grafting and atmospheric plasma activation [25-26]. Plasma oxidation has commonly been used in bonding elastomeric materials, such as PDMS. The energy comes from ions, electrons, and UV photons in the plasma, which break chemical bonds on the polymer surface to produce highly reactive free radicals and generate polar functional groups on the surface. Plasma treatment creates the desired charged groups and increases the overall surface energy, which in turn also increases hydrophilicity and wettability [15]. Through the generation of polar functional groups on the polymer surface, hydrogen or covalent bonds may be formed across the interface; strengthening the bonds between the two contacting surfaces.

Low temperature bonding of PMMA and cyclic olefin copolymer (COC) has been reported using O_2 plasma activation or UV/ozone surface treatment [16], however, the reported bond strength values limited these devices to low pressure applications. In a recent publication by ME Vlachopoulou et al [14], a method for bonding PMMA to PDMS via a surface modification technique using 3-aminopropyltriethoxysilane (APTES) to create covalent bonds was presented. The

drawback of this approach is the necessity of using a thin PDMS layer as an intermediate to bond two pieces of polymer substrates, such as PMMA to PMMA. Thus, channels do not have homogeneous wall materials, which limits the range of application of devices prepared in this manner.

In this work, an improved bonding method via surface modification of plastic and glass materials is presented. The bonding was performed through surface modification by plasma oxidation followed by application of silane reagents (tetraethyl orthosilicate or TEOS) to incorporate Si functionalities on the polymer surface, facilitating siloxane bonds between the two polymers (Fig. 3.1). This bonding process is simple, robust, and cost-effective, making it applicable to a wide range of polymer substrates (PMMA, PC, APET, PDMS and glass) and native Si-containing materials, such as glass or PDMS.

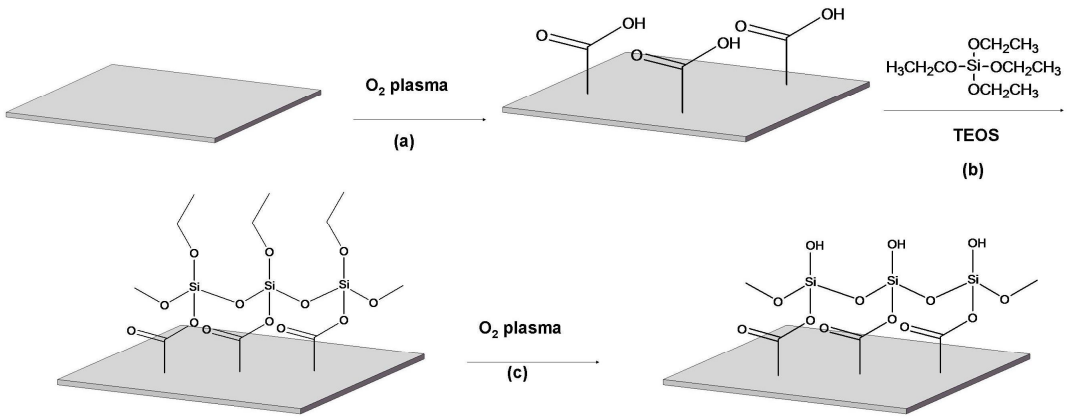

Fig. 3.1 Schematic of the PMMA surface modification using oxygen plasma and TEOS.

3.4 Experimental

3.4.1 Chemicals/materials

Tetraethylorthosilicate (TEOS ≥99.0%), isopropyl alcohol (99.5%), and Corning cover glass no.1 (24 x 60 mm) were obtained from Sigma-Aldrich (Milwaukee, WI, USA) and were used as received. Rhodamine B was obtained from Lambda Physik (Acton, MA, USA). SU-8 3050 and SU-8 developer were obtained from Microchem (Newton, MA, USA). Polyetherimide (PEI), polycarbonate (PC), polymethylmethacrylate (PMMA) were obtained from McMaster-Carr (Santa Fe Springs, CA, USA). Amorphous polyethylene terephthalate (APET) was obtained from ALRO Plastics (Jackson, MI, USA). Polydimethylsiloxane (PDMS) Sylgard 184 was obtained from Dow Corning (Midland, MI, USA), consisting of a base polymer and curing agent. PDMS was mixed in a 10:1 ratio of monomer to the curing agent, poured onto a clean unpatterned glass slide, and thermally cured for 3 h at 60^{o}C.

3.4.2. Microfabrication

The SU-8 master was fabricated on a silicon wafer via a standard photolithography technique using a maskless exposure system (SF-100, Intelligent Micro Patterning, LLC, St. Petersburg, FL, USA). SU-8 3050 was spun on the wafer at a thickness of ~100 μm according to a recently published program [22].

The process used for two-stage embossing was published previously [8]. In the first step of the embossing process, the positive features of the SU-8 master

were hot embossed into a PEI substrate (T_g~ 210^{o}C) using a hot press (Fred S. Carver Inc., Summit, NJ, USA). The resulting imprint produced negative features in the PEI substrate. In the second imprinting step, the PEI was used as a secondary master to emboss features into PMMA (T_g ~106^{o}C), APET (T_g ~75^{o}C), and PC (T_g ~150^{o}C) substrates. The two stage embossing process results in a final product with features that faithfully reproduce the primary master.

3.4.3 Surface modification-assisted bonding procedure

3.4.3.1 Bonding of two polymer substrates (PMMA, APET, PC)

A schematic of the PMMA surface modification-assisted bonding procedure is shown in Fig. 3.2. Prior to bonding, the surfaces of the polymers were treated using a home built oxygen plasma system. The RF source was obtained from XEI Scientific (Redwood City, CA, USA). The substrates were placed inside the plasma chamber, and the plasma was operated at 20 Watts and 100 mTorr for 90 sec. Immediately following the plasma treatment, both surfaces were silanized using 10% TEOS solution in 60:40 (v/v) isopropyl alcohol:water at 50^{o}C for 30 minutes. Next, the functionalized surfaces were activated a second time with the oxygen plasma under the same conditions as described above. After plasma exposure, the two surfaces were brought into contact and pressed together. Bonding temperatures and pressures of different type of polymers were optimized and determined experimentally (Table 3.1). A post-annealing bake was performed for 2 hours at 60^{o}C to increase bond strength.

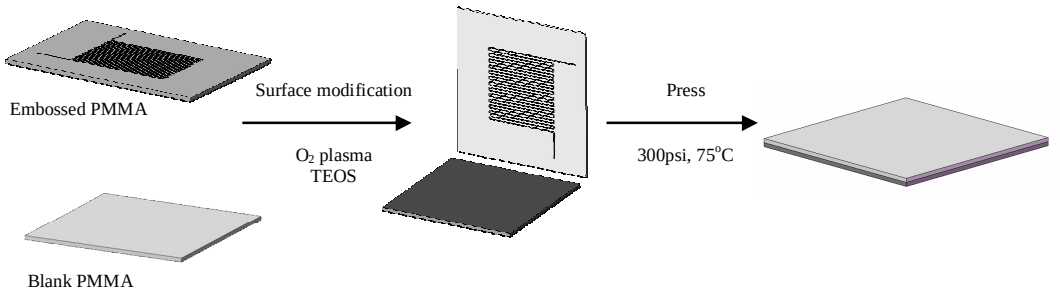

Fig. 3.2 Schematic of the PMMA surface modification-assisted bonding procedure. Both the embossed and blank PMMA pieces were surface modified with oxygen plasma and TEOS treatment. Following exposure to oxygen plasma, the two pieces were brought into contact and pressed together at 300 psi, 75°C until bonding occurred.

3.4.3.2 Bonding of a polymer substrate to an Si-containing substrate (PDMS or glass)

This method was used to bond polymer substrates and Si-containing substrates to produce hybrid chips, i.e. PMMA-glass or PMMA-PDMS. For substrates that contain Si at the surface, the TEOS treatment can be omitted. The procedure described in section 3.4.3.1 was employed on the polymer substrates. Prior to bonding, both the polymer substrate and the Si-containing substrate (such as PDMS) were exposed to an oxygen plasma and brought into contact, followed by the bonding protocol described in Table 3.1.

Table 3.1. Bonding procedures for a variety of materials using a novel surface modification method.

Bonding materials	Pressure applied (psi)	Temperature (^{o}C)	Time (min)
Bonding of PMMA based materials to PMMA or glass	300	75	20
Bonding of APET based materials to APET or glass	150	60	20
Bonding of PC based materials to PC or glass	300	110	20
Bonding of PMMA/APET/PC based materials to PDMS	Clamp	50 (oven)	60

3.4.4 Characterization

Water contact angle measurements were taken before and after surface modification treatment using an FTÅ 135 Contact Angle and Video Analysis System (First Ten Angstroms, Portsmouth, VA, USA). 5.0 µL of water was pipeted onto the polymer surface, contact angles were measured in triplicate and the average contact angle for each substrate was reported.

Bond strength between the two contacting surfaces was determined by measuring tensile strength using an Instron 5500R tensile tester (Instron, Norwood, MA, USA). Two pieces of PMMA (25.4 x 25.4 x 1.6 mm) were bonded using the procedure described in section 2.3.1. The bonded samples were clamped into the grips of the tensile tester, and pulled away from one another at a rate of 0.06 mm/sec. The force at which the bonded PMMA failed was recorded and divided by the cross sectional area of the bonded surface to obtain the tensile strength of bonding. The reported values are the average of at least three individual measurements tested for each method of bonding (PMMA samples bonded with and without the surface modification procedure).

The morphology of the bonded microchips was studied using an FEI Quanta 600F scanning electron microscope (SEM) (FEI Company, Hillsboro, Oregon, USA) operated at 5 kV. The microchips were frozen in liquid nitrogen and fractured to obtain the cross-section images.

3.5 Results and discussion

The use of this surface modification technique for bonding of microfluidic devices provides an inexpensive, straightforward, accessible method to produce polymer or hybrid microchips. The procedure is attractive as it provides a general method for the bonding of polymer substrates to adjacent polymer layers, but also to Si-containing substrates such as glass or PDMS. The method also obviates the need for high bulk temperatures (thermal bonding) and strong solvents (solvent bonding). Permanent bonding of polymers can be achieved at temperatures below T_g. As shown in Table 3.1, this technique is applicable to the bonding of various types of substrates by careful selection of an appropriate bonding temperature and pressure. These parameters can readily be altered and optimized depending on the type(s) of polymer(s) used and their properties (such as T_g). Therefore, the bonding method is not limited to the substrates chosen for this study.

In this work, the surface of PMMA was modified by oxygen plasma exposure, followed by TEOS treatment. The exact chemistry occurring at the surface of the polymer during oxygen plasma treatment is complex and still poorly understood [15, 25]; however, studies have shown that as the plasma bombards the surface with high-energy oxygen gas molecules, active species that strongly interact with the polymer surface are generated, resulting in polar functional groups. These may include functional groups containing oxygen, such as carboxyl groups, oxides, acid anhydrides and aldehydes, which contribute to the polarity of the surface [15]. According to the reaction scheme shown in Fig. 3.1a, exposure to

the oxygen plasma is postulated to result in conversion of a fraction of the native PMMA backbone into carboxylic acid groups, making the surface more hydrophilic. The acidic groups on the surface may then facilitate bonding of TEOS, as shown in Fig. 3.1b. The carboxylic acid groups on the PMMA surface may then react with the ethoxy groups on TEOS to introduce Si-containing functionalities on the PMMA surface. Subsequent exposure to the oxygen plasma converts the reactive ethoxy groups at the polymer surface into silanol groups (Fig. 3.1c). When two modified pieces of PMMA are brought into contact, siloxane (Si-O-Si) bonds are formed across the interface. Covalent bonding between a surface-modified polymer and an Si-containing substrate (i.e. PDMS or glass) can also be achieved using this surface modification process.

The extent of surface modification was assessed via water contact angle measurement. The average contact angle measurement for an unmodified PMMA surface was 75 ± 3^{o} (Fig. 3.3). This is in agreement with a previously published value of 73 ± 3^{o} for a native PMMA substrate [27]. Following oxygen plasma exposure and TEOS treatment, the surface contact angle was re-measured. A decrease in contact angle after plasma activation was observed: the initial contact angle for the oxygen plasma treated substrate was 20 ± 2^{o}, and increased to 36 ± 3^{o} after drying overnight at room temperature. The angle increased further to 65 ± 2^{o} after TEOS treatment. Next, plasma oxidation was performed on the TEOS-modified surface. The contact angle was measured and decreased to 34 ± 2^{o}, which indicates an increase in polarity or hydrophilicity of PMMA surface after plasma

activation, thus confirming our postulation that the polymer surface was converted into silanol groups as a result of the surface modification process. The contact angle results clearly indicate that there is a substantial change in the surface chemistry of the PMMA surface.

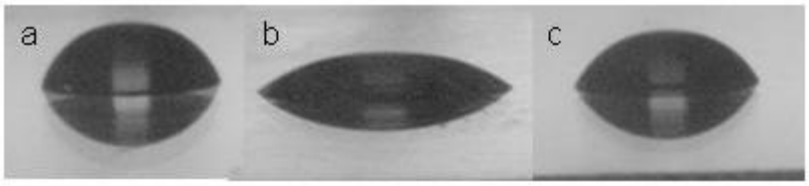

Fig. 3.3 Water contact angle measurements on a) native PMMA (75 ± 3^{o}), b) O_2 plasma treated PMMA (36 ± 3^{o}), and c) O_2 plasma and TEOS treated PMMA (65 ± 2^{o}).

The stability of the PMMA surface after plasma oxidation and surface modification was evaluated by re-measuring its contact angle after washing the treated surface with water and isopropanol, followed by oven drying at 60^{o}C for 1 hour. No measurable changes were observed in the results. Furthermore, TEOS-treated polymer samples were stored at room temperature for 7 days and contact angles were re-measured. The results did not show any measureable change for any of the samples, indicating a stable surface modification procedure.

The contact angles measured for untreated amorphous PET (APET) and polycarbonate (PC) were 71 ± 4^{o} and 82 ± 2^{o}, respectively, which correlate to reported values of 75 ± 4^{o} and 80 ± 3^{o} [18, 27]. After oxygen plasma activation and drying, the contact angle decreased to 33 ± 3^{o} for APET and 41 ± 3^{o} for PC. The

increase in hydrophilicity of the plasma-treated samples implies that the plasma had sufficient energy to break the hydrophobic polymer backbone and introduce polar groups (presumably carboxylic groups) onto the surface that were used in the ensuing surface modification step with TEOS. Table 3.2 gives a summary of contact angle measurements for PMMA, APET, and PC substrates following oxygen plasma and TEOS treatment.

Table 3.2 Water contact angle measurements for a variety of polymers following oxygen plasma and TEOS treatments. Each reported value is the mean of at least three samples for each substrate, and three measurements were performed at different locations on any given substrate. The +/- values correspond to standard deviation of the mean.

Materials	Native	O_2 plasma	TEOS
PMMA	75 ± 3^o	36 ± 3^o	65 ± 2^o
APET	71 ± 4^o	33 ± 3^o	61 ± 3^o
PC	82 ± 2^o	41 ± 3^o	71 ± 3^o

The viability of the bonding technique was tested for the fabrication of a microfluidic chip having a serpentine channel feature with dimensions of 400 μm width, 100 μm depth, and 1 m length (Fig. 3.4). This dimension was chosen for proof-of-concept studies. The bonding approach was repeated to produce channels with features as low as 100 μm width, 20 μm depth, and 3 cm length and as large as 3 mm width, 100 μm depth, and 2 cm length to demonstrate the applicability of this technique to bond channel of varying range of dimensions. A photograph of the fabricated PMMA microchip is shown in Fig. 3.4c. Ten chips were fabricated

using the surface-modification bonding technique and tested for leakage to demonstrate device integrity. A solution of Rhodamine B dye was introduced at the inlet of the microchannel. No leaks were observed in or between the channels. Fig. 3.4d shows a photograph of the dye solution flowing through the PMMA channels.

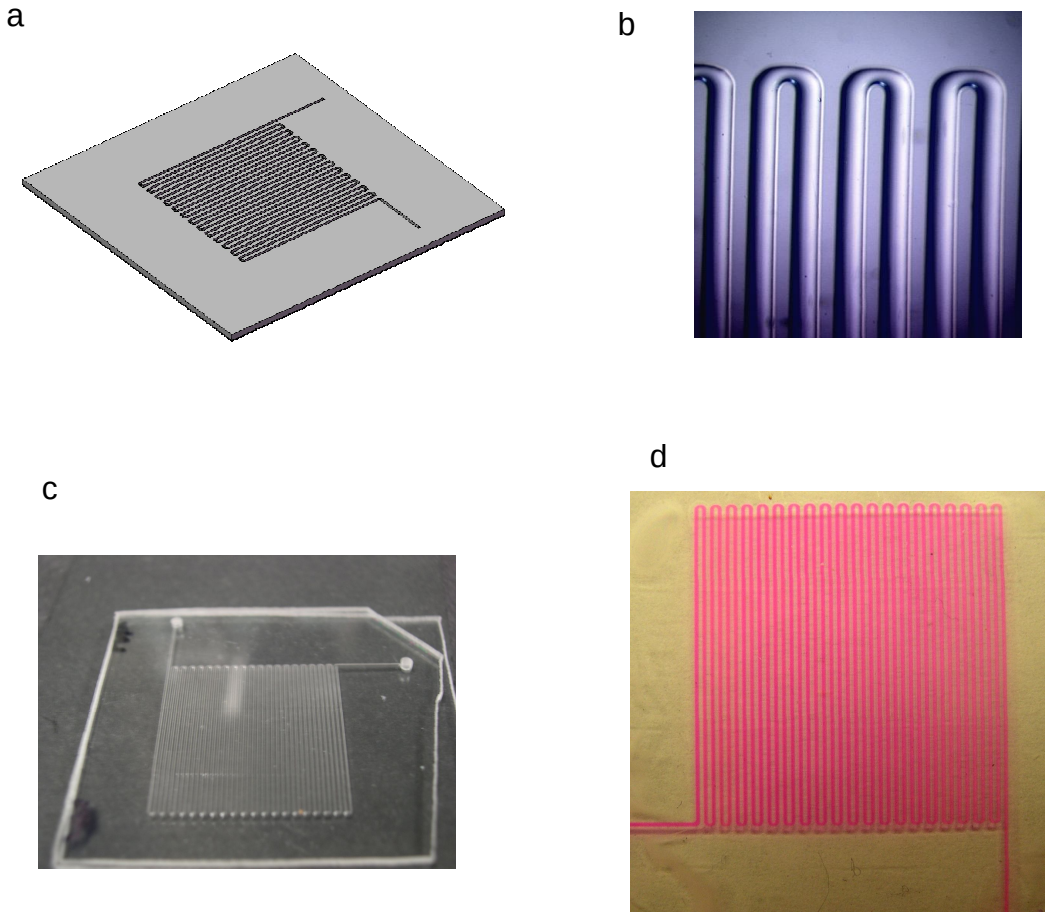

Fig. 3.4 a) A representation of the fabricated microchannel created via two-stage embossing, b) a photograph of the microchannel (400 μm width, 100 μm depth, and 1 m length), c) PMMA-PMMA microchip fabricated with surface-modification bonding technique, and d) bonding test with rhodamine B dye to check for leaks. The channel was formed by sealing the PMMA-PMMA chips by surface modification technique.

The surface modification and bonding process was evaluated for various polymer substrates (PMMA, APET, and PC). The bonding procedure was repeated ten times for each substrate to demonstrate the reproducibility of the technique. Fig. 3.5 shows SEM images of a PMMA-PMMA microchip bonded using the surface modification technique. The cross-sections of three adjacent microchannels and the magnified view are shown in Fig. 3.5a and b, respectively. Despite the low aspect ratio of the channels, no evidence of channel wall deformation was seen to result from the bonding process. These results clearly demonstrate the utility of this bonding method in microchip fabrication.

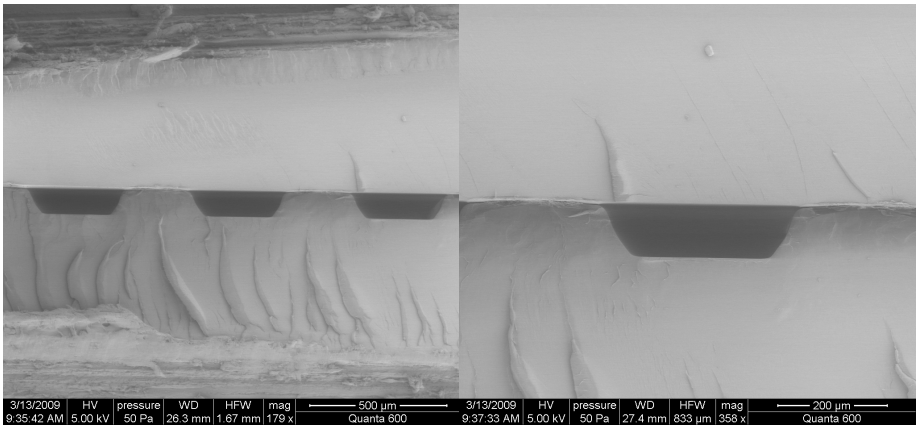

Fig. 3.5 SEM images of PMMA-PMMA microchip showing the microchannel cross-section: a) the cross-section of three adjacent channels, b) a magnified view of one channel shown in a).

Bonding of PMMA substrates (T_g is 106^oC) was carried out at a temperature of 75^oC. As expected, no bonding was observed for untreated PMMA chips at this temperature. Therefore, bonding of the surface modified chips at this temperature may be attributable to the relatively strong chemical interactions occurring at the modified polymer surface.

Many μTAS applications still require the use of glass due to the benefits that glass substrates offer. In this study, direct bonding of organic polymers (such as PMMA, APET, or PC) to inorganic substrates (such as Si or glass) was also demonstrated using the O_2 plasma/TEOS surface modification technique. The two substrates, however, have very different thermo-mechanical properties, namely Young's modulus and thermal expansion coefficient. For example, these properties differ by more than a factor of 10 for PMMA and glass substrates [28]. Thus, bonding of these two substrates required strict control of pressure and temperature to prevent fracturing the glass during the bonding process. Based on experimental observations, temperature was one of the most important parameters to control. In order to avoid bond failure at the PMMA/glass interface, cooling rate was decreased and optimized to minimize thermal stress between the two pieces.

Bond strength was evaluated by tensile strength measurement of the bonded PMMA/PMMA microchips. An average bond strength of 4000 kN/m^2 was measured for the O_2 plasma/TEOS treated samples. The bond strength obtained for the PMMA samples was greater than previously reported values for other bonding procedures. The tensile strength values for thermal bonding and plasma bonding of

PMMA chips were 1000 kN/m^2 and 600 kN/m^2, respectively [15]; thus a significant improvement in bond strength was achieved for PMMA samples bonded using the O_2 plasma/TEOS technique.

The O_2 plasma/TEOS bonding technique described here offers robust microchips that are amenable to high pressure applications such as chromatography, where a high internal pressure is often required. The higher bonding strength produced using this technique presents an ideal alternative for polymer microchip bonding that obviates the need for high bulk temperatures (thermal bonding) and strong solvents (solvent bonding).

3.6 Conclusions

An improved method for bonding polymer devices via a surface modification technique (oxygen plasma and TEOS treatment) was presented. This technique readily produced complete microfluidic chips without the need to use strong solvents or high temperatures. The method was straightforward and the integrity of microfluidic features was successfully preserved after bonding. A high bond strength was realized, with a value approaching that of solvent bonded chips.

This fabrication method provides a cost-effective, simple, and versatile approach to bonding polymer-based microdevices. The technique lends itself readily to many polymers and Si-containing substrates, such as PDMS and glass, facilitating device production for a variety of applications and even enabling hybrid chip fabrication.

3.7 Acknowledgement

The authors thank Teresa Sawyer and Bill Warnes for assistance with SEM experiments and tensile strength testing, and Tae-Hyeong Kim for his help with chip design.

3.8 References

[1] A. Manz, N. Graber, H.M. Widmer, Miniaturized total chemical analysis systems: A novel concept for chemical sensing, Sens. Actuators, B 1 (1990) 244-248.

[2] Y.J. Pan, R.J. Yang, A glass microfluidic chip adhesive bonding method at room temperature, J. Micromech. Microeng. 16 (2006) 2666-2672.

[3] G.E. Yue, M.G. Roper, C. Balchunas, A. Pulsipher, J.J. Coon, J. Shabanowitz, D.F. Hunt, J.P. Landers, J.P. Ferrance, Protein digestion and phosphopeptide enrichment on a glass microchip, Anal. Chim. Acta 564 (2006) 116–122.

[4] S.A. Soper, A.C. Henry, B. Vaidya, M. Galloway, M. Wabuyele, R.L. McCarley, Surface modification of polymer-based microfluidic devices, Anal. Chim. Acta 470 (2002) 87–99.

[5] S.R. Nugen, P.J. Asiello, J.T. Connelly, A.J. Baeumner, PMMA biosensor for nucleic acids with integrated mixer and electrochemical detection, Biosens. Bioelectron. 24 (2009) 2428–2433.

[6] Y. Sun, Y.C. Kwok, Polymeric microfluidic system for DNA analysis, Anal. Chim. Acta 556 (2006) 80–96.

[7] J.C. McDonald, D.C. Duffy, J.R. Anderson, D.T. Chiu, H. Wu, O.J.A. Schueller, G.M. Whitesides, Fabrication of microfluidic systems in poly(dimethylsiloxane), Electrophoresis 21 (2000) 27-40.

[8] M.T. Koesdjojo, Y.H. Tennico, J.T. Rundel, V.T. Remcho, Twostage polymer embossing of co-planar microfluidic features for microfluidic devices, Sens. Actuators, B 131 (2008) 692.

[9] Y. Sun, Y.C. Kwok, N.T. Nguyen, Low-pressure, high temperature thermal bonding of polymeric microfluidic devices and their applications for electrophoretic separations, J. Micromech. Microeng. 16 (2006) 1681-8.

[10] F.J. Blanco, M. Agirregabiria, J. Garcia, J. Berganzo, M. Tijero, M.T. Arroyo, J.M. Ruano, I. Aramburu, K. Mayora, Novel three-dimensional embedded SU-8 microchannels fabricated using a low temperature full wafer adhesive bonding, J. Micromech. Microeng. 14 (2004) 1047–56.

[11] D.C. Duffy, J.C. McDonald, O.J.A. Schueller, G.M. Whitesides, Rapid prototyping of microfluidic systems in poly(dimethylsiloxane), Anal. Chem. 70 (1998) 4974–84.

[12] J. Rossier, F. Reymond, P.E. Michel, Chips for electrochemical and biochemical analysis, Electrophoresis 23 (2002) 858–67.

[13] M.T. Koesdjojo, Y.H. Tennico, V.T. Remcho, Fabrication of a Microfluidic System for Capillary Electrophoresis Using a Two-Stage Embossing Technique and Solvent Welding on Poly(methyl methacrylate) with Water as a Sacrificial Layer, Anal. Chem. 80 (2008) 2311-2318.

[14] M.E. Vlachopoulou, A. Tserepi, P. Pavli, P. Argitis, M. Sanopoulou, K. Misiakos, A low temperature surface modification assisted method for bonding plastic substrates, J. Micromech. Microeng. 19 (2009) 015007.

[15] L. Brown, T. Koerner, J.H. Horton, R.D. Oleschuk, Fabrication and characterization of poly(methylmethacrylate) microfluidic devices bonded using surface modifications and solvents, Lab Chip 6 (2006) 66–73.

[16] C. W. Tsao, L. Hromada, J. Liu, P. Kumar, D. L. DeVoe, Low temperature bonding of PMMA and COC microfluidic substrates using UV/ozone surface treatment, Lab Chip 7 (2007) 499-505.

[17] W. Chen, T.J. McCarthy, Chemical Surface Modification of Poly(ethylene terephthalate), Macromolecules 31 (1998) 3648–3655.

[18] Z. Hao, H. Chen, X. Zhu, J. Li, C. Liu, Modification of amorphous poly(ethylene terephthalate) surface by UV light and plasma for fabrication of an electrophoresis chip with an integrated gold microelectrode, J. Chromatogr. A 1209 (2008) 246-52.

[19] Y. Liu, D. Ganser, A. Schneider, R. Liu, P. Grodzinski, N. Kroutchinina, Microfabricated Polycarbonate CE Devices for DNA Analysis, Anal. Chem. 73 (2001) 4196-4201.

[20] G.T. Roman, T. Hlaus, K.J. Bass, T.G. Seelhammer, C.T. Culbertson, Sol−Gel Modified Poly(dimethylsiloxane) Microfluidic Devices with High

Electroosmotic Mobilities and Hydrophilic Channel Wall Characteristics, Anal. Chem. 77 (2005) 1414–1422.

[21] X. Zhu, G. Liu, Y. Guo, Y. Tian, Study of PMMA thermal bonding, Microsyst Technol. 13 (2007) 403–407.

[22] M.T. Koesdjojo, C.R. Koch, V. T. Remcho, Technique for microfabrication of polymeric-based microchips from an SU-8 master with temperature-assisted vaporized organic solvent bonding, Anal. Chem. 81 (2009) 1652.

[23] T. Ussing, L. V. Petersen, C. B. Nielsen, B. Helbo, L. Højslet, Micro laser welding of polymer microstructures using low power laser diodes, Int. J. Adv. Manuf. Technol. 33 (2007) 198–205.

[24] R. T. Kelly, T. Pan, A. T. Woolley, Phase-Changing Sacrificial Materials for Solvent Bonding of High-Performance Polymeric Capillary Electrophoresis Microchips, Anal. Chem. 77 (2005) 3536-3541.

[25] J. Chai, F. Lu, B. Li, D. Y. Kwok, Wettability Interpretation of Oxygen Plasma Modified Poly(methyl methacrylate), Langmuir 20 (2004) 10919-10927.

[26] C.W. Tsao, D. L. DeVoe, Bonding of thermoplastic polymer microfluidics, Microfluid Nanofluid. 6 (2009) 1–16.

[27] H. Shadpour, H. Musyimi, J. Chen, S. A. Soper, Physiochemical properties of various polymer substrates and their effects on microchip electrophoresis performance, J. Chromatogr. A. 1111 (2006) 238–251.

[28] G. A. C. M. Spierings, J. Haisma, Direct bonding of organic materials, Appl. Phys. Lett. 64 (1994) 3246.

CHAPTER 4

ON-CHIP APTAMER-BASED SANDWICH ASSAY FOR THROMBIN DETECTION EMPLOYING MAGNETIC BEADS AND QUANTUM DOTS

4.1 Abstract

In this paper, we report the development of an on-chip aptamer-based fluorescence assay for protein detection and quantification based on sandwich ELISA principles. Thrombin was selected as a model analyte to validate the assay design, which involves two DNA thrombin aptamers recognizing two different epitopes of the protein. Aptamer-functionalized magnetic beads were utilized to capture the target analyte, while a second aptamer, functionalized with quantum dots, was employed for on-chip detection. The binding of thrombin to the two aptamers via sandwich assay was monitored by fluorescence microscopy. The sandwich assay was performed on disposable microfluidic devices, fabricated on double-sided tapes and polymeric materials using a laser cutting approach. The approach enabled rapid thrombin detection with high specificity. Experimental conditions, such as reagent consumption and incubation time, were optimized in the microchip platform for the lowest limit of detection, highest specificity and shortest assay time. The analytical performance of the microchip based assay was compared to that in the well plate format (generally utilized for ELISA-based methodologies). The results show that microfluidic chip proved to be a rapid and efficient system for aptamer-based thrombin assays, requiring only minimal

(microliter) reagent use. This work demonstrated the successful application of on-chip aptamer-based sandwich assays for detection of target proteins of biomedical importance.

4.2 Introduction

Aptamers are RNA or single stranded DNA molecules that selectively bind to various molecular targets, such as small molecules, proteins, nucleic acids, cells, or microorganisms.[1,2] They bind to molecular targets with high specificity and affinity, making them attractive alternatives to the commonly used antibodies. Aptamers are selected in-vitro from a large oligonucleotides pool through a process called SELEX (Systematic Evolution of Ligands by Exponential Enrichment), and are therefore less expensive and tedious to produce. Added advantages to antibodies, such as their relative ease of isolation and modifications (host animal not required for production), tailored binding affinity and resistance against denaturation, make them suitable candidates for use as protein detection.

One of the most commonly studied proteins for molecular targets in aptamer-based assays is thrombin, the last enzyme protease involved in the coagulant cascade, which converts fibrinogen to insoluble fibrin that forms the fibrin gel.[3] The concentration of thrombin in blood varies considerably, and can be almost absent in the blood of healthy subjects. However, it can reach to low-micromolar concentrations during the coagulation process, and even low levels (low nM) of thrombin can be generated in the early hemostatic process.[4]

Consequently, aptamer-based assays for thrombin detection are viable diagnostic tools for monitoring the thrombin level in plasma or blood in the clinical area.

The DNA aptamers-binding thrombin have been extensively investigated.[5] They consist of two G-quartet conformations that selectively bind to α-thrombin.[6-8] These aptamers are widely used as model systems due to their ability to bind thrombin in two specific epitopes: 1) a relatively short 15-base DNA aptamer, 5′-GGTTGGTGTGGTTGG-3′, also known as HD-1, which binds exosite I of thrombin (fibrinogen binding sites), and 2) a 29-base DNA aptamer, referred to as HD-22, which binds to exosite II of thrombin (a heparin-binding aptamer).[9] This property has facilitated the development of aptamer sandwich assays for the detection of thrombin with higher specificity than direct immunoassays.

Detection of various target molecules using aptamers as the molecular recognition component has been studied previously using aptamer-based fluorescent reporter, electronic aptamer-based sensors, potassium ion detector, gold nanoparticles, and quantum dots or luminescent semiconductor nanocrystals.[10-16] Quantum dots are inorganic fluorescent materials (semiconductor nanocrystals) that offer unique optical properties, such as greater photo-stability, high quantum yield, resistant against chemical degradation, and broad absorption with narrow emission spectra (allowing multiplexing).They offer brighter and prolonged fluorescent lifetimes (less photobleaching compared to conventional organic fluorophores).[17-18] Moreover, their surfaces are easily modified with distinct class of molecules or theraupetic agents, such as antibodies, aptamers, and

peptides for binding of specific molecules. As a result, quantum dots have been utilized in the development of sensitive and specific targeted imaging and diagnostic tools for biomedical applications, such as cell imaging, bacteria detection, immunoassay, and labeling probes.[19-21]

Magnetic beads have been widely used as a powerful tool in numerous bioassays.[22-27] Their use as solid supports due to their biocompatibility, stability and easily modified surface, allows for straightforward conjugation with biomolecules of interest. Possessing a large surface-to-volume ratio, magnetic beads provide a relatively large numbers of binding sites for biochemical reactions; which offer higher efficiency of interactions between the samples and reagents, resulting in faster assay kinetics. Their superparamagnetic property is a key component that allows them to be externally controlled by permanent magnets. Analysis of complex samples can be carried out without pre-enrichment or purification steps. Separation of these beads from the matrix components is simplified, eliminating the need for sample clean-up and allowing enhanced extraction capability and signal sensitivity.

Magnetic beads can be coupled with microfluidic technology for a system that offers rapid analysis, high separation efficiences, and improved sensitivity.[28-30] Permanent magnets can be used to extract and concentrate these beads in the microchannel. This eliminates the tedious process of creating frits in a microchannel. Moreover, the magnetic beads can be positioned anywhere on the

microchip, and can be easily unloaded for downstream analysis by simply removing the magnet.

Microfluidic platform offers a unique alternative approach for the integration of bioassays.[31-32] It requires minimal reagent use, hence the amount of captured analytes can be greatly reduced, which in turn minimizes analysis cost and time. The use of inexpensive polymeric materials, such as polymetylmethacrylate (PMMA) or polycarbonate (PC) for device fabrication makes microchips ideal candidates for disposable solutions. Polymeric chips exhibit similar properties to glass, but are less expensive, easier to fabricate, biocompatible, and have low autofluorescence. Procedures developed in conventional platforms, such as well plates or reaction tubes, are readily transferable (in most instances) to channels in microchips. Moreover, the use of a microfluidic device simplifies the labor-intensive, tedious, and time-consuming washing steps usually required in the traditional ELISA format.

Currently, there are many commercial methods used to produce microfluidic chips, including photolithography, micromachining, laser ablation, thermal embossing, and injection molding. In this work, microchannels are fabricated using laser ablation technique on double-sided adhesive tapes and various polymer substrates. Laser cutting approach is capable of producing features in the order of sub-microns with great precision. The channels are cut on double-sided adhesives with the laser, and then sealed with plastic polymers on both sides. Patterning is done on a UV laser tool designed for micro-machining.

Similar cutting process has been developed using a cutting plotter, called xurography.[33-35] This process uses a knife blade to directly cut the microfluidic designs into various films or plastic substrates. Gale et al reported a DNA melting analysis performed on a microchip fabricated using a Graphtec knife plotter to manufacture the tape-bonded microchannels with dimensional accuracy of 10μm.[36-37] Laser provides a more accurate cutting tool to produce the microchannels compared to other cutting techniques. It is an ideal approach in rapid prototyping process to create microfluidic devices accurately and consistently.

In this paper we report the development of microfluidic aptamer-based assays employing the use of magnetic beads and quantum dots. Traditional assay processes usually involve multiple washing steps for each sample at significant time and labor cost. Our approach enabled the conduct of magnetic beads-based aptamer sandwich assays in a microfluidic platform capable of performing on-chip washing procedures that accelerated and simplified the assay process. Furthermore, the microchip design allowed for simultaneous detection and quantification of target analytes. Thrombin was used as the target analyte to provide experimental validation of the sandwich assay based on ELISA principles. Two aptamers-binding thrombin (aptamer A and B) were utilized to selectively bind thrombin at two different epitopes. Aptamer-functionalized magnetic beads were used to capture and concentrate the thrombin. After addition of the secondary aptamer (labeled with Qdot® nanocrystals), thrombin was detected by

fluorescence microscopy (see Fig. 4.1). The approach enabled rapid, sensitive and specific thrombin detection with reduced costs and minimized material consumption. The analytical performance of the assay in the microfluidic format was compared to well plate format in terms of sensitivity, linearity, reproducibility, and total analysis time.

a)

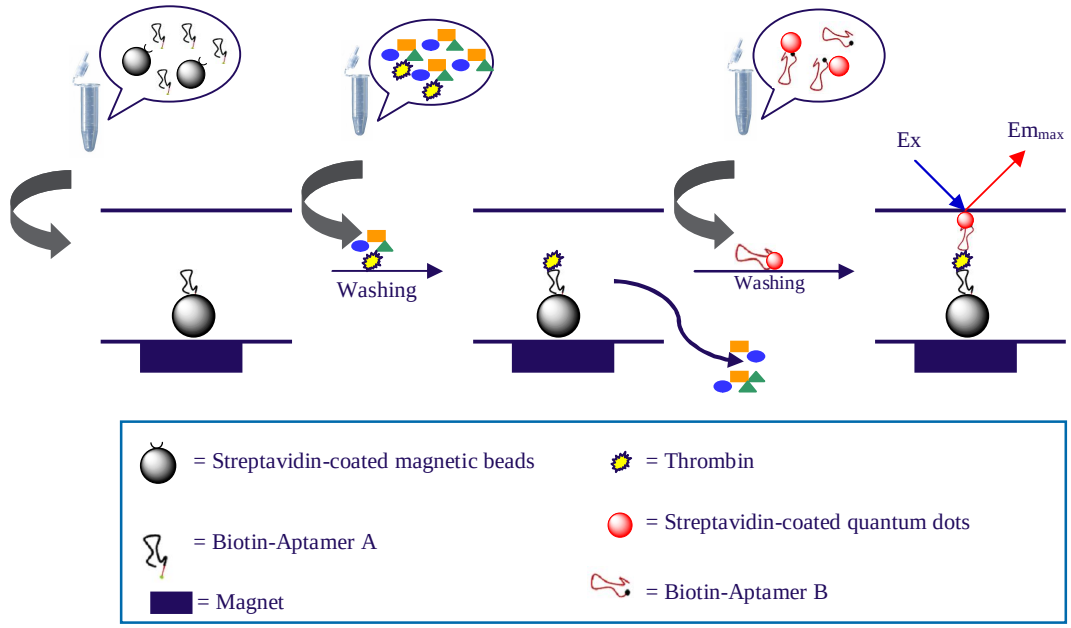

b) Sequences of aptamers:

1) Aptamer A: 5'-biotin-GGTTGGTGTGGTTGG-3'

2) Aptamer B: 5'-biotin-AGTCCGTGGTAGGGCAGGTTGGGGTGACT-3'

3) Mutated aptamer (control):

5'-biotin-CAGTCCGTAATAAAGCAGGTTAAAATGACTTCGTGGAA-3'

Fig. 4.1 a) Schematic reaction of aptamer-based sandwich assays, and b) Sequences of aptamers.

4.3 Experimental

4.3.1 Materials and reagents

Polymetylmethacrylate (PMMA) and polycarbonate (PC) were purchased from McMaster-Carr (Chicago, IL, USA). DNA thrombin-binding aptamers, Dynabeads® MyOne™ Streptavidin C1, Qdot® Streptavidin 655 and 525 were obtained from Life Technologies (Eugene, OR, USA). Human α-thrombin and prothrombin were obtained from Haematologic Technologies, Inc. (Essex Junction, VT, USA). Reagents used for buffer preparation (tris(hydroxylmethyl)aminomethane, magnesium chloride, potassium chloride, sodium chloride, bovine serum albumin), biotin, and human serum albumin were purchased from Sigma-Aldrich (St. Louis, MO, USA). Neodymium permanent magnets (grade N42) were purchased from K&J Magnetics (Jamison, PA, USA).

4.3.2 Microfabrication

The process was carried out using 3M Optically Clear Adhesive 8272 double-sided adhesive tapes (Boling Brook, IL, USA) on various polymer substrates. The microchannels were cut with a laser on a double-sided tape, and then sealed with plastic polymers on both sides. The top, bottom cover slips, and the adhesive layer can be quickly and easily patterned. Channel patterning was done with a 5 watt 355nm ESI UV laser tool designed for micro-machining (Portland, OR, USA). Individual cut layers were assembled as illustrated in Fig. 4.2.

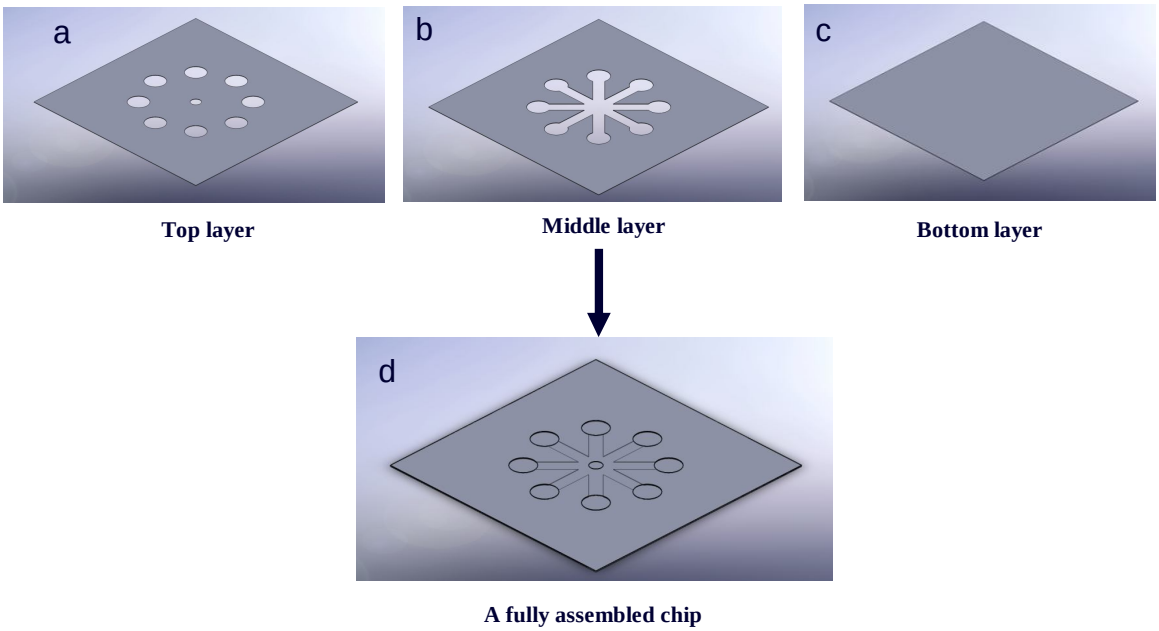

Fig. 4.2 Schematic design of the 3 layers microchip. a) top layer, made of PC or PMMA, b) middle layer, double-sided adhesives, for channel fabrication, c) bottom layer, PC or PMMA, as the enclosure, and d) a fully assembled chip with eight analyses performed simultaneously.

4.3.3 Chip Designs and Assembly

A photograph of the fabricated microchip is shown in Fig. 4.3. The device consists of inlet reservoirs of 4 mm in diameter and 50 μm in depth, used as the reaction chambers (Fig. 4.3a). Each chip consists of multiple channels (each with a dimension of 2 mm width, 10 mm length, and 50 μm depth), which allows for eight individual analyses to be performed simultaneously.

The disposable chip is positioned directly above the stationary component of the device (fixture) made of PMMA with dimensions of 4 cm width, 4 cm length, and 3.2 mm depth (Fig. 4.3b). 4-mm diameter holes are drilled in order to

permanently fix the permanent magnets on the fixture. These magnets are used to localize the magnetic beads in the microchambers.

The waste reservoir serves as a vacuum manifold (Fig. 4.3c) to accommodate simultaneous washing of reagents from the multiple channels. The reagents are flushed out by the applied negative pressure from a syringe pump through an Upchurch Scientific NanoPort (Oak Harbor, WA, USA), creating a vacuum system for washing.

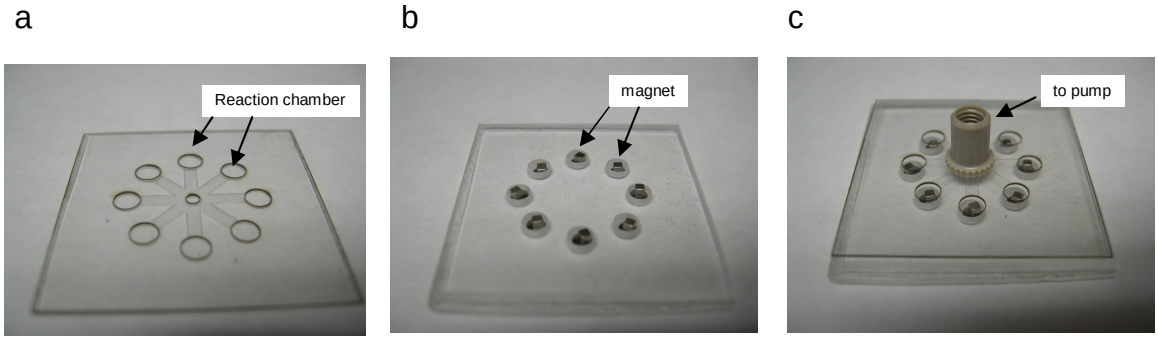

Fig. 4.3 Photographs of the microchip used for magnetic beads-based aptamer assays. a) A disposable plastic microchip containing 8 reaction chambers, b) a fixture to hold multiple NdFeB permanent magnets, and c) a photograph of the fully assembled device with a NanoPort for connection to a syringe pump.

4.3.4 Instrumentation

4.3.4.1 Studies in well plate format

The measurements were conducted in 96 well plates with Tecan Infinite M1000 plate reader (Research Triangle Park, NC, USA). Quantum dots fluorescence signal was monitored at 655 ± 5 nm (excitation wavelength at 400 ± 20 nm).

4.3.4.2 Studies in microfluidic chip format

On-chip experiments were performed on described microfluidic devices. The microchip outlet was connected to Harvard 33 twin syringe pump (Holliston, MA, USA) through the NanoPort. The pump was programmed in the withdrawal mode, which continuously pumping at a flow rate of 100 μL/min. Detection was performed on a Zeiss Axio Imager M1m fluorescence microscope (Thornwood, NY, USA), equipped with Qdot® 655 filter cubes.

Before use, the reaction chambers on the microchip were positioned directly above the magnets. Samples containing magnetic beads were loaded into the chambers, creating a solid support. Next, the target analytes were introduced into each chamber, followed by incubation steps to allow analyte interaction with the aptamer-functionalized magnetic beads. After incubation, excess matrix components were rinsed with the buffer solution and removed to waste by the negative pressure created from the syringe pump. Finally, quantification of the target analytes was completed on the fluorescence microscope.

4.3.5 Conjugation and optimization of magnetic beads and quantum dots to the biotinylated aptamers

Biotinylated aptamers were conjugated via streptavidin-biotin interaction on the streptavidin-coated magnetic beads or quantum dots. Prior to use, aptamers were thermally treated at 95^{o}C for 1 min, followed by cooling for 10 minutes. Previous studies have shown that thermal treatment unfolds the aptamer structure, allowing biotin at the 5' end to interact freely with streptavidin at the magnetic beads and quantum dots surface.[38]

Optimization of the conjugation for maximum coverage of magnetic beads and quantum dots with aptamers was performed using a Qubit® fluorometer (Life Technologies, Eugene, OR, USA). Streptavidin-conjugated quantum dots (Qdot® nanocrystals) were covalently linked to 5'-biotin aptamers with an optimized molar ratio of 1 to 10 (see supplementary materials in section 4.7). The conjugation reaction was carried out in tubes under gentle mixing for 30 minutes. The Qdot®-aptamer conjugates were centrifuged with a Pall Nanosep® device with a 30K MWCO membrane (Ann Arbor, MI USA) for 10 minutes at 12000 x g twice. The unreacted aptamers fractions were collected, labeled, then detected with Quant-iT™ ssDNA assay kits (Life Technologies, Eugene, OR, USA), on a Qubit® fluorometer.

Similarly, conjugation of aptamers to magnetic beads was optimized for maximum aptamer binding (see section 4.7). Streptavidin- magnetic beads were conjugated to 5'-biotin aptamers under gentle mixing for 30 minutes. As

previously described, the aptamers were collected, labeled by Quant-iT™ ssDNA assay kits, and detected using a Qubit® fluorometer.

4.3.6 Binding measurements

4.3.6.1 Studies in well plate format

Thrombin binding was performed in centrifuge tubes by mixing 50 μL of 1 μM aptamer A (conjugated to 1 mg/mL magnetic beads) and 50 μL of thrombin solutions. A series of thrombin standards with concentrations ranging from 0 to 204 nM were prepared. The reaction mixture was incubated at room temperature for 15 minutes. After 15 minutes, the solution was separated from the beads by triplicate rinsing in the binding buffer (50 mM Tris.HCl buffer containing 140mM NaCl, 1 mM $MgCl_2$, 5 mM KCl, and 0.1% BSA, pH 7.4). Next, 100 μL of 100 nM aptamer B-conjugated to 10 nM Qdot® nanocrystals was added to the beads. The solution was allowed to incubate for 15 minutes, followed by triplicate rinsing as described above. Finally, the beads were resuspended in 100 μL of the binding buffer, and transferred to 96 well plates for fluorescence measurements.

4.3.6.2 Studies in microfluidic chip format

The on-chip assays followed similar protocols described in section 4.3.6.1. Three μL of 1 μM aptamer A (conjugated to 1 mg/mL magnetic beads) was introduced into the reaction chambers; the magnetic beads were trapped in the chambers by magnets underneath. Rinsing was performed on-chip to remove

excess/unbound aptamers. Next, 3 μL of thrombin solutions of various concentrations were added, followed by a 5-minute incubation period. Unbound thrombin and excess matrix components were washed on-chip by the binding buffer. Finally, 6 μL of 100 nM aptamer B-conjugated to 10 nM Qdot® nanocrystals was introduced into the chamber and reacted for 5 minutes, followed by another washing step. Thrombin detection was performed on a fluorescence microscope to capture fluorescence images and intensity measurements.

4.3.7 Analytical performances

The fluorescence signal was reported in a dose-response curve for thrombin. Since plasma samples often contain the proteins involve in the coagulant cascades, such as prothrombin and HSA, these two analytes were also evaluated under the same experimental conditions to evaluate the assay specificity. Analytical performance in terms of specificity, detection limit, linearity, and reproducibility were assessed.

4.4 Results and Discussions

4.4.1 96 well plates assays

The aptamer-coated magnetic beads were utilized as solid supports for thrombin concentration and removal of excess protein and other unbound materials. With the use of a magnet, the separation of magnetic bead from unreacted components can be accomplished by repetitive washings. In a typical

experiment, a minimum of three washes is necessary to ensure complete rinsing. While this procedure is relatively easy and simple, it can be very time-consuming and labor-intensive when the process needs to be replicated numerous times for many samples.

A thrombin dose-response curve was carried out to demonstrate the binding of thrombin to aptamers using magnetic beads and Qdot® 655. Fig. 4.4 shows the dose-response curve of thrombin in the 96 well plate obtained from a series of titration experiments. Thrombin solutions with concentrations ranging from 0 to 204 nM (or 7.5 μg/mL) were incubated with aptamer A and aptamer B conjugates. The results in Fig. 4.4a show intensities of the measured fluorescence signals increasing with higher thrombin concentrations, which correspond well with a typical behavior of sandwich assays.

Fig. 4.4b depicts fluorescence intensities against log of thrombin concentrations. An increase in signal for thrombin with concentrations greater than 14 ng/mL was observed, until reaching its saturation point at thrombin concentration of approximately 4 μg/mL. A linear response was obtained for thrombin with concentrations ranging from 100 to 950 ng/mL (R^2=0.9975). Limit of detection (LOD) of 18 ng/mL was determined. This concentration value was calculated by the evaluation of the average response of the blank plus three times the standard deviation. Experiments were repeated five times to evaluate the reproducibility of the assay. The assay shows an average of 14% CV, calculated as the mean of all the concentrations tested.

a)

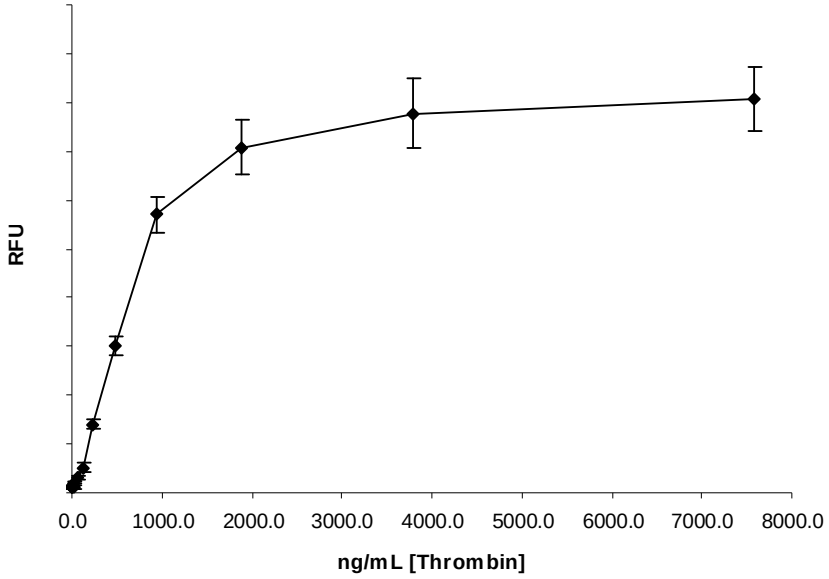

b)

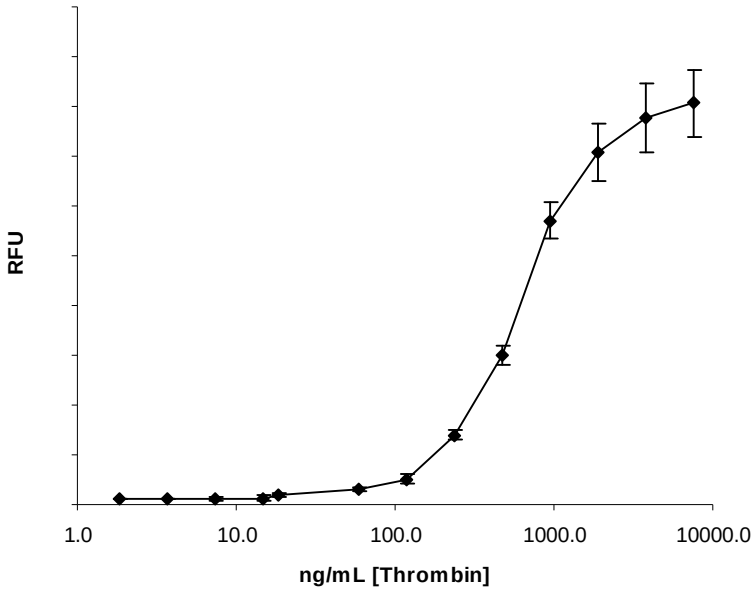

Fig. 4.4 Dose-response curve of the magnetic beads-based aptamer sandwich assay for thrombin. Assay was performed in the 96 well plate format. a) linear scale, and b) logarithmic scale.

Negative control experiments were carried out with aptamers that were previously reported as non-specific for thrombin. A mutated aptamer with a sequence shown in Fig. 4.1b was used.[9] The fluorescence signal of various concentration of thrombin binding to aptamer A and B was compared to the binding of 2 μg/mL of thrombin to the mutated aptamer (Fig. 4.5a). Results show that there is no change in the fluorescence intensity with response to the interaction between thrombin and the mutated aptamer. This confirms that this aptamer indeed does not bind to thrombin under assay conditions. It may have altered the conformation of the aptamer G-quartets, which prevents its binding.

Binding assay specificity for thrombin was tested using different other analytes: HSA and prothrombin. HSA is naturally present in blood at high concentrations, while thrombin is almost absent in healthy subjects. The assay was performed with 5 mg/mL HSA (700 fold in excess to thrombin), and the resulting signal was compared with that obtained for thrombin, as shown in Fig. 4.5b. The results are comparable with a blank, which demonstrates that the assay is not affected by the presence of this protein. Prothrombin is a structurally similar thrombin precursor. Low non-specific binding was observed resulting from interaction of 72 μg/mL prothrombin to the aptamers. These control experiments confirm that only thrombin binds to aptamer A and B, and that the change of both aptamer structures and fluorescence signals are resulted from the specific interaction between thrombin to the aptamers in presence of other plasma proteins.

a)

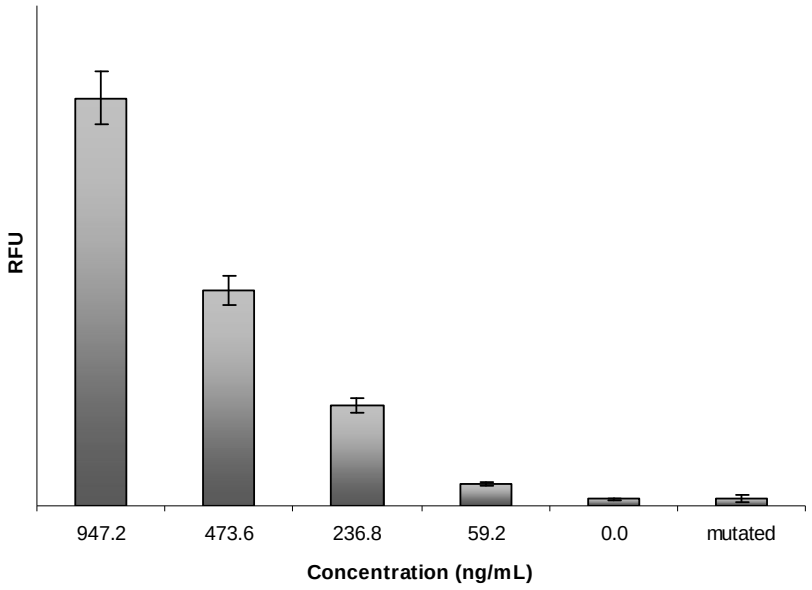

b)

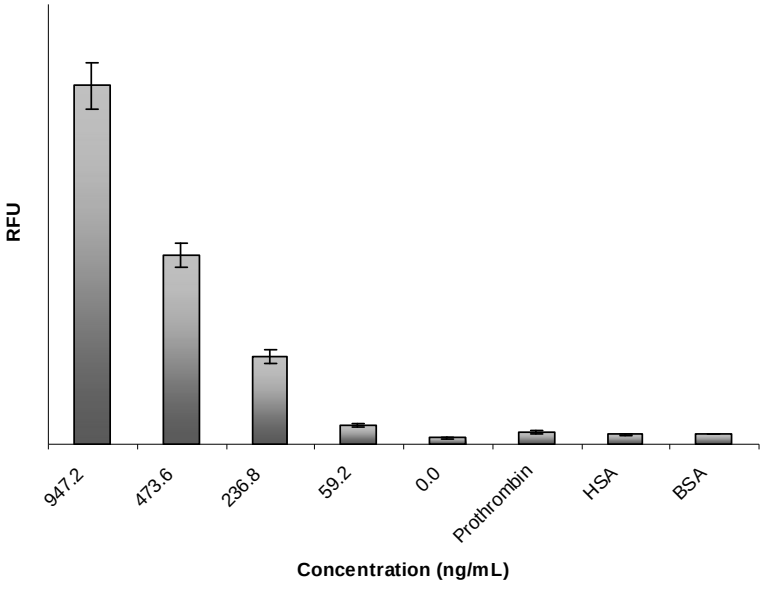

Fig. 4.5 Specificity of the assay in response to: a) mutated aptamers binding to thrombin (2μg/mL), and b) aptamer A and B binding to thrombin and thrombin-related compounds, such as prothrombin (72μg/mL) and HSA (5mg/mL).

4.4.2 Microfluidic chip assays

Fig. 4.3 shows photographs of the developed microfluidic device that enables magnetic bead-aptamer-based assays for the detection and quantification of thrombin. The platform enables the precise manipulation of small number of beads, and the rapid removal of unreacted components. The novel design greatly simplifies the usual technical difficulty of trapping a controlled quantity of beads by the use of external magnets located underneath the "reaction chamber". Proposed approach allowed the functionalized magnetic beads to be retained directly inside the chamber, instead of trapping the beads somewhere along the microchannel (typically performed in a magnetic bead-based assays) which often leads to sorption of particles on the channel walls and loss of particles (and compromised quantitative results) in the process. The integration of the disposable microfluidic component to a pump (serves as a vacuum manifold) facilitates automated on-chip washing for simpler and more rapid analysis. The device operation is facile, robust and efficient in removing excess unbound molecules) in a rapid, automated fashion. With the current design, each chip consists of multiple chambers to enable eight analyses to be performed simultaneously. The platform can be used for measurements of various analytes in parallel (multiplexed applications).

The on-chip magnetic beads-based aptamer assays were examined with fluorescence microscopy. Fig. 4.6 shows an image of immobilized magnetic beads subjected to thrombin assay in brightfield mode and fluorescence mode. The

magnetic beads were successfully concentrated in chambers using permanent magnets placed directly below the microchip. Fig. 4.6b shows the same captured beads in the fluorescence mode. The profile of the fluorescent beads shown in Fig.4.6b corresponds well to the brightfield image shown in Fig. 4.6a. Emission of the Qdot® 655 red fluorescence from the captured beads indicates binding of thrombin to both aptamers via the sandwich assay.

Each reaction chamber (Fig. 4.6c) contains aptamers-coated beads which captured different amounts of thrombin. The aptamers labeled with Qdot® 655 were introduced into the chambers. Rinsing was performed on-chip and thrombin binding was evaluated by fluorescence microscope. Fig. 4.6c represents fluorescence images of the aptamer-coated beads incubated with increasing concentrations of thrombin (0-4 μg/mL). Higher thrombin concentrations exhibit brighter red signal observed in the right side of the figure and show consistent decrease in brightness as the thrombin concentration decreases.

a) b)

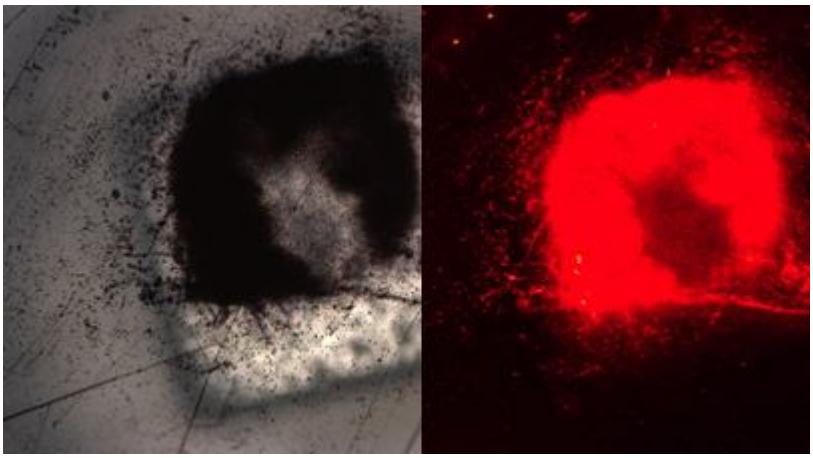

c)

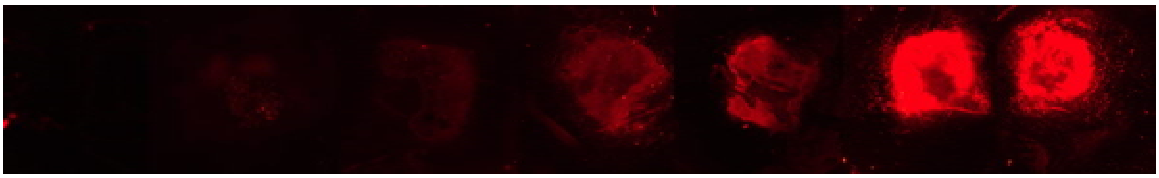

Fig. 4.6 Images of microchip reaction chamber following sandwich assay procedures: a) brightfield mode, b) fluorescence mode, and c) fluorescence images of aptamer-coated beads incubated with increasing concentration of thrombin (from left to right).

A series of proposed assay was performed on-chip to generate a calibration plot and determine the dose-dependent response for thrombin. The mean fluorescence intensity as a function of thrombin concentration obtained from five replicates was plotted in Fig. 4.7. The curve shows an expected sigmoidal response in fluorescence intensity to the log of thrombin concentration (Fig. 4.7b). A limit of detection of 10 ng/mL was determined with a linear range of 100-1000 ng/mL. The average standard deviation was 8%, demonstrating the reproducibility of the assay.

a)

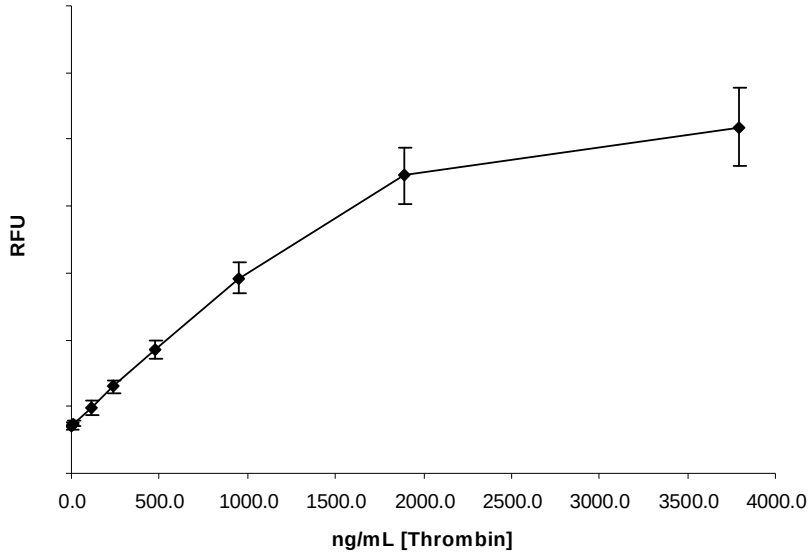

b)

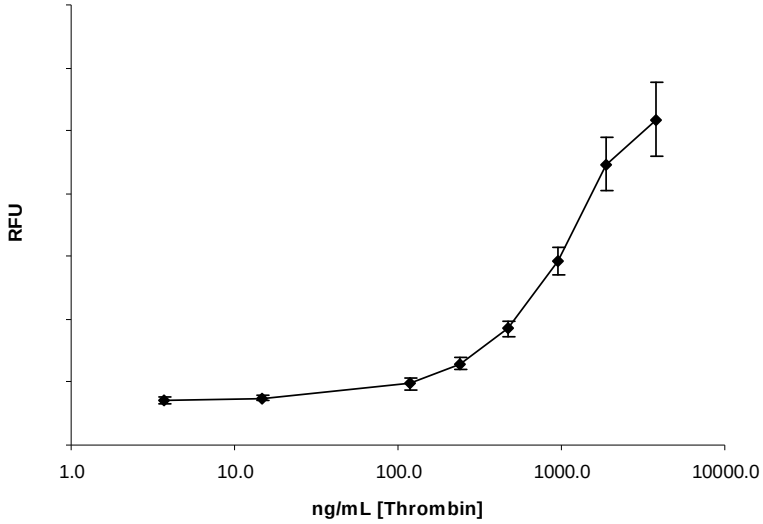

Fig. 4.7 On-chip dose-response curve for thrombin. a) linear scale, and b) logarithmic scale.

Results obtained in microchip format show increase in signal sensitivity and reproducibility compared with microplate format. On-chip assays offer additional benefits with simplified washing procedures (compared to the tedious and laborious washing steps in well plate format), faster analysis time, and minimal reagents consumption. The entire process from beads trapping to detection can be completed in less than an hour.

Different quantum dots may be imaged simultaneously. To demonstrate its potential use in multiplexing, the sandwich assay principle was performed for thrombin detection using two different quantum dots (red Qdot® 655 and green Qdot® 525). Fig. 4.8 shows the successful thrombin binding, confirmed by the red and green fluorescence signals exhibited from the captured beads that correspond to the emission of Qdot® 655 and 525, respectively. The results show a potential in using this assay for other target analytes in multiplexing applications. By immobilizing different aptamers with different quantum dots, multiplexing for multiple protein detections are feasible.

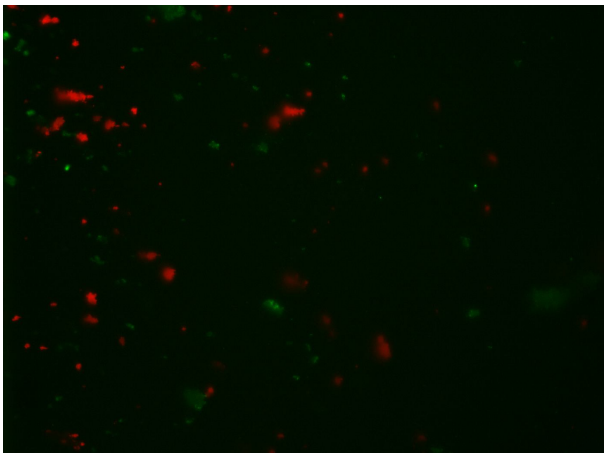

Fig. 4.8 Sandwich assay on a mixed bed of Qdot® 655/525, both immobilized on 1μm magnetic beads for thrombin detection.

4.5 Conclusions

We reported here an innovative approach for bioassay development by integrating microfluidics technologies with magnetic beads separation and fluorescence detection. The approach was investigated with an aptamer-based sandwich assay for a simultaneous detection and quantification of thrombin. The microfuidic platform offers high sensitivity (LOD of 10 ng/mL), specificity, and reproducibility (CV = 8%). Furthermore, the simplified on-chip washing process allows for high throughput processing with minimal time and materials/reagents consumption. The work has demonstrated the potential of this new approach for applications in protein analysis for diagnosis or fundamental research.

4.6 Acknowledgements

The authors would like to acknowledge Dean Tsou, Vanessa Adams, Schuyler Corry, and Joe Bartel for assistance with reagents and expertise.

4.7 Supplementary materials

Optimization of the assay parameters

The first step in the optimization of aptamer and magnetic beads immobilization was to determine the binding capacity of the magnetic beads. The graph shown in Fig. 4.9 represents different aptamer concentrations added into a constant amount of beads. The concentrations of the aptamers were increased until the beads reach their maximum capacity. The response signal represents the concentration of aptamers labeled with Quant-iT™ ssDNA assay kit and detected with Qubit® fluorometer.[39] The plot indicates the degree of saturation that occurs at approximately 1 μM aptamer A conjugated to 1 mg/mL beads.

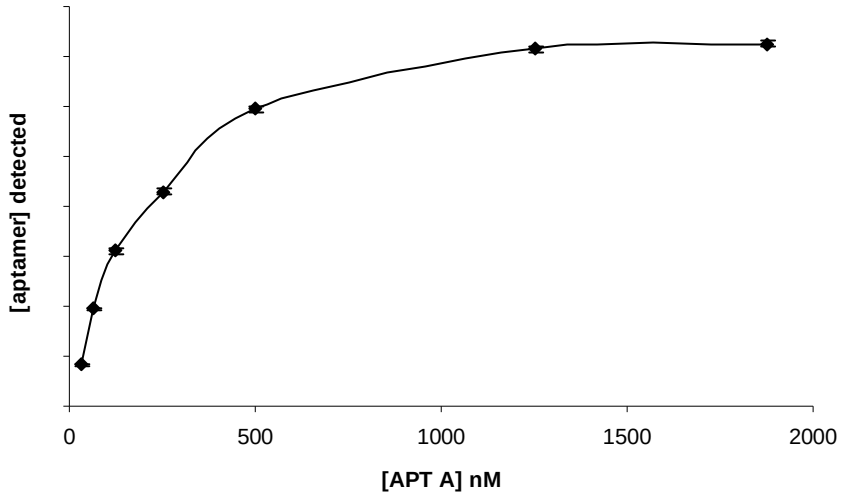

Fig. 4.9 Binding curve of biotinylated aptamer to streptavidin magnetic beads; analysis performed with Quant-iT™ ssDNA assay, and detected by Qubit® fluorometer.

The steps shown in Fig. 4.10a were performed to determine the optimum binding ratio between aptamer and quantum dots. Initially, excess aptamers of different concentrations were added to a constant concentration of quantum dots. The filtration step followed using a centrifugal device with a certain molecular weight cutoff membrane (MWCO) to separate the excess or nonspecifically bound aptamers. Unbound aptamers (with smaller size compared to the membrane pores) passed through the membrane and were efficiently separated, subsequently collected, labeled by Quant-iT™ ssDNA assay, and detected with Qubit® fluorometer.[39] The signal detected represents the concentration of free aptamers measured. A low concentration of free aptamers ensures maximum binding between quantum dots and the aptamers. The plot in Fig. 4.10b indicates the maximum binding ratio of 10 aptamers per quantum dots.

a)

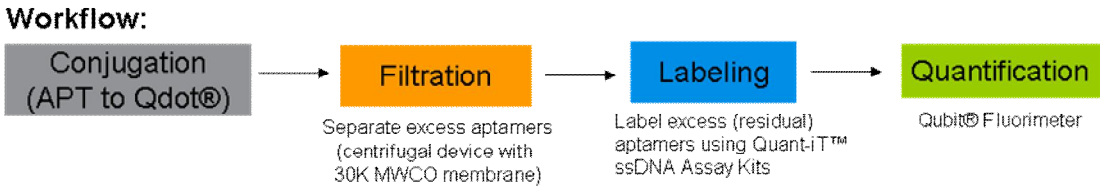

b)

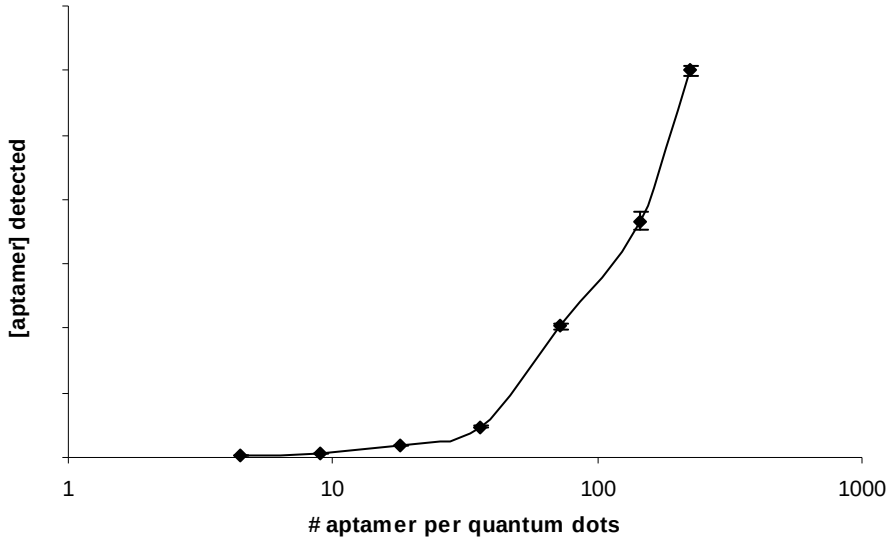

Fig. 4.10 a) Workflow for conjugation of aptamer to quantum dots, and b) the curve correlates the concentration of unbound aptamer to the amount of aptamers conjugated to quantum dots.

4.8 References

(1) Ellington, A. D.; Szostak, J. W. *Nature* **1990**, *346*, 818-822.

(2) Tuerk, C.; Gold, L. *Science* **1990**, *249*, 505-510.

(3) Holland, C.A.; Henry, A.T.; Whinna, H.C.; Church, F.C. *FEBS Letters* **2000**, *484*, 87-91.

(4) Shuman, M.A.; Majerus, P.W. *J Clin Invest.* **1976**, *58*, 1249-1258.

(5) Bock, L. C.; Griffin, L. C.; Latham, J. A.; Vermaas, E. H.; Toole, J. J. *Nature* **1992**, *355*, 564-566.

(6) Macaya, P.; Schultze, F. W.; Smith, J. A.; Roe, Feigon, J. *Proc. Natl. Acad. Sci. U.S.A.* **1993**, *90*, 3745-3749.

(7) Smirnov, I.; Shafer, R. H. *Biochemistry* **2000**, *39*, 1462-1468.

(8) Paborsky, L. R.; McCurdy, S. N.; Griffin, L. C.; Toole, J. J.; Leung, L. L. *J. Biol. Chem.* **1993**, *268*, 20808-20811.

(9) Tasset, D. M.; Kubik, M. F.; Steiner, W. *J. Mol. Biol.* **1997**, *272*, 688-698.

(10) Nutiu, R.; Li, Y.F. *J. Am. Chem. Soc.* **2003**, *125*, 4771–4778.

(11) Radi, A.E.; O'Sullivan, C.K. *Chem. Commun*. **2006**, *32*, 3432–3434.

(12) Baker, B.R.; Lai, R.Y.; Wood, M.S.; Doctor, E.H.; Heeger, A.J.; Plaxco, K.W. *J. Am. Chem. Soc*. **2006**, *128*, 3138–3139.

(13) Sapsford, K.E.; Pons, T.; Medintz, I.L.; Mattoussi, H. *Sensors* **2006**, *6*, 925-953.

(14) Hernandez' F.J.; Dondapati, S.K.; Ozalp, V.C.; Pinto, A.; O'Sullivan, C.K.; Klar, T.A.; Katakis, I. *J. Biophotonics*. **2009**, *2*, 227 – 231.

(15) Huang, C.C.; Chang, H.T. *Chem. Commun.* **2008**, *28*, 1461-1463.

(16) Chen, Z.; Li, G.; Zhang, L.; Jiang, J. Li, Z.; Peng, Z.; Deng, L. *Anal. Bioanal. Chem.* **2008**, *392*, 1185-1188.

(17) Michalet, X.; Pinaud, F.F.; Bentolila, L.A.; Tsay, J.M.; Doose, S.; Li, J.J.; Sundaresan, G.; Wu, A.M.; Gambhir, S.S.; Weiss, S. *Science* **2005**, *307*, 538–544.

(18) Medintz, I.L.; Uyeda, H.T.; Goldman, E.R.; Mattoussi, H. *Nat. Mater.* **2005**, *4*, 435–446.

(19) Goldman, E.R.; Medintz, I.L; Mattoussi, H. *Anal. Bioanal. Chem.* **2006**, *384*, 560–563.

(20) Wu, X,Y.; Liu, H.J.; Liu, J.Q.; Haley, K.N.; Treadway, J.A.; Larson, J.P.; Ge, N.F.; Peale, F.; Bruchez, M.P. *Nat. Biotech.* **2003**, *21*, 41–46.

(21) Edgar, R.; McKinstry, M.; Hwang, J.; Oppenheim, A.B.; Fekete, R.A.; Giulian, G.; Merril, C.; Nagashima, K.; Adhya, S. *Proc Natl Acad Sci USA* **2006**, *103*, 4841–4845.

(22) Centi, S.; Tombelli, S.; Minunni, M.; Mascini, M. *Anal. Chem.* **2007**, *79*, 1466-1473.

(23) Strehlitz, B.; Nikolaus, N.; Stoltenburg, R. *Sensors* **2008**, *8*, 4296-4307.

(24) Fischer, N.O.; Tarasow, T.M.; Tok, J.B.H. *Anal. Biochem.* **2008**, *373*, 121–128.

(25) Dwarakanath, S.; Satyanarayana, S.; Bruno, J.G.; Vattem, D.; Rao, P.M.; Ikanovic, M.; Phillips T. *Journal of Clinical Ligand Assay* **2006**, *29*, 136-142.

(26) Kawde, A.N.; Rodriguez, M.C.; Lee, T.M.H.; Wang, J. *Electrochemistry Communications* **2005**, *7*, 537-540.

(27) Tombelli, S.; Minunni, M.; Mascini, M. *Biosens. Bioelectron.* **2005**, *20*, 2424-2434.

(28) Lou, X.; Qian, J.: Xiao, Y.; Viel, L.; Gerdon, A.E.; Lagally, E.T.; Atzberger, P.; Tarasow, T.M.; Heeger, A.J.; Soh, H.T. *Proc. Natl. Acad. Sci. USA* **2009**, *106*, 2989-2994.

(29) Gijs, M.A.M. *Microfluid. Nanofluid.* **2004**, *1*, 22–40.

(30) Gijs, M.A.M.; Lacharme, F.; Lehmann, U. *Chem. Rev.* **XXXX**, *xxx*, 000–000

(31) Bronzeau, S.; Pamme, N. *Anal. Chim. Acta* **2008**, *609*, 105-112.

(32) Park, H.; Lee, M.; Seong, G.H.; Choo, J.; Lee, E.K.; Park, J.Y.; Lee, S.; Lee, K.H.; Choi, Y.W. *Bull. Korean Chem. Soc*. **2008**, *29*, 1297-1298.

(33) Bartholomeusz, D.A.; Boutte, R.W.; Andrade, J.D. *J. Micromech. System* **2005**, *14*, 1364-1374.

(34) Kim, J.; Surapaneni, R.; Gale, B.K. *Lab on a Chip* **2009**, *9*, 1290-1293.

(35) Kumar, R.; Smith, R.L.; Pappas, M.G. *Chip and Tips* **2009**

(36) Greer, J.; Sundberg, S.O.; Wittwer, C.T.; Gale, B.K. *J. Micromech. Microeng*. **2007**, 17, 2407-2413.

(37) Sundberg, S.O.; Wittwer, C.T.; Greer, J.; Pyror, R.J.; Elenitoba, J.; Gale, B.K. *Biomed. Microdevices* **2007**, *9*, 159-166.

(38) Baldrich, E.; Restrepo, A.; O'Sullivan, C.K. *Anal. Chem*. **2004**, *76*, 7053-7063.

(39) Quant-it™ ssDNA assay kits (for use with the Qubit® fluorometer) manuals. http://probes.invitrogen.com/media/pis/mp10212.pdf

CHAPTER 5

SUMMARY AND CONCLUSIONS

The area of micro total analysis systems (μTAS), also called "lab on a chip", miniaturized analysis systems, is a rapidly developing field. The benefits it offers include reduced component size, decreased consumption of reagents and sample, reduced waste generation, reduced analysis time, and increased synthesis rate due to short mixing time. It also offers many promising analytical tools that may enhance the effectiveness and performance of routine chemical analysis. They allow for the integration of fluid delivery, sample handling, chemical or biochemical analysis (such as extraction, separation by chromatography or electrophoresis), and detection systems into a single device for a complete on-chip analysis. This interfacing allows highly integrated parallel operations, making complex analyses simpler to perform.

The development of a μTAS system is presented in this dissertation by covering three main research subjects. This study started with the utilization of magnetic particles for an in-line extraction in confines of capillary columns. The work continued with the development of bonding techniques for creating polymer-based microfluidic devices through surface modification process. The two previous projects combined allowed us to integrate the properties of magnetic

particles in a microfluidic format by developing a device that enables on-chip magnetic beads-based bioassays.

In chapter 2, I synthesized magnetic particles consisted of silica-clad iron oxide nanoparticles that were functionalized with C18 groups. The particles demonstrated high saturation magnetization and superparamagnetic properties. I utilized these particles as extraction sorbents in a capillary setup. Simple permanent magnets were used to perform an inline extraction method. This approach allowed for extraction, elution, and detection of multiple target analytes to be performed in a single configuration. The method is simple by eliminating the use of frits for sorbents immobilization, and the option of recovering the sorbents after each use making it cost effective. This approach is especially advantageous when the analysis involves samples containing particulate matter, such that sample preparation can be greatly simplified. The use of this approach extends to other areas by using various extraction sorbents on different analytical tools depending on their applications.

In Chapter 3, I presented a bonding method that was used to form channels in microchip and other functional features for making microfluidic devices [1]. The channels were fabricated according to the published methods developed in our group [2-3]. Briefly, an SU-8 master was created by photolithography process, followed by a two-stage embossing technique, which involved two polymer substrates with different glass transition temperatures (T_g), polyetherimide (PEI; T_g~216^{o}C) and poly(methyl methacrylate) (PMMA; T_g~105^{o}C). The resulting

PMMA substrate possessed the same features as those of the SU-8 master. A novel bonding method was developed to form a complete microchannel by enclosing the embossed PMMA with another blank PMMA piece. Bonding was achieved through surface modification by plasma oxidation treatment, followed by the application of silane reagents (tetraethyl orthosilicate or TEOS) to incorporate Si functionalities on the polymer surface. The bonding occurred by facilitating siloxane bonds between the two polymers. This method presents several advantages compared to other bonding methods, such as thermal bonding or solvent welding [3-4]. This technique readily produced complete microfluidic chips without the need to use strong organic solvents or high temperatures. The method was straightforward and integrity of the microfluidic features was successfully preserved after bonding. A high bond strength (4000 kN/m^2) was realized, with a value approaching that of solvent bonded chips. Lastly, this fabrication method provides a cost-effective, simple, robust, and versatile approach to bonding polymer-based microdevices. The technique lends itself readily to many polymers (such as PMMA, PC, or APET) and Si-containing substrates, such as PDMS and glass, facilitating device production for a variety of applications and even enabling hybrid chip fabrication.

Magnetic beads can be coupled with microfluidic technology for a system that offers rapid analysis, high separation efficiences, and improved sensitivity. Permanent magnets can be used to extract and concentrate these beads in the microchannel. This way, tedious process in creating frits in a microchannel is

eliminated. Moreover, they can be positioned anywhere on the microchip, and easily unloaded for downstream analysis by simply removing the magnet. In chapter 4, I utilized the benefits of magnetic beads properties and microfluidic technology to develop an innovative approach in bioassay analysis. Specifically, I developed a device capable of conducting a magnetic beads-fluorescence assay based on sandwich ELISA principles for thrombin detection and quantification. Two DNA thrombin aptamers were utilized to selectively bind thrombin at two different epitopes. Aptamer-functionalized magnetic beads were used to capture and concentrate the thrombin, while a second aptamer, functionalized with quantum dots, was employed for on-chip detection. The device allowed us to perform an on-chip assay that is rapid, sensitive and specific for thrombin detection, with the benefits of reduced costs and minimized material consumption. The assay design described here is not limited to thrombin as the target analyte or aptamer as the molecular recognition elements, thus the system can be optimized for the detection of multiple proteins of complex matrices.

In conclusion, this work has opened up a new chapter in the development of magnetic beads-based materials and devices in a wide variety of applications, ranging from diagnostics to fundamental research. A device that enables a simple, more time-efficient, economical, and sensitive approach is very attractive and useful in chemical or biochemical analysis. A significant challenge that remains as an impediment to the broader application of μTAS is the use of manual handling that is often still required for sample introduction. This can result in varying

amount of samples that are introduced; lowering reproducibility of the analysis. In order to fully realize the benefits of μTAS, further techniques need to be developed and optimized to accommodate a more rapid and consistent analysis. Recently, the development of automation technologies in micro technology is continuously emerging. A fully automated system provides us with higher throughput that enables rapid and consistent sample handling and fluid manipulation on the microchip without human intervention. This improves the process even further with enhanced assay efficiencies and system robustness. Most importantly, a full realization of μTAS that enables the integration of several steps of analyses all in one chip, from sampling, sample processing, and separation to detection can be achieved.

References

[1] Y.H. Tennico, M.T. Koesdjojo, S. Kondo, D.T. Mandrell, V.T. Remcho. *Sensors and Actuators B*, **2010**, *143*, 799

[2] M.T. Koesdjojo, Y.H. Tennico, J.T. Rundel, V.T. Remcho. *Sensors and Actuators B,* **2008**, *131*, 692

[3] M.T. Koesdjojo, C.R. Koch, V.T. Remcho**.** *Anal. Chem.*, **2009**, *81* (4), 1652–1659

[4] M.T. Koesdjojo Y.H. Tennico V.T. Remcho**.** *Anal. Chem.*, **2008**, *80* (7), 2311–2318